

Semiempirical Molecular Orbital Models based on the Neglect of Diatomic Differential Overlap Approximation

Tamara Husch, Alain C. Vaucher, and Markus Reiher*

ETH Zürich, Laboratorium für Physikalische Chemie,
Vladimir-Prelog-Weg 2, 8093 Zürich, Switzerland.

October 30, 2018

Abstract

Semiempirical molecular orbital (SEMO) models based on the neglect of diatomic differential overlap (NDDO) approximation efficiently solve the self-consistent field equations by rather drastic approximations. The computational efficiency comes at the cost of an error in the electron-electron repulsion integrals. The error may be compensated by the introduction of parametric expressions to evaluate the electron-electron repulsion integrals, the one-electron integrals, and the core-core repulsion. We review the resulting formalisms of popular NDDO-SEMO models (such as the MNDO(/d), AM1, PM x , and OM x models) in a concise and self-contained manner. We discuss the approaches to implicitly and explicitly describe electron correlation effects within NDDO-SEMO models and we dissect strengths and weaknesses of the different approaches in a detailed analysis. For this purpose, we consider the results of recent benchmark studies. Furthermore, we apply bootstrapping to perform a sensitivity analysis for a selection of parameters in the MNDO model. We also identify systematic limitations of NDDO-SEMO models by drawing on an analogy to Kohn–Sham density functional theory.

*corresponding author: markus.reiher@phys.chem.ethz.ch.

1 Introduction

The driving force for the development of semiempirical molecular orbital (SEMO) models has always been the desire to accelerate quantum chemical calculations. At the outset of the development of SEMO models in the middle of the last century,^{1–10} the goal was to carry out electronic structure calculations for small molecules, which was not routinely possible with *ab initio* electronic structure methods at that time. Since then, theoretical chemistry has seen a remarkable development in terms of computational resources, but also in terms of *ab initio* methodology.¹¹ One must not forget that most electronic structure methods which we apply routinely today, such as Kohn–Sham density functional theory (KS-DFT)¹² and coupled cluster theory,¹³ were developed concurrently with today’s SEMO models. As a consequence of algorithmic and methodological developments,¹¹ accurate *ab initio* electronic structure methods have long replaced SEMO models in their original areas of application (electronic structure calculations for small molecules). Nevertheless, SEMO models did not become extinct. Instead, they opened up different areas of application which can broadly be divided into three categories (see also Ref. 14 for a recent review): (i) simulations of very large systems such as proteins^{15–22} and those with thousands of small molecules,^{23,24} (ii) calculations for a large number of isolated and unrelated medium-sized molecules, e.g., in virtual high-throughput screening schemes for materials discovery^{25,26} and docking-and-scoring of potential drug candidates,^{27–32} and (iii) entirely new applications such as real-time quantum chemistry where ultra-fast SEMO models allow the perception of visual and haptic feedback in real time when manipulating medium-sized molecular structures.^{33–40}

In this work, we review, dissect, and analyze SEMO models which apply the neglect of diatomic differential overlap (NDDO) approximation⁸ (NDDO-SEMO models). These models are currently among the most popular SEMO models⁴¹ and all members of this class of SEMO models share the same conceptual framework. Another class of semiempirical models, which is under continuous development, are tight-binding versions of KS-DFT.^{42–48} We will not discuss these density-functional tight-binding models as the focus of this work is on NDDO-SEMO models.

The central NDDO approximation drastically reduces the computational effort associated with the calculation of electron–electron repulsion integrals (ERIs), and hence, leads to a significant speed-up.⁸ However, it took over ten years to successfully incorporate the NDDO approximation in a useful SEMO model (see Figure 1), the *Modified Neglect of Diatomic Overlap* (MNDO) model proposed in 1977.^{49,50}

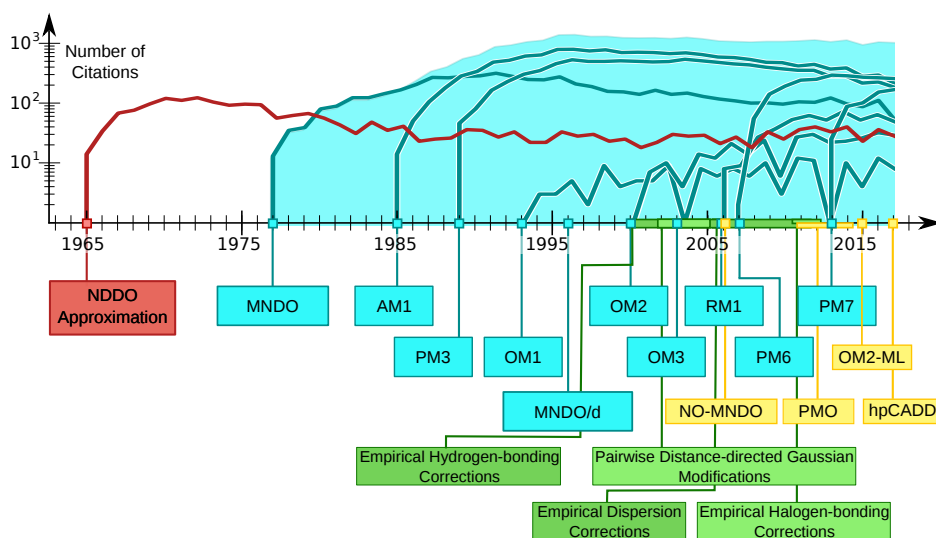


Figure 1: Chronology of key steps in the development of NDDO-SEMO models starting with the introduction of the NDDO approximation in 1965⁸ (highlighted in red) and reaching until today. Popular NDDO-SEMO models (MNDO,⁵⁰ AM1,⁵¹ PM3,⁵² MNDO/d,^{53,54} RM1,⁵⁵ PM6,⁵⁶ PM7,⁵⁷ OM1,⁵⁸ OM2,⁵⁹ and OM3⁶⁰) are highlighted in blue, novel suggestions (NO-MNDO,⁶¹ PMO,^{62–66} OM2-ML,⁶⁷ and hpCADD⁶⁸) in yellow, and semiclassical correction terms in green. The number of citations of the original publications^{50–60} was assessed with Google Scholar.⁶⁹

Since that time, small adjustments were made to the original MNDO model which gave rise to different closely related models such as AM1,⁵¹ PM3,⁵² MNDO/d,^{53,54} RM1,⁵⁵ PM6,⁵⁶ and PM7.⁵⁷ In the nineties of the last century, the development of another family of NDDO-SEMO models began, the *Orthogonalization-Corrected Models* OM1,⁵⁸ OM2,⁵⁹ and OM3.⁶⁰

Although the development efforts were consistently accompanied by articles, reviews, and books,^{41,70–82} there is no single resource which contains the detailed formalisms of the NDDO-SEMO models in a form which enables their facile implementation. Currently, for example, the implementation of a modern NDDO-SEMO model such as PM7 requires the consultation of at least ten references.^{49,50,52,53,56,57,83–86} Some of these references contain errors or misprints (which are clarified later on in this work) and some of them may be hard to obtain because they are books and dissertations written over forty years ago, some of them in German. Furthermore, the varying notation, adoption of jargon, and introduction of acronyms may hamper an in-depth understanding. An in-depth understanding is, however, mandatory

to be able to implement NDDO-SEMO models following the original references. As a concise and self-contained presentation of the formalism of these models is appropriate to understand their central ideas, we intend to provide such an overview in this work.

In recent years, a variety of semiclassical correction terms was designed to correct for specific flaws of NDDO-SEMO models, e.g., for hydrogen-bonding interactions,^{87–93} dispersion interactions,^{87,90–92,94} halogen-bonding interactions,^{91,95} and other pairwise interactions.^{96,97} The form of these terms is documented in a self-contained manner in the respective publications. The introduction of these terms does not explicitly affect the electronic structure part of the models. Hence, we refer to a recent review by Christensen *et al.*⁹⁸ on this topic and we instead focus on the question of how NDDO-SEMO models attempt to approximate the electronic structure problem in this work.

This review is organized as follows: We first briefly introduce the notation and the quantum chemical foundations necessary to discuss NDDO-SEMO models which makes this review self-contained (Section 2). NDDO-SEMO models share, apart from the NDDO approximation, the application of a minimal basis set and the restriction of the number of explicitly considered electrons. We outline the formalism essential to all NDDO-SEMO models (Section 3) before moving on to specific NDDO-SEMO models (Sections 4–6). After discussing how NDDO-SEMO models are assembled, we discuss how (static and dynamical) electron correlation effects are captured. Generally, there are two strategies to tackle this problem: The calibration of parameters incorporated in NDDO-SEMO models against accurate reference data and the explicit description of electron correlation effects (Sections 7 and 8). We summarize the current state of knowledge with respect to both of these aspects and draw some more general conclusions for the prospects of NDDO-SEMO models (Section 9).

2 Setting the Stage

Electronic structure methods aim at the solution of the electronic Schrödinger equation,

$$\mathcal{H}_{\text{el}}\Psi_{\text{el}}^{\{\tilde{\mathbf{R}}_I\}}(\{\mathbf{r}_i\}) = E_{\text{el}}^{\{\tilde{\mathbf{R}}_I\}}\Psi_{\text{el}}^{\{\tilde{\mathbf{R}}_I\}}(\{\mathbf{r}_i\}), \quad (1)$$

which asserts that we can calculate the electronic energy $E_{\text{el}}^{\{\tilde{\mathbf{R}}_I\}}$ from the electronic wave function $\Psi_{\text{el}}^{\{\tilde{\mathbf{R}}_I\}}(\{\mathbf{r}_i\})$ by applying the electronic Hamiltonian operator \mathcal{H}_{el} . In the Born–Oppenheimer approximation, $E_{\text{el}}^{\{\tilde{\mathbf{R}}_I\}}$ and

$\Psi_{\text{el}}^{\{\tilde{\mathbf{R}}_I\}}(\{\mathbf{r}_i\})$ depend parametrically on the fixed (indicated by the tilde and by giving them as superscripts) coordinates of the N atomic nuclei ($\{\tilde{\mathbf{R}}_I\}$) of a system. The electronic wave function $\Psi_{\text{el}}^{\{\tilde{\mathbf{R}}_I\}}(\{\mathbf{r}_i\})$ depends on the coordinates of n electrons ($\{\mathbf{r}_i\}$). The Hamiltonian operator \mathcal{H}_{el} contains operators for the n kinetic energy contributions of the electrons and for the electrostatic pair interaction energies of electrons and the N atomic nuclei (in Hartree atomic units (a.u.)),

$$\mathcal{H}_{\text{el}} = \sum_{i=1}^n \left(-\frac{1}{2} \nabla_i^2 - \sum_{I=1}^N \frac{Z_I}{|\mathbf{r}_i - \tilde{\mathbf{R}}_I|} \right) + \sum_{i=1}^n \sum_{j>i}^n \frac{1}{|\mathbf{r}_i - \mathbf{r}_j|} + \sum_{I=1}^N \sum_{J>I}^N \frac{Z_I Z_J}{|\tilde{\mathbf{R}}_I - \tilde{\mathbf{R}}_J|}. \quad (2)$$

The gradient defined for the coordinates of electron i is denoted as ∇_i and Z_I denotes the nuclear charge of the I -th nucleus (note that capital letters denote quantities defined for atomic nuclei). It is convenient to collect the first two terms in a one-electron operator h_i , the third term in a two-electron operator $g_{(i,j)}$, and the nuclear interaction energy in V ,

$$\mathcal{H}_{\text{el}} = \sum_{i=1}^n h_i + \sum_{i=1}^n \sum_{j>i}^n g_{(i,j)} + V. \quad (3)$$

Since the early days of quantum mechanics, various approximations were developed to solve Eq. (1). In the following, we focus on Hartree–Fock (HF) theory to lay the foundation for the discussion of NDDO-SEMO models (see, e.g., Ref. 99 for a detailed presentation of HF theory in a one-electron basis set). The exact wave function $\Psi_{\text{el}}^{\{\tilde{\mathbf{R}}_I\}}(\{\mathbf{r}_i\})$ is approximated by the HF wave function $\Phi_{\text{el}}^{\text{HF},\{\tilde{\mathbf{R}}_I\}}(\{\mathbf{r}_i\})$, which is constructed as the antisymmetrized product of one-particle functions $\psi_i^{\{\tilde{\mathbf{R}}_I\}}(\mathbf{r}_i)$ (i.e., molecular spin orbitals),

$$\Psi_{\text{el}}^{\{\tilde{\mathbf{R}}_I\}}(\{\mathbf{r}_i\}) \approx \Phi_{\text{el}}^{\text{HF},\{\tilde{\mathbf{R}}_I\}}(\{\mathbf{r}_i\}) = \mathcal{A} \prod_{i=1}^n \psi_i^{\{\tilde{\mathbf{R}}_I\}}(\mathbf{r}_i). \quad (4)$$

Antisymmetrization of the product of one particle-states by means of the antisymmetrization operator \mathcal{A} implements the Pauli principle.¹⁰⁰ We approximate the spatial orbitals that enter the spin orbitals as linear combinations of M atom-centered basis functions $\chi_{\mu}^I = \chi_{\mu}^{\tilde{\mathbf{R}}_I}(\mathbf{r})$ (μ -th basis function of type χ centered on atom I) weighted with the expansion coefficients $x_{C^{\{\tilde{\mathbf{R}}_I\}}} = \{x_{C^{\mu i}}^{\{\tilde{\mathbf{R}}_I\}}\}$,

$$\psi_i^{\{\tilde{\mathbf{R}}_I\}}(\mathbf{r}) = \sum_{\mu=1}^M x_{C^{\mu i}}^{\{\tilde{\mathbf{R}}_I\}} \chi_{\mu}^{\tilde{\mathbf{R}}_I}(\mathbf{r}). \quad (5)$$

For the sake of brevity, we drop the superscripts $\{\tilde{\mathbf{R}}_I\}$ and $\tilde{\mathbf{R}}_I$ in the following. We require the χ -basis to be *locally orthogonal*, i.e., the overlap ${}^\chi S_{\mu\nu} = \langle \chi_\mu^I | \chi_\nu^J \rangle$ of different basis functions centered on the same atom must be zero,

$${}^\chi S_{\mu\nu} = \begin{cases} \langle \chi_\mu^I | \chi_\nu^J \rangle & I \neq J, \forall \mu, \nu \\ \delta_{\mu\nu} & I = J, \forall \mu, \nu \end{cases}, \quad (6)$$

in order to be able to apply the NDDO approximation. This is no general requirement for HF theory, but the introduction of another basis would complicate the notation. We will discuss this requirement in detail in Section 3.1.

The following equations are given for the spin-restricted formulation for the sake of simplicity. The central step underlying a canonical HF calculation in basis-set representation is then the iterative solution of the nonlinear Roothaan–Hall equation,

$${}^\chi \mathbf{F} {}^\chi \mathbf{C} = {}^\chi \mathbf{S} {}^\chi \mathbf{C} \boldsymbol{\epsilon}, \quad (7)$$

for which we first need to calculate the Fock matrix ${}^\chi \mathbf{F} = {}^\chi \mathbf{F}({}^\chi \mathbf{C})$ and the overlap matrix ${}^\chi \mathbf{S}$. We obtain the matrix of basis set expansion coefficients ${}^\chi \mathbf{C}$ and the diagonal matrix of orbital energies $\boldsymbol{\epsilon}$ as the solution of this generalized eigenvalue equation. The left superscript ‘ χ ’ continues to indicate that the calculations are carried out in the χ -basis. It is necessary to explicitly specify the basis because we will operate with different bases throughout this work. The matrix of orbital energies $\boldsymbol{\epsilon}$ is invariant under unitary matrix transformations by which one basis is transformed into another one. Consequently, $\boldsymbol{\epsilon}$ does not carry a superscript.

We can transform Eq. (7) to read

$${}^\chi \mathbf{S}^{-\frac{1}{2}} {}^\chi \mathbf{F} {}^\chi \mathbf{S}^{-\frac{1}{2}} {}^\chi \mathbf{S}^{\frac{1}{2}} {}^\chi \mathbf{C} = {}^\chi \mathbf{S}^{\frac{1}{2}} {}^\chi \mathbf{C} \boldsymbol{\epsilon}, \quad (8)$$

which may be re-written in a simpler way as

$$\boldsymbol{\phi} \mathbf{F} \boldsymbol{\phi} \mathbf{C} = \boldsymbol{\phi} \mathbf{C} \boldsymbol{\epsilon}, \quad (9)$$

where

$$\boldsymbol{\phi} \mathbf{F} = {}^\chi \mathbf{S}^{-\frac{1}{2}} {}^\chi \mathbf{F} {}^\chi \mathbf{S}^{-\frac{1}{2}} \quad (10)$$

and

$$\boldsymbol{\phi} \mathbf{C} = {}^\chi \mathbf{S}^{\frac{1}{2}} {}^\chi \mathbf{C}. \quad (11)$$

This constitutes a transformation of the Fock and coefficient matrices to the Löwdin orthogonalized¹⁰¹ ϕ -basis (indicated by a left superscript ‘ ϕ ’). The

Löwdin orthogonalized basis functions $\phi = \{\phi_\mu\}$ and the locally orthogonal basis functions $\chi = \{\chi_\mu^I\}$ are related through

$$\phi_\nu = \sum_{\mu=1}^M ({}^xS^{-\frac{1}{2}})_{\mu\nu} \chi_\mu^I. \quad (12)$$

Obviously, the basis functions ϕ_μ are not centered on a single atom and therefore do not carry a superscript ‘ I ’. The solution of the Roothaan–Hall equations in either basis (Eqs. (7) and (9)) requires a calculation of one-electron integrals and of ERIs. In this work, we employ Dirac’s bra-ket notation for the one-electron integrals,

$$\langle \chi_\mu^I | h | \chi_\nu^J \rangle = \int \chi_\mu^{*,I}(\mathbf{r}_1) \left[-\frac{1}{2} \nabla_1^2 - \sum_{I=1}^N \frac{Z_I}{|\mathbf{r}_1 - \tilde{\mathbf{R}}_I|} \right] \chi_\nu^J(\mathbf{r}_1) d^3r_1 \quad (13)$$

and the ERIs,

$$\langle \chi_\mu^I \chi_\nu^J | \chi_\lambda^K \chi_\sigma^L \rangle = \int \int \chi_\mu^{*,I}(\mathbf{r}_1) \chi_\nu^J(\mathbf{r}_1) \frac{1}{|\mathbf{r}_1 - \mathbf{r}_2|} \chi_\lambda^{*,K}(\mathbf{r}_2) \chi_\sigma^L(\mathbf{r}_2) d^3r_1 d^3r_2, \quad (14)$$

in the χ -basis. A Fock matrix element in the χ -basis is then evaluated as,

$${}^x F_{\mu\nu} = \langle \chi_\mu^I | h | \chi_\nu^J \rangle + \sum_{\lambda=1}^M \sum_{\sigma=1}^M {}^x P_{\lambda\sigma} \left[\langle \chi_\mu^I \chi_\nu^J | \chi_\lambda^K \chi_\sigma^L \rangle - \frac{1}{2} \langle \chi_\mu^I \chi_\sigma^L | \chi_\lambda^K \chi_\nu^J \rangle \right], \quad (15)$$

where the ERIs are contracted with elements of the density matrix ${}^x \mathbf{P}$. The elements of the density matrix in closed-shell systems are given by

$${}^x P_{\mu\nu} = 2 \sum_{i=1}^{n/2} {}^x C_{\mu i} {}^x C_{\nu i}, \quad (16)$$

(assuming real expansion coefficients). The Fock matrix elements in the ϕ -basis are assembled analogously,

$${}^\phi F_{\mu\nu} = \langle \phi_\mu | h | \phi_\nu \rangle + \sum_{\lambda=1}^M \sum_{\sigma=1}^M {}^\phi P_{\lambda\sigma} \left[\langle \phi_\mu \phi_\nu | \phi_\lambda \phi_\sigma \rangle - \frac{1}{2} \langle \phi_\mu \phi_\sigma | \phi_\lambda \phi_\nu \rangle \right]. \quad (17)$$

Eqs. (7) and (9) must be solved iteratively because the Fock matrix elements depend on the elements of the density matrix which is why the Roothaan–Hall equations are also known as the self-consistent field (SCF) equations.

For the following discussion, it is convenient to divide the Fock matrices into one-electron matrices \mathbf{H} and two-electron matrices \mathbf{G} . The two-electron matrices \mathbf{G} can be further divided into the Coulomb matrices \mathbf{J} and the exchange matrices \mathbf{K} , so that

$${}^x\mathbf{F} = {}^x\mathbf{H} + {}^x\mathbf{G} = {}^x\mathbf{H} + {}^x\mathbf{J} + {}^x\mathbf{K}, \quad (18)$$

and

$$\phi\mathbf{F} = \phi\mathbf{H} + \phi\mathbf{G} = \phi\mathbf{H} + \phi\mathbf{J} + \phi\mathbf{K}. \quad (19)$$

After reaching self consistency, the total electronic HF energy $E_{\text{el}}^{\{\tilde{\mathbf{R}}_I\},\text{HF}} = E_{\text{el}}^{\text{HF}}$ is calculated from the resulting density matrices, Fock matrices, and the nucleus-nucleus repulsion energy,

$$E_{\text{el}}^{\text{HF}} = \frac{1}{2} \sum_{\mu=1}^M \sum_{\nu=1}^M {}^xP_{\nu\mu} ({}^xH_{\mu\nu} + {}^xF_{\mu\nu}) + V, \quad (20)$$

and

$$E_{\text{el}}^{\text{HF}} = \frac{1}{2} \sum_{\mu=1}^M \sum_{\nu=1}^M \phi P_{\nu\mu} (\phi H_{\mu\nu} + \phi F_{\mu\nu}) + V. \quad (21)$$

3 General Considerations for the Formalism of NDDO-SEMO Models

All NDDO-SEMO models describe a way to efficiently approximate the Fock matrix. Formally, the assembly of the Fock matrix in the course of the iterative solution of the SCF equations requires the calculation, repeated processing, and (if possible) storage of M^4 ERIs. Consequently, a lot of effort was put into the development of strategies to reduce the computational cost associated with this step.¹⁰⁰

3.1 Neglect of Diatomic Differential Overlap

One of these strategies is the NDDO approximation⁸ which drastically reduces the number of ERIs that must be calculated explicitly to assemble $\phi\mathbf{G}$. The NDDO approximation,

$$\langle \phi_\mu \phi_\nu | \phi_\lambda \phi_\sigma \rangle \approx \delta_{IJ} \delta_{KL} \langle \chi_\mu^I \chi_\nu^J | \chi_\lambda^K \chi_\sigma^L \rangle, \quad (22)$$

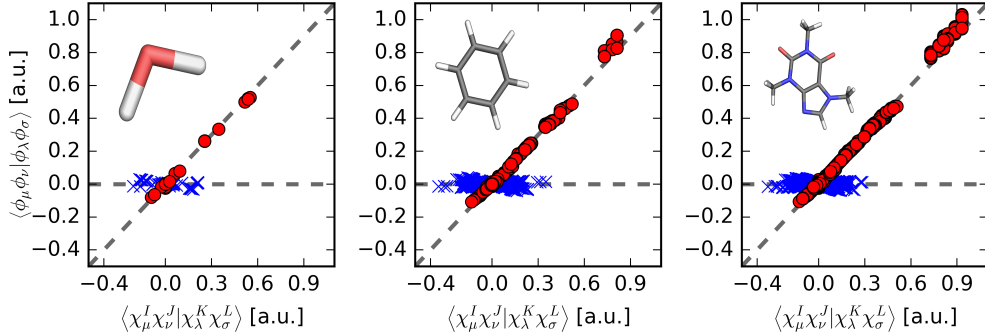


Figure 2: Comparison of the analytical values of $\langle \phi_\mu \phi_\nu | \phi_\lambda \phi_\sigma \rangle$ and $\langle \chi_\mu^I \chi_\nu^J | \chi_\lambda^K \chi_\sigma^L \rangle$ in a.u. for water (left), benzene (middle), and caffeine (right) in the OM2-3G basis set.^{58,60,117} The gray dashed lines indicate $\langle \phi_\mu \phi_\nu | \phi_\lambda \phi_\sigma \rangle = 0.0$ and $\langle \phi_\mu \phi_\nu | \phi_\lambda \phi_\sigma \rangle = \langle \chi_\mu^I \chi_\nu^J | \chi_\lambda^K \chi_\sigma^L \rangle$. Red circles encode ERIs where $I = J$ and $K = L$ in the χ -basis, and blue crosses encode ERIs where $I \neq J$ or $K \neq L$ in the χ -basis.

specifies how ERIs in the ϕ -basis may be approximated based on the values of the respective ERIs in the χ -basis. It is not immediately obvious why Eq. (22) should hold true, especially in view of Eq. (12), but numerical data suggest that there is some merit to the NDDO approximation.^{102–116} We additionally illustrate the NDDO approximation in Figure 2 for three examples. Eq. (22) asserts that $\langle \phi_\mu \phi_\nu | \phi_\lambda \phi_\sigma \rangle$ is negligibly small if $I \neq J$ or $K \neq L$, i.e., if χ_μ^I and χ_ν^J are centered on different atoms or if χ_λ^K and χ_σ^L are centered on different atoms. As a consequence, the formal scaling of the ERI evaluation step is reduced from $\mathcal{O}(M^4)$ to $\mathcal{O}(M^2)$. We see that this statement holds true for the three examples in Figure 2 because all blue crosses are located close to the horizontal dashed lines. Furthermore, Eq. (22) states that $\langle \phi_\mu \phi_\nu | \phi_\lambda \phi_\sigma \rangle$ is approximately equal to $\langle \chi_\mu^I \chi_\nu^J | \chi_\lambda^K \chi_\sigma^L \rangle$ when $I = J$ and $K = L$, e.g., the value of $\langle \phi_1 \phi_1 | \phi_1 \phi_1 \rangle$ is approximately equal to the value of $\langle \chi_1^I \chi_1^I | \chi_1^K \chi_1^K \rangle$. We see that this part of the NDDO approximation also holds true for the three examples that we considered for calculations in Figure 2 because the red circles are located close to the diagonal dashed lines.

Evidently, the NDDO approximation *emulates* a basis transformation for the ERIs, and hence, also for the two-electron matrix, i.e.,

$${}^\chi \mathbf{G}^{\text{NDDO}} \approx {}^\phi \mathbf{G} \quad (23)$$

and

$${}^\chi \mathbf{G}^{\text{NDDO}} \not\approx {}^\chi \mathbf{G}. \quad (24)$$

This means that the matrix elements ${}^\phi G_{\mu\nu}$ can be approximately determined based on ERIs in the χ -basis by

$$\begin{aligned} {}^\phi G_{\mu\nu} &\approx \chi G_{\mu\nu}^{\text{NDDO}} \\ &= \sum_{\lambda=1}^M \sum_{\sigma=1}^M \chi P_{\lambda\sigma}^{\text{NDDO}} \left(\delta_{IJ} \delta_{KL} \langle \chi_\mu^I \chi_\nu^J | \chi_\lambda^K \chi_\sigma^L \rangle - \delta_{IK} \delta_{JL} \frac{1}{2} \langle \chi_\mu^I \chi_\lambda^K | \chi_\nu^J \chi_\sigma^L \rangle \right). \end{aligned} \quad (25)$$

The NDDO approximation may also be formulated in the ϕ -basis,

$$\langle \phi_\mu \phi_\nu | \phi_\lambda \phi_\sigma \rangle \approx \delta_{IJ} \delta_{KL} \langle \phi_\mu \phi_\nu | \phi_\lambda \phi_\sigma \rangle, \quad (26)$$

which is, however, not very illuminating in the context of NDDO-SEMO models as it is not obvious what the meaning of I , J , K , and L in Eq. (26) actually is for the basis functions ϕ that are not centered on single atoms (see Eq. (6)). Additionally, it is important to note that all NDDO-SEMO models calculate the ERIs in the χ -basis and do not carry out an explicit basis transformation to the ϕ -basis. In order to understand how NDDO-SEMO models work, we need to understand how this implicit basis transformation occurs, i.e., Eq. (22).

We emphasize that the NDDO statement is not that the ERIs in the χ -basis are close to zero when $I \neq J$ or $K \neq L$. *Only* their corresponding ERIs in the ϕ -basis are approximately zero. Figure 2 also illustrates this statement as several ERIs for which $I \neq J$ or $K \neq L$ are as large as 0.3 a.u. in the χ -basis. It is therefore misleading to formulate the NDDO approximation in the χ -basis,

$$\langle \chi_\mu^I \chi_\nu^J | \chi_\lambda^K \chi_\sigma^L \rangle \approx \delta_{IJ} \delta_{KL} \langle \chi_\mu^I \chi_\nu^J | \chi_\lambda^K \chi_\sigma^L \rangle. \quad (27)$$

The NDDO approximation leads to uncontrollable errors for the ERIs in the ϕ -basis^{102–116} which propagate to all quantities based on these erroneous ERIs (most importantly to electronic energies).^{104,110–114,116,118–123} Most likely due to the uncontrollable errors and the lack of systematic improvability, the NDDO approximation has never found any use in *ab initio* theories.

In NDDO-SEMO models, the NDDO approximation is coupled to multiple other approximations, not least to correct for the errors introduced by the NDDO approximation itself.^{8,50,58,59,72} These additional approximations generally concern the calculation of the nonzero ERIs in the χ -basis, the elements of the one-electron matrix in the ϕ -basis, and V . Hence, we must specify for each NDDO-SEMO model which parametrized expressions were applied to evaluate these three quantities. Throughout this work, we mostly adhered to the original parameter abbreviations. We present a comparison

of the parameter abbreviations which we chose to the ones in the original literature in Tables 2 and 3 in Section 10.2.

3.2 Restriction to an Effective Valence Shell

NDDO-SEMO models further reduce the computational effort by restricting the number of explicitly considered electrons. When restricting the number of explicitly considered electrons, it is necessary to specify for each atom I which of its n_I electrons are considered valence (' v ') electrons ($n_{v,I}$) and which ones are considered core (' c ') electrons ($n_{c,I} = n_I - n_{v,I}$). Accordingly, each atomic core then exhibits a core charge Q_I ,

$$Q_I = Z_I - n_{c,I}. \quad (28)$$

Note that a rigorous distinction between core charge Q_I and nuclear charge Z_I is crucial for NDDO-SEMO models. Both quantities are required in parametric expressions in the formalism of some NDDO-SEMO models (see, e.g., Eq. (62) in Section 4.5.3). No rigorous method exists to justify a specific choice for $n_v = \sum_I n_{v,I}$ and $n_c = \sum_I n_{c,I}$. Within the NDDO-SEMO models, $n_{v,I}$ is restricted drastically so that $n_{v,I} = 1$, $n_{v,I} = 4$, $n_{v,I} = 5$, and $n_{v,I} = 6$ for hydrogen, carbon, nitrogen, and oxygen atoms, respectively.^{50,56,57,60} In fact, $n_{v,I} \leq 12$ for all elements, and in principle, no more than two s electrons, six p electrons, and ten d electrons could be considered per atom within the current formalism of the popular NDDO-SEMO models.^{50,56,57,60} We specify $n_{v,I}$ for all elements up to $Z_I = 83$ in Table 1 in Section 10.2. We note that usually it is considered better to avoid too large $n_{c,I}$ in *ab initio* calculations (see, e.g., Ref. 124 in which it was shown that a choice of $n_{v,I} = 4$ for lead and for titanium (as in PM6 and PM7) is not adequate to yield accurate electronic energies).

In *ab initio* theories, one may approximate the effects of the core electrons by an effective core potential (ECP),^{124,125} so that for n_v valence electrons, the full Hamiltonian (Eq. (2)) is replaced by an approximate valence-only Hamiltonian $\mathcal{H}_{\text{el},v}$,

$$\begin{aligned} \mathcal{H}_{\text{el},v} = & \sum_{i=1}^{n_v} \left(-\frac{1}{2} \nabla_i^2 + \sum_I^N \left(-\frac{Q_I}{|\mathbf{r}_i - \tilde{\mathbf{R}}_I|} + \text{ECP}_I \right) \right) \\ & + \sum_{i=1}^{n_v} \sum_{j>i}^{n_v} \frac{1}{|\mathbf{r}_i - \mathbf{r}_j|} + \sum_{I=1}^N \sum_{J>I}^N \frac{Q_I Q_J}{|\tilde{\mathbf{R}}_I - \tilde{\mathbf{R}}_J|}, \end{aligned} \quad (29)$$

or in short notation,

$$\mathcal{H}_{\text{el},v} = \sum_{i=1}^{n_v} h_{v,i} + \sum_{i=1}^{n_v} \sum_{j>i}^{n_v} g(i,j) + V_v. \quad (30)$$

The core-core repulsion energy is denoted as V_v and the effective one-electron operator is denoted as $h_{v,i}$. The effective one-electron operator $h_{v,i}$ incorporates an effective core potential describing the interaction with the core electrons of atom I , ECP_I . We will not specify the different functional forms for the ECPs which are applied in *ab initio* theories here (see, e.g., Refs. 124, 125 for recent reviews) because they differ strongly from the ones which are applied in NDDO-SEMO models today.^{126–129} We will discuss the form of ECP_I for each individual NDDO-SEMO model below.

3.3 Restriction of the Basis Set Expansion

Another way of reducing the computational effort is the restriction of the number of basis functions M in Eq. (5). Generally, the number of basis function which are activated for an atom I , M_I , is less than or equal to nine. For each atom, at most, one s -type, three p -type, and five d -type basis functions may be considered, i.e., the number of basis functions activated for a molecule is

$$M = \sum_{I=1}^N M_I \leq 9N. \quad (31)$$

All NDDO-SEMO models apply only one s -type basis function for hydrogen. For carbon, nitrogen, and oxygen, the NDDO-SEMO models activate one s -type basis function and three p -type basis function. The basis functions which are considered for an atom of a certain element type are given in Table 1 in Section 10.2.

The application of such a minimal valence-shell basis set has the practical advantage that the basis functions are inherently locally orthogonal (Eq. (6)), i.e., the NDDO approximation is straightforwardly applicable.^{110–114, 116, 121, 122} A minimal basis set is, however, generally unsuitable for the description of atoms in molecules. Conceptually, molecules are characterized by interacting atoms which polarize each other through additional external fields exerted by electrons and nuclei of the other atoms that distort the spherical symmetry of an atom. The description of the polarization of the electron density requires basis functions with a higher angular momentum. Consequently, it is common knowledge that calculations with a minimal basis sets do not yield reliable relative energies, force constants, electric dipole moments, static

dipole polarizabilities, and other properties.^{130–134} More specifically, it would, for example, not be possible to obtain satisfactory results for polarizabilities or for the description of non-covalent interactions at the full-configuration-interaction (FCI) limit when applying a minimal basis set.¹⁰⁰ A minimal basis set may, however, be sufficient to predict reasonable molecular equilibrium structures^{130–132,135} which led to a re-consideration of minimal-basis-set HF as a quick preliminary structure optimization method in recent years.^{136,137} Hence, the application of minimal basis sets may be adequate if the area of application of the NDDO-SEMO model is restricted accordingly.

4 The Modified Neglect of Diatomic Overlap (MNDO) Model

The MNDO model is the first successful SEMO model which is based on the NDDO approximation.^{49,50,138} The MNDO model activates one s - and three p -type basis functions (χ -basis) for carbon, nitrogen, oxygen, and fluorine.⁵⁰ Only one s -type basis function is retained for hydrogen.⁵⁰ The MNDO model was later on extended to a larger part of the periodic table (see, e.g, Ref. 139 and also Section 4.5.1). The Slater-type basis functions incorporate a parameter, the exponent ζ^{Z_I} , which depends on the element type (here indicated by the superscript atomic number Z_I) of the atom I on which the basis function χ is centered. The same ζ^{Z_I} is applied for s - and p -type basis functions, i.e., $\zeta_s^{Z_I} = \zeta_p^{Z_I}$.⁵⁰ We explicitly indicate for each parameter its dependencies (e.g., Z_I of the atom I on which a χ -basis function is centered or the orbital-type of the basis function χ , i.e., s , p , or more generally, the angular momentum of the μ -th χ -basis function $l(\mu)$).

4.1 Parametrization of One-Center ERIs

At most, one s -type basis function and three p -type basis functions are centered on one atom. Altogether, six unique nonzero one-center ERIs $\langle \chi_\mu^I \chi_\nu^I | \chi_\lambda^I \chi_\sigma^I \rangle$ may arise. Five of the six ERIs are substituted for element- and orbital-type-dependent parameters,

$$\gamma_{ss}^{Z_I} = \langle s^I s^I | s^I s^I \rangle, \quad (32)$$

$$\gamma_{pp}^{Z_I} = \langle p^I p^I | p^I p^I \rangle, \quad (33)$$

$$\gamma_{sp}^{Z_I} = \langle s^I s^I | p^I p^I \rangle, \quad (34)$$

$$\gamma_{pp'}^{Z_I} = \langle p^I p^I | p^I p^I \rangle, \quad (35)$$

and

$$\tilde{\gamma}_{sp}^{Z_I} = \langle s^I p^I | s^I p^I \rangle, \quad (36)$$

where we only indicate the orbital type (s or p) of the basis functions when specifying the ERIs. The magnetic quantum numbers do not need to be explicitly specified because otherwise rotational invariance could not be guaranteed.¹⁴⁰ Hence, it is only necessary to indicate for the p -type basis functions whether the magnetic quantum number is the same (no prime, e.g., $\langle p_x^I p_x^I | p_x^I p_x^I \rangle = \langle p^I p^I | p^I p^I \rangle$) or different (prime, e.g., $\langle p_x^I p_x^I | p_y^I p_y^I \rangle = \langle p^I p^I | p'^I p'^I \rangle$). The sixth one-center ERI is calculated from $\gamma_{pp}^{Z_I}$ and $\gamma_{pp'}^{Z_I}$,

$$\langle p^I p'^I | p^I p'^I \rangle = \frac{1}{2} (\gamma_{pp}^{Z_I} - \gamma_{pp'}^{Z_I}). \quad (37)$$

If $\gamma_{pp}^{Z_I} < \gamma_{pp'}^{Z_I}$, $\langle p^I p'^I | p^I p'^I \rangle$ will be negative which leads to issues in the determination of the two-center ERIs (see also Section 10.3). In the original MNDO model, $\langle p^I p'^I | p^I p'^I \rangle$ is always positive so that no issues arise, but $\gamma_{pp}^{Z_I}$ may be smaller than $\gamma_{pp'}^{Z_I}$ for extensions of the MNDO model.^{56,57,139} All other one-center ERIs in the minimal valence-shell basis (e.g., $\langle s^I p^I | s^I s^I \rangle$, $\langle s^I p^I | p^I p^I \rangle$, $\langle s^I p^I | p^I p'^I \rangle$, or $\langle p^I p^I | p^I p'^I \rangle$) are exactly zero.

4.2 Approximating the Two-Center ERIs

The two-center ERIs $\langle \chi_\mu^I \chi_\nu^I | \chi_\lambda^J \chi_\sigma^J \rangle$, $I \neq J$, can be interpreted as the electrostatic interaction between a charge distribution $\chi_\mu^I \chi_\nu^I$ centered on atom I and a charge distribution $\chi_\lambda^J \chi_\sigma^J$ centered on atom J . Each possible charge distribution $\chi_\mu^I \chi_\nu^I$ in the s , p minimal valence-shell basis is approximately represented as a truncated classical multipole expansion^{49,50,53,54} (see Ref. 49 or Section 10.4 for explicit formulae). Dewar and Thiel decided to specify four individual arrangements of discrete point charges for this purpose; a monopole q , a dipole $\mu_{x,y,z}$, a linear quadrupole $Q_{xx,yy,zz}$, and a square quadrupole $Q_{xy,xz,yz}$ (see Figure 3). The distances D_μ and D_Q between the point charges in each configuration were chosen such that the multipole moment of each point charge configuration approximated the one of the corresponding charge distribution which is ensured by calculating D_μ and D_Q based on ζ^{Z_I} (see Ref. 49 or Section 10.4). As soon as the positions of the point charges in space have been specified (by defining D_μ and D_Q and the local arrangements around the atomic nuclei), one can readily calculate the electrostatic potential energy as a sum over all possible electrostatic interactions of the point charges. The approximation of a two-center ERI as the electrostatic interaction of discrete point charges will, however, break down

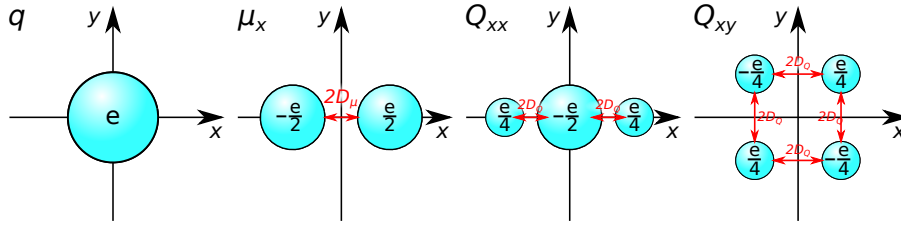


Figure 3: Illustration of the configuration of point charges (blue spheres) for the monopole q , the dipole μ_x , the linear quadrupole Q_{xx} , and the square quadrupole Q_{xy} . The charge for each point charge is given in units of the elementary charge. The point charges in μ_x are $2D_\mu$ apart, the ones in Q_{xx} $2D_Q$, and the ones in Q_{xy} $2D_Q$.

when the distance between the atomic nuclei,

$$\tilde{R}_{IJ} = |\tilde{\mathbf{R}}_I - \tilde{\mathbf{R}}_J|, \quad (38)$$

becomes small. We illustrate this at the example of the two-center ERI $\langle s^I s^I | s^J s^J \rangle$ which is approximated by the electrostatic interaction of a point charge located on I and one located on J . If $\tilde{R}_{IJ} = 0$, a singularity would arise for the electrostatic interaction between the two point charges. This would not be the case if we considered the electrostatic interaction of a charge distribution centered on I and one centered on J . As a consequence, the expression to calculate the electrostatic interaction between point charges is modified in an empirical manner in such a way that it yields the *one-center* ERIs (Eqs. (32)–(37)) in the limit $\tilde{R}_{IJ} = 0$, (‘Klopman formula’, Eq. (14) in Ref. 141),

$$\langle s^I s^I | s^J s^J \rangle \approx [s^I s^I | s^J s^J] = \left[\tilde{R}_{IJ}^2 + \left(\frac{1}{2\gamma_{ss}^{Z_I}} + \frac{1}{2\gamma_{ss}^{Z_J}} \right)^2 \right]^{-\frac{1}{2}}. \quad (39)$$

In the following, we denote an ERI calculated in the Klopman approximation by square brackets to easily distinguish them from analytically calculated ERIs (denoted in angle brackets). From Eq. (39) and Figure 4, we see that for large \tilde{R}_{IJ} (and constant $\gamma_{ss}^{Z_I}$ and $\gamma_{ss}^{Z_J}$), the term approaches the regular Coulomb interaction of two elementary point charges, $[s^I s^I | s^J s^J] \approx 1/\tilde{R}_{IJ}$. In the limit $\tilde{R}_{IJ} = 0$ (where $\gamma_{ss}^{Z_I} = \gamma_{ss}^{Z_J}$), the expression reduces to $[s^I s^I | s^I s^I] = \gamma_{ss}^{Z_I}$. The value of $\gamma_{ss}^{Z_I}$ determines how closely the approximate ERI follows the analytical one (see also Figure 4). Usually $\gamma_{ss}^{Z_I}$ is chosen such that the semiempirical two-center ERIs are smaller than the analytical values. E.g., Pariser and Parr,⁵ Dewar and Klopman,¹⁴² and Voigt¹⁴³ argued

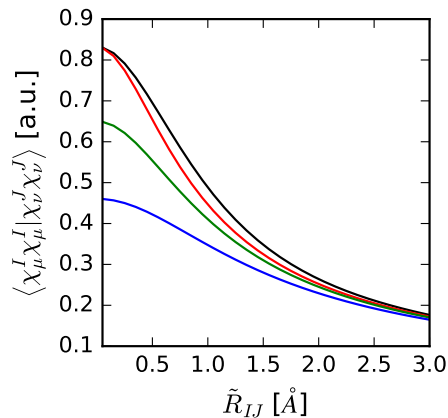


Figure 4: Dependence of $\langle \chi_\mu^I \chi_\mu^I | \chi_\nu^J \chi_\nu^J \rangle$ (black line) and $[\chi_\mu^I \chi_\mu^I | \chi_\nu^J \chi_\nu^J]$ on $\tilde{R}_{IJ} = |\tilde{\mathbf{R}}_{\text{H}_1} - \tilde{\mathbf{R}}_{\text{H}_2}|$ in an H_2 molecule described by an MNDO-3G basis. We applied a Gaussian-type basis set (denoted MNDO-3G) to calculate the analytical ERI values instead of the Slater-type basis set inherent to the MNDO model. We generated the MNDO-3G basis based on ζ^{Z_I} .⁵⁰ We chose different values for γ_{ss}^1 in Eq. (39): $\gamma_{ss}^1=0.83$ a.u. (analytical one-center ERI, red line), $\gamma_{ss}^1=0.65$ a.u. (green line), and $\gamma_{ss}^1=0.45$ a.u. (MNDO value,¹⁴⁴ blue line).

that in this way dynamic electron correlation effects can be emulated. We will analyze this claim in detail in Section 7.

For the other two-center ERIs, similar formulae as the one in Eq. (39) can be derived which yield the respective one-center ERI in the limit $\tilde{R}_{IJ} = 0$ (see Ref. 49 or Section 10.4). For the calculation of two-center ERIs, which involve at least one p -type basis function, a local coordinate system is adopted.⁴⁹ This local coordinate system is defined based on $\tilde{\mathbf{R}}_I$ and $\tilde{\mathbf{R}}_J$ (see Figure 5 and Section 10.6). The results obtained in this local coordinate system have to be transformed to yield the ERIs in the global coordinate system. The necessary transformations can be formulated in terms of rotation matrices⁸⁶ which are outlined in Section 10.6.

Issues with the presented approach were detected years after the introduction of the MNDO model. It was remarked^{53,145} that rotational invariance was not satisfied for the ERIs $[p_x^I p_y^I | p_x^J p_y^J]$ due to the chosen point charge configurations. It was then suggested⁵³ to impose rotational invariance by setting

$$[p_x^I p_y^I | p_x^J p_y^J] = 0.5 \left([p_x^I p_x^I | p_x^J p_x^J] - [p_x^I p_x^I | p_y^J p_y^J] \right). \quad (40)$$

Moreover, the Klopman approximation causes distinct errors in the ERIs^{146–148}

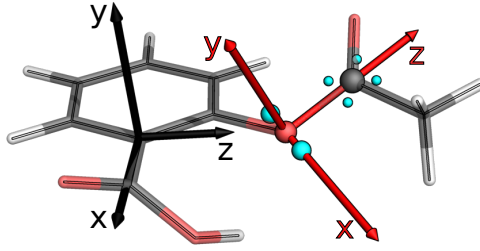


Figure 5: Illustration of the difference of the local (red axes) and global (black axes) coordinate systems when calculating $\langle s^I p_x^I | p_x^J p_z^J \rangle$ in aspirin. The positions of the point charges with which the charge distributions $s^I p_x^I$ and $p_x^J p_z^J$ are approximated are indicated by blue spheres.

which culminates in an infinite error in periodic electronic structure calculations.¹⁴⁹ To be able to apply the MNDO in periodic electronic structure calculations, an additional scaling factor has to be introduced to yield the exact limit for large \tilde{R}_{IJ} .^{149,150}

4.3 Assembling the Symmetrically Orthogonalized One-Electron Matrix

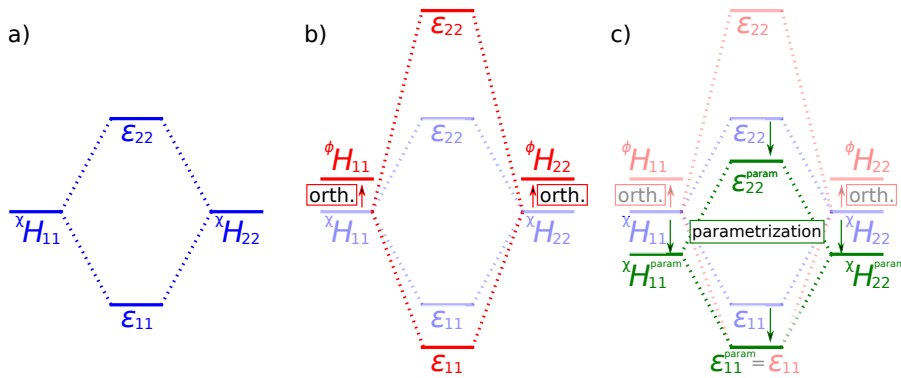


Figure 6: Illustration of the effect of parametrization when orthogonalization effects are not considered at the example of dihydrogen ($\chi = \{\chi_1^{H_1}, \chi_2^{H_2}\}$). a) Values of ϵ_{11} and ϵ_{22} when solving the eigenvalue equation ${}^{\chi}\mathbf{H} {}^{\chi}\mathbf{C} = {}^{\chi}\mathbf{C} \epsilon$ without considering ${}^{\chi}\mathbf{S}$. b) Value of ϵ_{11} and ϵ_{22} obtained when solving the eigenvalue equation ${}^{\phi}\mathbf{H} {}^{\phi}\mathbf{C} = {}^{\phi}\mathbf{C} \epsilon$. The eigenvalues are split asymmetrically with respect to the ${}^{\chi}H_{11} = {}^{\chi}H_{22}$ reference. c) Effect of parametrization to reproduce the lowest energy eigenvalue when solving the equation ${}^{\chi}\mathbf{H}^{\text{param}} {}^{\chi}\mathbf{C} = {}^{\chi}\mathbf{C} \epsilon$.

The MNDO model does not provide an explicit way to account for the change from the χ -basis to the ϕ -basis for the one-electron matrix \mathbf{H} .⁵⁰ It is assumed that the elements of ${}^\phi\mathbf{H}$ are approximately equal to ${}^\chi\mathbf{H}$ when an appropriate parametrization is chosen,⁷²

$${}^\phi\mathbf{H} \approx {}^\chi\mathbf{H}^{\text{param}}. \quad (41)$$

An example discussed in Refs. 58,59,151,152 explains why this is not generally possible (see Figure 6). We may consider the dihydrogen molecule (H_1-H_2) in a minimal basis set consisting of two $1s$ orbitals $\boldsymbol{\chi} = \{\chi_1^{H_1}, \chi_2^{H_2}\}$. For the moment, we neglect electron-electron interactions, i.e., we solve the eigenvalue equations,

$${}^\phi\mathbf{H} {}^\phi\mathbf{C} = {}^\phi\mathbf{C}\boldsymbol{\epsilon}, \quad (42)$$

in the ϕ -basis, or analogously in the χ -basis,

$${}^\chi\mathbf{H} {}^\chi\mathbf{C} = {}^\chi\mathbf{S} {}^\chi\mathbf{C}\boldsymbol{\epsilon}. \quad (43)$$

We now want to know whether it is possible to obtain the same $\boldsymbol{\epsilon} = \boldsymbol{\epsilon}^{\text{param}}$ when solving an eigenvalue equation of the type

$${}^\chi\mathbf{H}^{\text{param}} {}^\chi\mathbf{C} = {}^\chi\mathbf{C}\boldsymbol{\epsilon}^{\text{param}}, \quad (44)$$

where we neglect ${}^\chi\mathbf{S}$. When solving Eqs. (42) and (43), we see that $|{}^\phi H_{11} - \epsilon_{11}|$ and $|{}^\phi H_{11} - \epsilon_{22}|$ are equally large while $|{}^\chi H_{11} - \epsilon_{11}|$ and $|{}^\chi H_{11} - \epsilon_{22}|$ differ. Independently of the parametrization, it is not possible to obtain different $|{}^\chi H_{11}^{\text{param}} - \epsilon_{11}^{\text{param}}|$ and $|{}^\chi H_{11}^{\text{param}} - \epsilon_{22}^{\text{param}}|$ when solving Eq. (44) because ${}^\chi\mathbf{S}$ is neglected in Eq. (44) (see Figure 6).

Apart from this example, it is evident that orthogonalization effects,

$${}^\phi H_{\mu\nu} = \sum_{\lambda=1}^M \sum_{\sigma=1}^M \left({}^\chi S^{-\frac{1}{2}} \right)_{\mu\lambda} {}^\chi H_{\lambda\sigma} \left({}^\chi S^{-\frac{1}{2}} \right)_{\sigma\nu}, \quad (45)$$

cannot be captured by introducing element-dependent parameters which was, for instance, pointed out in Refs. 121,153–155. The matrix element ${}^\phi H_{\mu\nu}$ depends on contributions from all matrix elements of ${}^\chi\mathbf{H}$. Consequently, the parametrization would need to depend on the chemical environment of each atom in some manner. The MNDO parameters, however, are only element-dependent and do not depend on the chemical environment. Despite this inherent limitation, MNDO has been a very successful model and we will continue to discuss how the contributions to ${}^\phi\mathbf{H}^{\text{MNDO}}$ are evaluated in the following Sections (Sections 4.3.1 and 4.3.2). We assume that the inclusion of

empirical parameters accounts for orthogonalization effects in some average manner, and hence, retain the superscript ϕ for $\phi\mathbf{H}^{\text{MNDO}}$.

The parametric expressions applied for the evaluation of the matrix elements $\phi H_{\mu\nu}^{\text{MNDO}}$ differ depending on the number of atoms on which the corresponding basis functions χ_μ^I and χ_ν^J are centered: (i) χ_μ^I and χ_ν^I are centered on a single atom I (one-center one-electron matrix elements) and (ii) χ_μ^I and χ_ν^J are centered on different atomic nuclei $I \neq J$ (two-center one-electron matrix elements).

4.3.1 One-Center One-Electron Matrix Elements

In the case that χ_μ^I and χ_ν^I are centered on the same atom, the analytical matrix elements in the χ -basis are given by

$${}^xH_{\mu\nu} = \left\langle \chi_\mu^I \left| -\frac{1}{2} \nabla^2 \right| \chi_\nu^I \right\rangle - \left\langle \chi_\mu^I \left| \frac{Q_I}{|\mathbf{r}_i - \tilde{\mathbf{R}}_I|} \right| \chi_\nu^I \right\rangle - \sum_{\substack{J=1 \\ J \neq I}}^N \left\langle \chi_\mu^I \left| \frac{Q_J}{|\mathbf{r}_i - \tilde{\mathbf{R}}_J|} \right| \chi_\nu^I \right\rangle. \quad (46)$$

These first two terms in the right hand side of Eq. (46) only refer to the atom I ('one-center' one-electron contributions to ${}^xH_{\mu\nu}$). The remaining 'two-center' one-electron contributions to ${}^xH_{\mu\nu}$ describe the electrostatic attraction between the charge distribution $\chi_\mu^I \chi_\nu^I$ and the atomic cores $J \neq I$.

In view of Eq. (46), it is apparent why Dewar and Thiel suggested⁵⁰ to calculate $\phi H_{\mu\nu}^{\text{MNDO}}$ by means of

$$\phi H_{\mu\nu}^{\text{MNDO}} = U_{l(\mu)l(\nu)}^{Z_I} - \sum_{\substack{J=1 \\ J \neq I}}^N Q^J [\chi_\mu^I \chi_\nu^I | s^J s^J]. \quad (47)$$

The element- and orbital-type-dependent parameter $U_{l(\mu)l(\nu)}^{Z_I}$ comprises all one-center one-electron contributions in Eq. (46). The one-center one-electron terms are exactly zero in a locally orthogonal basis when $\mu \neq \nu$,

$$U_{l(\mu)l(\nu)}^{Z_I} = \begin{cases} \text{const.} & \mu = \nu \\ 0 & \mu \neq \nu \end{cases}. \quad (48)$$

The parameter $U_{l(\mu)l(\nu)}^{Z_I}$ may not depend on the magnetic quantum number to ensure rotational invariance,^{8,140} and hence, at most two parameters, $U_{ss}^{Z_I}$ and $U_{pp}^{Z_I}$, arise per element. Within a given χ -basis, $U_{ss}^{Z_I}$ and $U_{pp}^{Z_I}$ can be calculated exactly and are transferable between molecules. The MNDO model,

however, attempts to approximate the matrix element in the ϕ -basis,

$$\phi H_{\mu\nu} = \left\langle \phi_\mu \left| -\frac{1}{2} \nabla^2 \right| \phi_\nu \right\rangle - \left\langle \phi_\mu \left| \frac{Q_I}{|\mathbf{r}_i - \tilde{\mathbf{R}}_I|} \right| \phi_\nu \right\rangle - \sum_{\substack{J=1 \\ J \neq I}}^N \left\langle \phi_\mu \left| \frac{Q_J}{|\mathbf{r}_i - \tilde{\mathbf{R}}_J|} \right| \phi_\nu \right\rangle. \quad (49)$$

In the ϕ -basis, the first two terms obviously depend on the chemical environment of the atom I which is neglected by introducing constant $U_{ss}^{Z_I}$ and $U_{pp}^{Z_I}$. It is assumed that the calibration of $U_{ss}^{Z_I}$ and $U_{pp}^{Z_I}$ will implicitly lead to a modeling of average orthogonalization effects and will also absorb the effects from the core electrons.⁵⁹

A two-center contribution to Eq. (46) is approximated by the negative electrostatic interaction energy of $\chi_\mu^I \chi_\nu^I$ with a model charge distributions $s^J s^J$, $J \neq I$ scaled with Q_J in Eq. (47). Pople and Segal proposed¹⁵⁶ to apply this so-called Goeppert-Mayer-Sklar approximation (named for its relation to an equation proposed in Ref. 157) after observing that the application of the analytical expression in Eq. (46) led to far too short bond lengths for several diatomic molecules.¹⁵⁶ A decade after their proposal, Coffey analyzed the Goeppert-Mayer-Sklar approximation in more detail and concluded that a fortunate error cancellation occurs, so that¹⁵⁸

$$\begin{aligned} \left\langle \phi_\mu \left| \frac{Q_J}{|\mathbf{r}_i - \tilde{\mathbf{R}}_J|} \right| \phi_\nu \right\rangle &= \left\langle \chi_\mu^I \left| \frac{Q_J}{|\mathbf{r}_i - \tilde{\mathbf{R}}_J|} \right| \chi_\nu^I \right\rangle \\ &\quad - Q^J \langle \chi_\mu^I \chi_\nu^I | s^J s^J \rangle + Q^J \langle \chi_\mu^I \chi_\nu^I | s^J s^J \rangle \\ &\quad + \left(\left\langle \phi_\mu \left| \frac{Q_J}{|\mathbf{r}_i - \tilde{\mathbf{R}}_J|} \right| \phi_\nu \right\rangle - \left\langle \chi_\mu^I \left| \frac{Q_J}{|\mathbf{r}_i - \tilde{\mathbf{R}}_J|} \right| \chi_\nu^I \right\rangle \right) \\ &\approx Q^J \langle \chi_\mu^I \chi_\nu^I | s^J s^J \rangle. \end{aligned} \quad (50)$$

The first two terms in Eq. (50) are the so-called ‘penetration integrals’,¹⁵⁷

$$\langle \chi_\mu^I \chi_\nu^I, J \rangle \approx \left\langle \chi_\mu^I \left| \frac{Q^J}{|\mathbf{r}_i - \tilde{\mathbf{R}}_J|} \right| \chi_\nu^I \right\rangle - Q^J \langle \chi_\mu^I \chi_\nu^I | s^J s^J \rangle, \quad (51)$$

approximately cancel the orthogonalization effects, $\left\langle \phi_\mu \left| \frac{Q_J}{|\mathbf{r}_i - \tilde{\mathbf{R}}_J|} \right| \phi_\nu \right\rangle - \left\langle \chi_\mu^I \left| \frac{Q_J}{|\mathbf{r}_i - \tilde{\mathbf{R}}_J|} \right| \chi_\nu^I \right\rangle$ which are required to transform ${}^x H_{\mu\nu}$ from the χ - into the ϕ -basis (see Figure 1 in Ref. 158). Hence, the Goeppert-Mayer-Sklar approximation entails an implicit basis set transformation from the χ - to the ϕ -basis. The orthogonalization effects, which Coffey considered,¹⁵⁸ also included orthogonalization of the core orbitals to the valence orbitals. Hence,

the application of Eq. (50) may also be interpreted as the emulation of the application of an approximate effective core potential. Unfortunately, Coffey’s analysis was restricted to the C_2 molecule and included several additional approximations (such as an averaging of one- and two-electron integrals).¹⁵⁸ It is not evident whether (and appears improbable^{155,159} that) Coffey’s analysis can easily be generalized to arbitrary polyatomic molecules. The success of the MNDO model indicates, however, that — at least in the context of all other invoked approximations — the Goeppert-Mayer–Sklar approximation is a satisfactory one.

4.3.2 Two-Center One-Electron Matrix Elements

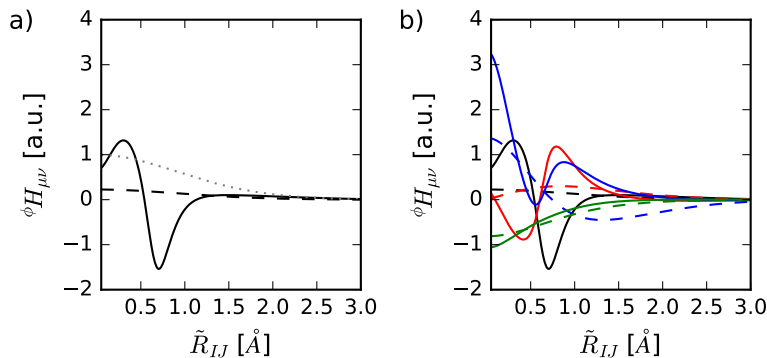


Figure 7: Dependence of $\phi H_{\mu\nu}$ (solid lines) and $\phi H_{\mu\nu}^{\text{MNDO}}$ (dashed lines) on the distance \tilde{R}_{IJ} in a C_2 molecule described in an MNDO-3G basis ($\chi = \{\chi_1^{C_1}, \chi_2^{C_1}, \chi_3^{C_1}, \chi_4^{C_1}, \chi_5^{C_2}, \chi_6^{C_2}, \chi_7^{C_2}, \chi_8^{C_2}\}$ where the first and fifth basis functions are $2s$, the second and sixth are $2p_x$, the third and seventh are $2p_y$, and the fourth and eighth are $2p_z$ basis functions). a) $\phi H_{15}^{\text{MNDO}}$ with the best-fit parameter $\beta_s^6 = 0.1$ a.u. (black line) and χS_{15} (gray dotted line). b) $\phi H_{15}^{\text{MNDO}}$ with $\beta_s^6 = 0.1$ a.u. (black lines), $\phi H_{18}^{\text{MNDO}}$ with $\beta_s^6 = \beta_p^6 = -0.3$ a.u. (red lines), $\phi H_{48}^{\text{MNDO}}$ with $\beta_s^6 = 1.3$ a.u. (blue lines), and $\phi H_{26}^{\text{MNDO}}$ with $\beta_s^6 = -0.2$ a.u. (green lines).

In the case that χ_μ^I and χ_ν^J are centered on different atomic nuclei ($I \neq J$), the matrix elements $\phi H_{\mu\nu}^{\text{MNDO}}$ are taken to be proportional to $\chi S_{\mu\nu}$,

$$\phi H_{\mu\nu}^{\text{MNDO}} = \frac{\beta_{l(\mu)}^{Z_I} + \beta_{l(\nu)}^{Z_J}}{2} \chi S_{\mu\nu}. \quad (52)$$

The mean of two element- and orbital-type-dependent parameters $\beta_{l(\mu)}^{Z_I}$ and $\beta_{l(\nu)}^{Z_J}$ yields the proportionality factor. In analogy to the parameters $U_{ss}^{Z_I}$

and $U_{pp}^{Z_I}$, at most two parameters arise per element, $\beta_s^{Z_I}$ and $\beta_p^{Z_I}$. Taking $\phi H_{\mu\nu}^{\text{MNDO}}$ to be proportional to $\chi S_{\mu\nu}$ has a long history^{8,50} and the initial idea is ascribed to Mulliken.¹⁶⁰ Generally, Eq. (52) was, however, found to be a poor approximation to the analytical value of $\phi H_{\mu\nu}$, irrespective of the chosen values for $\beta_{l(\mu)}^{Z_I}$.^{155,161–163} This can be attributed to the fact that $\phi H_{\mu\nu}$ is not necessarily proportional to $\chi S_{\mu\nu}$ ^{155,161–163} (for an example, see Figure 7). Hence, not even the nodal structure of $\phi H_{\mu\nu} = \phi H_{\mu\nu}(\tilde{R}_{IJ})$ is captured correctly. This finding appears puzzling in view of the success of the MNDO model, apparently Eq. (52) suffices to obtain satisfactory results, e.g., for heats of formation in this context.

4.4 Empirical Modification of Core-Core Repulsion Energy

The core-core repulsion energy in the MNDO model, V_v^{MNDO} , is also determined from a parametric expression. The substitution of the analytical expression,

$$V_v = \sum_{I=1}^N \sum_{J>I}^N \frac{Q_I Q_J}{\tilde{R}_{IJ}}, \quad (53)$$

for a parametric one cannot be physically motivated. Empirically, it was determined that a parametric expression needs to be introduced to decrease the average core-core repulsion energy to define a useful NDDO-SEMO model.^{8,50} The parametric expression to evaluate V_v^{MNDO} ,

$$\begin{aligned} V_v^{\text{MNDO}} &= \sum_{I=1}^N \sum_{J>I}^N Q_I Q_J [s^I s^I | s^J s^J] \cdot f_{IJ}^{\text{MNDO}} \\ &= \sum_{I=1}^N \sum_{J>I}^N Q_I Q_J \left[\tilde{R}_{IJ}^2 + \left(\frac{1}{2\gamma_{ss}^{Z_I}} + \frac{1}{2\gamma_{ss}^{Z_J}} \right)^2 \right]^{-\frac{1}{2}} \cdot f_{IJ}^{\text{MNDO}}, \end{aligned} \quad (54)$$

features two key modifications with respect to Eq. (53). Firstly, the pairwise point-charge interaction is substituted by a scaled interaction of the charge distributions $s^I s^I$ and $s^J s^J$ which is evaluated in the Klopman approximation (cf. Eq. (39)). Secondly, each core-core interaction energy is scaled by f_{IJ}^{MNDO} ,

$$f_{IJ}^{\text{MNDO}} = 1 + \exp\left(-\alpha^{Z_I} \tilde{R}_{IJ}\right) + \exp\left(-\alpha^{Z_J} \tilde{R}_{IJ}\right), \quad (55)$$

where α^{Z_I} is an element-dependent parameter. The introduction of these modifications provides a large flexibility for the MNDO model, but this flexibility comes at a high price. Most strikingly, V_v^{MNDO} is finite for $\tilde{R}_{IJ} = 0$.

More specifically, $f_{IJ}^{\text{MNDO}} = 3.0$ and $V_v^{\text{MNDO}} = 3Q_I^2\gamma_{ss}^{Z_I}$ in the limit $\tilde{R}_{IJ} = 0$ for a homonuclear diatomic system (see also Figure 8). Obviously, this limit is entirely artificial. For intermediate values of \tilde{R}_{IJ} , the parameter α^{Z_I} determines how fast f_{IJ}^{MNDO} declines from three ($\tilde{R}_{IJ} = 0$) to one ($\tilde{R}_{IJ} \rightarrow \infty$) if α^{Z_I} is not negative. This appears to be a constraint invoked during the calibration of α^{Z_I} . Hence, in the limit of large \tilde{R}_{IJ} , V_v^{MNDO} will tend toward V_v , as it should. Depending on the choice of α^{Z_I} , V_v^{MNDO} may be larger or smaller than V_v for a given \tilde{R}_{IJ} .

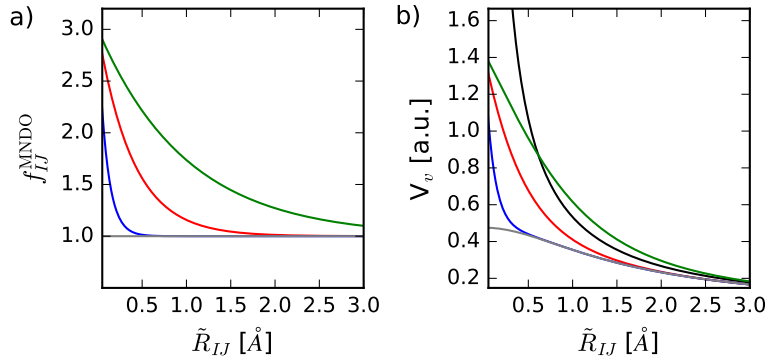


Figure 8: Dependence of a) f_{IJ}^{MNDO} and b) V_v^{MNDO} on \tilde{R}_{IJ} in an H_2 molecules. We calculated the MNDO scaling factors f_{IJ}^{MNDO} and V_v^{MNDO} with $\alpha^1 = 1.0 \text{ \AA}^{-1}$ (green lines), $\alpha^1 = 2.5 \text{ \AA}^{-1}$ (red lines), $\alpha^1 = 10.0 \text{ \AA}^{-1}$ (blue lines), and $\alpha^1 = \infty$ (i.e., $f_{IJ}^{\text{MNDO}} = 1$, gray lines). We compare V_v^{MNDO} to V_v (black line).

The scaling factor is not calculated according to Eq. (55) when the element pair is N–H ($Z_I = 7$ and $Z_J = 1$) or O–H ($Z_I = 8$ and $Z_J = 1$). Dewar and Thiel found⁵⁰ that they could achieve a better agreement with experimental data when they instead applied the scaling factor $f'_{IJ}{}^{\text{MNDO}}$ for these element pairs,

$$f'_{IJ}{}^{\text{MNDO}} = 1 + \tilde{R}_{IJ} \exp\left(-\alpha^{Z_I=7,8} \tilde{R}_{IJ}\right) + \exp\left(-\alpha^{Z_J=1} \tilde{R}_{IJ}\right). \quad (56)$$

Because there is no theoretical foundation for the introduction of Eqs. (54) and (55), it remains unclear why the application of Eq. (56) yields a better agreement with experimental data. We note that $f'_{IJ}{}^{\text{MNDO}} = 2$ in the limit $\tilde{R}_{IJ} = 0$. The modification does, hence, not rectify the theoretically unsatisfactory situation of finite core-core repulsion energies in the limit $\tilde{R}_{IJ} = 0$. The scaling factor $f'_{IJ}{}^{\text{MNDO}}$ also tends to one for large \tilde{R}_{IJ} . For given α^{Z_I} , $f'_{IJ}{}^{\text{MNDO}} < f_{IJ}^{\text{MNDO}}$ for all \tilde{R}_{IJ} .

4.5 Direct Descendants of the MNDO Model

4.5.1 Extension to d Orbitals: The MNDO/d Model

The acronym ‘MNDO/d’ denotes the extension of the MNDO model from an s, p basis to an s, p, d basis.^{53,54} The consideration of d -type basis functions requires, on the one hand, the specification of additional orbital-type-dependent parameters per element, and on the other hand, an adjustment of the parametric expressions themselves.

The number of unique nonzero one-center ERIs increases from six (see Eqs. (32)–(37)) for an s, p basis to 58 for an s, p, d basis. These 58 one-center ERIs are determined analytically⁸⁴ from a set of auxiliary orbital exponents $\zeta_s^{Z_I}$, $\zeta_p^{Z_I}$, and $\zeta_d^{Z_I}$.^{53,54} The auxiliary orbital exponents are derived from the fitted parameters $\gamma_{ss}^{Z_I}$, $\gamma_{pp}^{Z_I}$, and the newly introduced parameter $\gamma_{dd}^{Z_I}$. Note that these auxiliary orbital exponents are different from the set of Slater exponents $\zeta_s^{Z_I}$, $\zeta_p^{Z_I}$, and $\zeta_d^{Z_I}$ which are, e.g., applied to calculate the overlap integrals. The formulae for calculating the one-center ERIs from the auxiliary Slater exponents $\zeta_s^{Z_I}$, $\zeta_p^{Z_I}$, and $\zeta_d^{Z_I}$ are given in Refs. 84,85. It appears that several of the formulae presented in Ref. 84 (Eqs. (17), (51), (53), (54), (56), and (57)) contain typographical mistakes which we correct in Section 10.5 (Eqs. (134*), (168*), (170*), (171*), (173*), and (174*)). These errors affect the one-center ERIs of the types $\langle p_z^I d_{z^2}^I | p_x^I d_{xz}^I \rangle$, $\langle p_z^I d_{z^2}^I | p_y^I d_{yz}^I \rangle$, $\langle s^I d_{z^2}^I | p_x^I p_x^I \rangle$, $\langle s^I d_{z^2}^I | p_y^I p_y^I \rangle$, $\langle p_y^I p_y^I | s^I d_{x^2-y^2}^I \rangle$, $\langle p_z^I s^I | p_z^I d_{z^2}^I \rangle$, $\langle p_z^I p_z^I | s^I d_{z^2}^I \rangle$, $\langle p_z^I p_x^I | s^I d_{xz}^I \rangle$, $\langle p_z^I p_y^I | s^I d_{yz}^I \rangle$, $\langle p_x^I p_x^I | s^I d_{x^2-y^2}^I \rangle$, and $\langle p_x^I p_z^I | s^I d_{xy}^I \rangle$.

Thiel and Voityuk also extended the formalism to approximate two-center ERIs in a point-charge model to charge distributions including d -type orbitals.^{53,54} For this purpose, they introduced a new quadrupole point charge configuration $\tilde{Q}_{xy,xz,yz}$ (see also Figure 19 in Section 10.5). One can then straightforwardly apply the concepts of the multipole expansion introduced in Section 4.2 and derive the necessary formulae for all possible combinations of arising multipoles (see Refs. 53,54,164,165 and Section 10.5).

The two-center ERIs are also applied to calculate the core-core repulsion energy (Eq. (54)) and contributions to the one-electron matrix (Eq. (47)). In these equations, the atomic core I was described by a charge distribution $s^I s^I$ which involves the parameter $\gamma_{ss}^{Z_I}$. The MNDO/d formalism makes these expressions independent from the parameter $\gamma_{ss}^{Z_I}$. Therefore, the atomic core I is described by a spherical charge distribution ϱ_{core}^I . The electrostatic interaction energy with this charge distribution is computed within the Klopman–

Ohno approximation, so that Eq. (54) is substituted for

$$\begin{aligned}
V_v^{\text{MNDO/d}} &= \sum_{I=1}^N \sum_{J>I}^N Q_I Q_J [\varrho_{\text{core}}^I | \varrho_{\text{core}}^J] \cdot f_{IJ}^{\text{MNDO}} \\
&= \sum_{I=1}^N \sum_{J>I}^N Q_I Q_J \left[\tilde{R}_{IJ}^2 + (\vartheta_{\text{core}}^{Z_I} + \vartheta_{\text{core}}^{Z_J})^2 \right]^{-\frac{1}{2}} \cdot f_{IJ}^{\text{MNDO}},
\end{aligned} \tag{57}$$

where $\vartheta_{\text{core}}^{Z_J} = 1/(2\gamma_{ss}^{Z_I})$ for elements which do not activate d -type orbitals and $\vartheta_{\text{core}}^{Z_J} \neq 1/(2\gamma_{ss}^{Z_I})$ for elements which activate d -type orbitals. Similar adjustments are necessary for the formula to calculate the one-electron matrix (Eq. (47)) which is now evaluated as

$$\phi_{\mu\nu}^{\text{MNDO}} = U_{l(\mu)l(\nu)}^{Z_I} - \sum_{\substack{J=1 \\ J \neq I}}^N Q^J [\chi_{\mu}^I \chi_{\nu}^I | \varrho_{\text{core}}^J]. \tag{58}$$

Additionally, we have to specify the parameters $U_{dd}^{Z_I}$, $\beta_d^{Z_I}$, and $\zeta_d^{Z_I}$ to assemble the one-electron matrix.

4.5.2 The Austin Models (AM x)

The *Austin model 1* (AM1)⁵¹ differs from the MNDO model in the way in which the scaling factor for the pairwise core-core repulsion energies is determined,

$$V_v^{\text{AM1}} = \sum_{I=1}^N \sum_{J>I}^N Q_I Q_J [s^I s^I | s^J s^J] \cdot f_{IJ}^{\text{AM1}}. \tag{59}$$

The scaling factor f_{IJ}^{AM1} is defined as the sum of the scaling factor f_{IJ}^{MNDO} (Eq. (55)) and an element-specific number of additional Gaussian functions A^{Z_I} ,^{51,166}

$$\begin{aligned}
f_{IJ}^{\text{AM1}} &= f_{IJ}^{\text{MNDO}} + \sum_{a=1}^{A^{Z_I}} K_a^{Z_I} \exp \left(-L_a^{Z_I} \left(\tilde{R}_{IJ} - M_a^{Z_I} \right)^2 \right) \\
&\quad + \sum_{a=1}^{A^{Z_J}} K_a^{Z_J} \exp \left(-L_a^{Z_J} \left(\tilde{R}_{IJ} - M_a^{Z_J} \right)^2 \right).
\end{aligned} \tag{60}$$

The shape of the a -th Gaussian function is characterized by the element-dependent parameters $K_a^{Z_I}$, $L_a^{Z_I}$, and $M_a^{Z_I}$. The sign of $K_a^{Z_I}$ determines

whether the a -th Gaussian increases (positive sign) or decreases (negative sign) f_{IJ}^{AM1} at a given \tilde{R}_{IJ} . $L_a^{Z_I}$ determines the width of the Gaussian; it must be positive because f^{AM1} would otherwise tend to infinity for large \tilde{R}_{IJ} . $M_a^{Z_I}$ specifies where the a -th Gaussian is centered and, hence, for which \tilde{R}_{IJ} additional repulsive or attractive interactions are added. If more than one

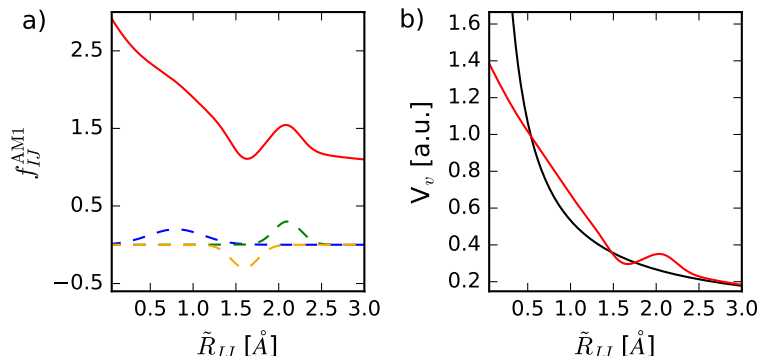


Figure 9: Dependence of a) f_{IJ}^{AM1} (red line) and b) V_v^{AM1} (red line) on \tilde{R}_{IJ} in H_2 . Diagram a) illustrates the contributions of the 3 Gaussian functions (dashed lines) with $K_0^1 = 0.10$, $L_0^1 = 5.0 \text{ \AA}^{-2}$, $M_0^1 = 0.80 \text{ \AA}$ (blue dashed line), $K_1^1 = -0.15$, $L_1^1 = 20.0 \text{ \AA}^{-2}$, $M_1^1 = 1.6 \text{ \AA}$ (orange dashed line), and $K_2^1 = 0.15$, $L_2^1 = 20.0 \text{ \AA}^{-2}$, $M_2^1 = 2.1 \text{ \AA}$ (green dashed line). b) Comparison of V_v^{AM1} (red line) with V_v (black line).

Gaussian is added to the scaling factor ($A^{Z_I} > 1$), f_{IJ}^{AM1} becomes a quite involved function. It can decrease the core-core repulsion energy at certain distances (e.g., at $\tilde{R}_{IJ} = 1.6 \text{ \AA}$ in Figure 9) and increase it at other distances (e.g., at $\tilde{R}_{IJ} = 2.1 \text{ \AA}$ in Figure 9). Hence, f_{IJ}^{AM1} offers a tremendous flexibility and allows for tightly focused fine-tuning to achieve a better agreement with reference data. Simultaneously, the addition of Gaussian functions introduces a high degree of arbitrariness, which has already been noted by Dewar and co-workers when they introduced this modification.⁵¹

A popular reparameterization of AM1⁵¹ was presented by Rocha *et al.* under the name *Recife model 1* (RM1).⁵⁵ Its formalism is identical to that of AM1.⁵⁵

The AM1 model was also generalized to include d orbitals (AM1/d¹⁶⁷) in the same way in which MNDO was generalized to MNDO/d. Additionally,

the scaling factor f_{IJ}^{AM1} is usually slightly modified for heavier elements,¹⁶⁷

$$f_{IJ}^{\prime, \text{AM1}} = 1 + 2x^{Z_I, Z_J} \exp\left(-\alpha^{\prime Z_I, Z_J} \tilde{R}_{IJ}\right) + \sum_{a=1}^{A^{Z_I}} K_a^{Z_I} \exp\left(-L_a^{Z_I} \left(\tilde{R}_{IJ} - M_a^{Z_I}\right)^2\right) + \sum_{a=1}^{A^{Z_J}} K_a^{Z_J} \exp\left(-L_a^{Z_J} \left(\tilde{R}_{IJ} - M_a^{Z_J}\right)^2\right), \quad (61)$$

so that it contains element-pair-dependent parameters x^{Z_I, Z_J} (denoted as δ in Ref. 167) and $\alpha^{\prime Z_I, Z_J}$.¹⁶⁷

The acronym AM1* denotes a popular reparameterization of the AM1/d model^{168–176} which is implemented in the EMPIRE suite of programs.¹⁵⁰

4.5.3 The Parametrized Models (PM x)

Stewart introduced three popular NDDO-SEMO models, the *parametrized models* (PM x , $x = 3, 6, 7$).^{52, 56, 57} The parametrized models regard *all* element-dependent parameters as independent⁵² and the element-dependent parameters are calibrated individually, hence the name. The MNDO/d model specifies a set of auxiliary orbital exponents $\zeta_s^{\prime Z_I}$, $\zeta_p^{\prime Z_I}$, and $\zeta_d^{\prime Z_I}$ which are deduced from the parameters $\gamma_{ss}^{Z_I}$, $\gamma_{pp}^{Z_I}$, and $\gamma_{dd}^{Z_I}$, respectively. In the PM x models, the conceptual relation of the auxiliary orbital exponents to $\gamma_{ss}^{Z_I}$, $\gamma_{pp}^{Z_I}$, and $\gamma_{dd}^{Z_I}$ is ignored for main-group elements.⁵⁶ For several transition metals, the one-center ERIs $\langle s^I s^I | d_{z_2}^I d_{z_2}^I \rangle = \langle s^I s^I | d_{x^2-y^2}^I d_{x^2-y^2}^I \rangle = \langle s^I s^I | d_{xy}^I d_{xy}^I \rangle = \langle s^I s^I | d_{xz}^I d_{xz}^I \rangle = \langle s^I s^I | d_{yz}^I d_{yz}^I \rangle$ and $\langle s^I d_{z_2}^I | s^I d_{z_2}^I \rangle = \langle s^I d_{x^2-y^2}^I | s^I d_{x^2-y^2}^I \rangle = \langle s^I d_{xy}^I | s^I d_{xy}^I \rangle = \langle s^I d_{xz}^I | s^I d_{xz}^I \rangle = \langle s^I d_{yz}^I | s^I d_{yz}^I \rangle$ are also considered parameters independent of $\zeta_s^{\prime Z_I}$ and $\zeta_d^{\prime Z_I}$.⁵⁶

The formalism of the PM3 model (s, p basis) is identical to that of the AM1 model. It differs from the AM1 model only in the values of the parameters, and in the way in which they are determined.⁵²

The PM6 model (s, p, d basis), by contrast, features several modifications with respect to PM3 and, hence, AM1.⁵⁶ Most prominently, the parametric expression which is applied to calculate V_v , was modified even further. In general, the PM6 core-core repulsion energy, V_v^{PM6} , is given by

$$V_v^{\text{PM6}} = \sum_{I=1}^N \sum_{J>I}^N \left\{ Q_I Q_J [\varrho_{\text{core}}^I | \varrho_{\text{core}}^J] \cdot f_{IJ}^{\text{PM6}} + 10^{-8} \text{eV} \left(\frac{Z_I^{1/3} Z_J^{1/3}}{\tilde{R}_{IJ}} \right)^{12} \right\}. \quad (62)$$

Eq. (62) resembles Eq. (57) (MNDO/d core-core repulsion energy), but applies a different scaling factor, f_{IJ}^{PM6} , and adds an additional term to each pairwise interaction. This additional term re-introduces a singularity for $\tilde{R}_{IJ} = 0$ (see also Figure 10). One could therefore conclude that the expression is physically more consistent. The term was designed to resemble the repulsive part of the Lennard-Jones potential.⁵⁶ The prefactor of 10^{-8} electron volt (eV) is an empirical choice which is not further commented on in Ref. 56. It appears to be chosen such that V_v^{PM6} is only affected by the Lennard-Jones-like term for very small \tilde{R}_{IJ} .

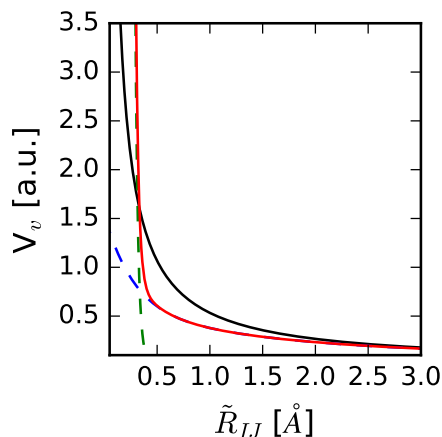


Figure 10: V_v^{PM6} (red line) and V_v (black line) in a.u. for H_2 for various distances \tilde{R}_{IJ} in \AA . V_v^{PM6} is decomposed in the contribution of the first term in Eq. (61) (blue dashed line) and that of the second term in Eq. (61) (green dashed line).

The scaling factor f_{IJ}^{PM6} was constructed in analogy to the scaling factor which was proposed for heavier elements for the AM1/d model¹⁶⁷ (Eq. (61)),

$$f_{IJ}^{\text{PM6}} = 1 + 2x^{Z_I, Z_J} \exp\left(-\alpha'^{Z_I, Z_J} \left(\tilde{R}_{IJ} + 0.0003\text{\AA}^{-5} \tilde{R}_{IJ}^6\right)\right) + K^{Z_I} \exp\left(-L^{Z_I} \left(\tilde{R}_{IJ} - M^{Z_I}\right)^2\right) + K^{Z_J} \exp\left(-L^{Z_J} \left(\tilde{R}_{IJ} - M^{Z_J}\right)^2\right) \quad (63)$$

It also contains element-pair-dependent parameters x^{Z_I, Z_J} and α'^{Z_I, Z_J} . In comparison to Eq. (6) in Ref. 56, we replaced x^{Z_I, Z_J} for $2x^{Z_I, Z_J}$; this is necessary to achieve an agreement with the implementation in MOPAC¹⁷⁸ with the parameter values reported for x^{Z_I, Z_J} in Ref. 56. Stewart restricted the number of additional Gaussian functions to one per element, so that we do

not have to specify an index anymore for the parameters characterizing the Gaussian functions (i.e., K^{Z_I} , L^{Z_I} , and M^{Z_I} instead of $K_a^{Z_I}$, $L_a^{Z_I}$, and $M_a^{Z_I}$, respectively). In comparison to f'_{IJ} ^{AM1}, a term $0.0003\text{\AA}^{-5}\tilde{R}_{IJ}^6$ was added to the exponential scaling function. Apparently, this modification enabled a better agreement with reference data for rare-gas compounds.⁵⁶ The PM6 model defines additional special expressions which are only applied for certain compound classes or for the evaluation of the scaling factors for certain atom pairs (i.e., C–H, N–H, O–H, C–C, and Si–O). We discuss these minor modifications in Section 10.7.

Disturbingly, the PM6 model contains special corrections to the heats of formations at 298 K, $\Delta H_f^{298\text{K}}$, for several compound classes. In the PM6 model, the predicted $\Delta H_f^{298\text{K}}$ in kcal mol⁻¹ is empirically modified depending on a measure for the non-planarity of the amine nitrogen atom, ϕ ,⁵⁶

$$\Delta H_f^{298\text{K}} = \Delta H_f^{298\text{K,PM6}} - 0.5 \text{ kcal mol}^{-1} \exp(-10\phi). \quad (64)$$

The measure for the non-planarity of the amine nitrogen atom is determined as 2π minus the sum of the three bond angles involving the amine nitrogen atom. For a perfectly planar amine, $\Delta H_f^{298\text{K}}$ is reduced by 0.5 kcal mol⁻¹. With an increasing pyramidalization of the amine, $\Delta H_f^{298\text{K}}$ is reduced by a smaller amount. Additionally, the PM6 model (as implemented in MOPAC) includes an undocumented modification to $\Delta H_f^{298\text{K}}$ when the computed bond order for a carbon–carbon bond exceeds 2.5, as for example, in acetylenic bonds. A contribution of 12.0 kcal mol⁻¹ is added to $\Delta H_f^{298\text{K}}$ for every detected acetylenic bond, e.g., MOPAC outputs $\Delta H_f^{298\text{K}} = 57.4 \text{ kcal mol}^{-1}$ for acetylene. If one applies the formulae specified in Ref. 56 instead, one would obtain $\Delta H_f^{298\text{K}} = 45.4 \text{ kcal mol}^{-1}$ for this molecule.

The PM7 model was introduced as the successor of the PM6 model in 2013.⁵⁷ The largest changes were again made to the core-core repulsion energy. It became evident that it is essential that the two-center ERIs decrease to the exact value at large distances when applying a SEMO model in periodic calculations.¹⁴⁹ Hence, Eq. (39) was modified so that the ERI $[s^I s^I | s^J s^J]$ is approximated as,

$$\begin{aligned} [s^I s^I | s^J s^J]^{\text{PM7}} &= \frac{1}{\tilde{R}_{IJ}} \exp\left(-0.22\text{\AA}^{-2}(\tilde{R}_{IJ} - 7.0\text{\AA})^2\right) \\ &+ \left(1 - \exp\left(-0.22\text{\AA}^{-2}(\tilde{R}_{IJ} - 7.0\text{\AA})^2\right)\right) \\ &\times \left[\tilde{R}_{IJ}^2 + \left(\frac{1}{2\gamma_{ss}^{Z_I}} + \frac{1}{2\gamma_{ss}^{Z_J}}\right)^2\right]^{-\frac{1}{2}}. \end{aligned} \quad (65)$$

The value 7.0 Å was apparently chosen as some random distance which is far larger than usual bond lengths.⁵⁷ This equation is also consulted to evaluate V_v^{PM7} ,

$$V_v^{\text{PM7}} = \sum_{I=1}^N \sum_{J>I}^N \left\{ Q_I Q_J [\varrho_{\text{core}}^I | \varrho_{\text{core}}^J]^{\text{PM7}} \cdot f_{IJ}^{\text{PM6}} + 10^{-8} \text{eV} \left(\frac{Q_I^{1/3} Q_J^{1/3}}{\tilde{R}_{IJ}} \right)^{12} \right\}. \quad (66)$$

In Eq. (66), we did not include the additional empirical corrections for hydrogen bonding and dispersion interactions which are inherent to the PM7 model and described in Refs. 57, 89. Note that the description of dispersion interactions in PM7 creates a conceptual problem as pointed out by Grimme *et al.*:¹⁷⁹ Ref. 57 states that the dispersion energy is damped down and truncated at longer distances. This is obviously not sensible for dispersion interactions which are long-range interactions and was also shown to cause significant errors for larger systems.^{180, 181}

5 The Orthogonalization-Corrected Models (OM x)

The OM x ($x = 1, 2, 3$) models activate one s -type basis functions for hydrogen and one s - and three p -type basis functions for carbon, nitrogen, oxygen, and fluorine.^{58–60, 151, 152, 182} Each of these basis function consists of three primitive Gaussian functions,^{58, 60, 117} and hence, we denote the basis sets for the OM1, OM2, and OM3 models with OM1-3G, OM2-3G, and OM3-3G, respectively. The OM x -3G basis sets are based on the ECP-3G basis set.¹¹⁷ The exponents of the primitive Gaussian functions of the ECP-3G basis are scaled with $(\zeta^{Z_I})^2$ to yield the OM x -3G basis sets. The factor ζ^{Z_I} is a parameter of the respective OM x model.⁶⁰ The OM x models currently do only provide parameters for hydrogen, carbon, nitrogen, oxygen, and fluorine.⁶⁰

5.1 Approximation of Electron-Electron Repulsion Integrals

In analogy to MNDO-type models, the five one-center ERIs $\langle \chi_\mu^I \chi_\nu^I | \chi_\lambda^I \chi_\sigma^I \rangle$ arising in the minimal s, p basis are substituted for the parameters $\gamma_{ss}^{Z_I}$, $\gamma_{pp}^{Z_I}$, $\gamma_{sp}^{Z_I}$, $\gamma_{pp'}^{Z_I}$, and $\tilde{\gamma}_{sp}^{Z_I}$ (see also Eqs. (32)–(36)).

Within the OM x models, the value of the two-center ERIs $\langle \chi_\mu^I \chi_\nu^I | \chi_\lambda^J \chi_\sigma^J \rangle$, $I \neq J$ is determined analytically. The analytical values of the two-center ERIs are

then scaled with the so-called Klopman–Ohno factor f_{IJ}^{KO} when assembling $\phi \mathbf{G} \approx \chi \mathbf{G}^{\text{NDDO}}$,

$$\langle \chi_\mu^I \chi_\nu^I | \chi_\lambda^J \chi_\sigma^J \rangle^{\text{OMx}} = f_{IJ}^{\text{KO}} \cdot \langle \chi_\mu^I \chi_\nu^I | \chi_\lambda^J \chi_\sigma^J \rangle \quad (67)$$

The Klopman–Ohno factor f_{IJ}^{KO} is given as the quotient of the MNDO-type ERI $[s^I s^I | s^J s^J]$ (Eq. (39)) and the analytical ERI $\langle s^I s^I | s^J s^J \rangle$,⁵⁸

$$f_{IJ}^{\text{KO}} = \frac{[s^I s^I | s^J s^J]}{\langle s^I s^I | s^J s^J \rangle} = \frac{\left[\tilde{R}_{IJ}^2 + \left(\frac{1}{2\gamma_{ss}^{ZI}} + \frac{1}{2\gamma_{ss}^{ZJ}} \right)^2 \right]^{-\frac{1}{2}}}{\langle s^I s^I | s^J s^J \rangle}. \quad (68)$$

When χ_μ^I , χ_ν^I , χ_λ^J , and χ_σ^J are s -type basis functions, the product of f_{IJ}^{KO} and $\langle s^I s^I | s^J s^J \rangle$ reduces to the MNDO-type model,

$$\begin{aligned} \langle s^I s^I | s^J s^J \rangle^{\text{OMx}} &= \frac{[s^I s^I | s^J s^J]}{\langle s^I s^I | s^J s^J \rangle} \langle s^I s^I | s^J s^J \rangle \\ &= [s^I s^I | s^J s^J]. \end{aligned} \quad (69)$$

In the case of one basis function, χ_μ^I , χ_ν^I , χ_λ^J , or χ_σ^J , not being an s -type basis function, the two-center ERI is still scaled with f_{IJ}^{KO} .

Let us now examine how this Klopman–Ohno scaling affects the value which enters the two-electron matrices. Generally, f_{IJ}^{KO} tends to one in the limit $\tilde{R}_{IJ} \rightarrow \infty$, i.e., the unscaled analytical value for $\langle \chi_\mu^I \chi_\nu^I | \chi_\lambda^J \chi_\sigma^J \rangle$ is applied. It would be theoretically satisfactory if we had a smooth transition from the one-center ERIs $\langle \chi_\mu^I \chi_\nu^I | \chi_\lambda^I \chi_\sigma^I \rangle = \gamma_{ss}^{ZI}, \gamma_{pp}^{ZI}, \gamma_{sp}^{ZI}, \gamma_{pp'}^{ZI}$, or $\tilde{\gamma}_{sp}^{ZI}$ to the two-center ERIs $f_{IJ}^{\text{KO}} \cdot \langle \chi_\mu^I \chi_\nu^I | \chi_\lambda^J \chi_\sigma^J \rangle$. This situation would occur if the analytical one-center limits were chosen for $\gamma_{ss}^{ZI}, \gamma_{pp}^{ZI}, \gamma_{sp}^{ZI}, \gamma_{pp'}^{ZI}$, and $\tilde{\gamma}_{sp}^{ZI}$. If $\gamma_{ss}^{ZI} = \langle s^I s^I | s^I s^I \rangle$, f_{IJ}^{KO} would be one in the limit $\tilde{R}_{IJ} = 0$,

$$f_{II}^{\text{KO}} = \frac{\gamma_{ss}^{ZI}}{\langle s^I s^I | s^I s^I \rangle} = \frac{\langle s^I s^I | s^I s^I \rangle}{\langle s^I s^I | s^I s^I \rangle} = 1. \quad (70)$$

Hence, all two-center ERIs are scaled with a factor of one in the limit $\tilde{R}_{IJ} = 0$ and the analytical one-center limit is recovered. In this case, the scaled two-center ERIs differ negligibly from the analytical two-center ERIs (see Figure 11).

Usually, γ_{ss}^{ZI} is, however, chosen to be significantly smaller than the analytical one-center ERI limit ($\langle s^I s^I | s^I s^I \rangle - \gamma_{ss}^{ZI} = 0.36$ a.u. in our example in Figure 11). Consequently, a theoretically unsatisfactory situation arises which we illustrate at the example of the $\langle s^I p_z^I | s^J p_z^J \rangle$ ERI in

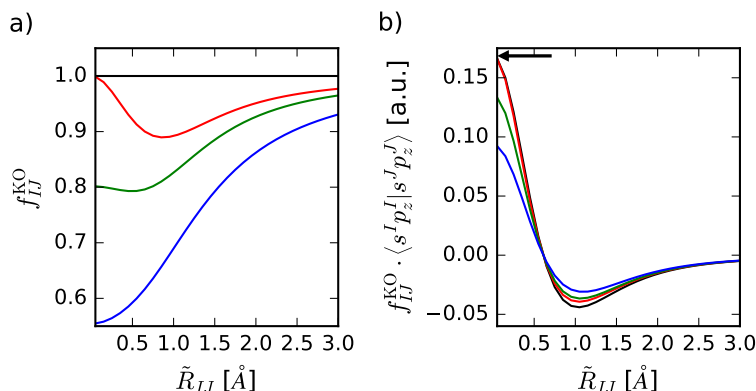


Figure 11: Dependence of a) the Klopman–Ohno factor f_{IJ}^{KO} and b) the value of f_{IJ}^{KO} multiplied by $\langle s^I p_z^I | s^J p_z^J \rangle$ on \tilde{R}_{IJ} in a C_2 molecule described by an OM2-3G basis. We show the values for $f_{IJ}^{\text{KO}} = 1$ (black lines), Eq. (67) with $\gamma_{ss}^6 = \langle s^I s^I | s^I s^I \rangle = 0.81$ a.u. (analytical one-center limit, red lines), Eq. (67) with $\gamma_{ss}^6 = 0.65$ a.u. (green lines), and Eq. (67) with $\gamma_{ss}^6 = 0.45$ a.u. (OMx value,^{58–60} blue lines). The analytical one-center limit $\langle s^I p_z^I | s^I p_z^I \rangle = 0.17$ a.u. is highlighted by a black arrow and the OMx one-center limit $\gamma_{sp}^{\text{ZI}} = 0.42$ a.u. is not shown here.

C_2 . The parametrized one-center ERI limits of interest are $\gamma_{ss}^6 = 0.45$ a.u. and $\gamma_{sp}^6 = 0.42$ a.u.¹⁸³ We then observe a discontinuity from the point $\tilde{R}_{IJ} = 0$ where $\langle s^I p_z^I | s^J p_z^J \rangle^{\text{OMx}} = \gamma_{sp}^6 = 0.42$ a.u. to the point $\tilde{R}_{IJ} \ll 1$ where $\langle s^I p_z^I | s^J p_z^J \rangle^{\text{OMx}} = f_{IJ}^{\text{KO}} \langle s^I p_z^I | s^J p_z^J \rangle = 0.09$ a.u. While these discontinuities are unsatisfactory, they do not appear to lead to practical issues in the calculations.

5.2 Approximation of the Symmetrically Orthogonalized One-Electron Matrix

An exact orthogonalization of $\chi\mathbf{H}$ (e.g., by the transformation $\chi\mathbf{S}^{-\frac{1}{2}} \chi\mathbf{H} \chi\mathbf{S}^{-\frac{1}{2}}$) was initially attempted, but did not provide a useful model to calculate electronic energies^{58,59,182} as confirmed by other studies.^{122,154,159,184–187} Kolb and Thiel therefore decided to develop approximate orthogonalization corrections to be added to $\chi\mathbf{H}$.^{58,182} These^{58,59,151,182} and other^{162,188–190} approximate orthogonalization corrections, are based on an expansion of $\chi\mathbf{S}^{-\frac{1}{2}}$ into a power series,

$$\chi\mathbf{S}^{-\frac{1}{2}} = (\mathbf{1} + \chi\mathbf{S}')^{-\frac{1}{2}} = \mathbf{1} - \frac{1}{2}\chi\mathbf{S}' + \frac{3}{8}\chi\mathbf{S}'^2 - \frac{5}{16}\chi\mathbf{S}'^3 + \mathcal{O}(\chi\mathbf{S}'^4), \quad (71)$$

where ${}^x\mathbf{S}'$ is defined as

$${}^x\mathbf{S}' = {}^x\mathbf{S} - \mathbf{1}. \quad (72)$$

The transformation of ${}^x\mathbf{H}$ to ${}^\phi\mathbf{H}$,

$${}^\phi\mathbf{H} = ({}^x\mathbf{S})^{-\frac{1}{2}} {}^x\mathbf{H} ({}^x\mathbf{S})^{-\frac{1}{2}} = (\mathbf{1} + {}^x\mathbf{S}')^{-\frac{1}{2}} {}^x\mathbf{H} (\mathbf{1} + {}^x\mathbf{S}')^{-\frac{1}{2}} \quad (73)$$

is then approximated as

$$\begin{aligned} {}^\phi\mathbf{H} \approx & {}^x\mathbf{H} - \frac{1}{2}({}^x\mathbf{S}' {}^x\mathbf{H} + {}^x\mathbf{H} {}^x\mathbf{S}') + \frac{3}{8}({}^x\mathbf{S}'^2 {}^x\mathbf{H} + {}^x\mathbf{H} {}^x\mathbf{S}'^2) \\ & + \frac{1}{4} {}^x\mathbf{S}' {}^x\mathbf{H} {}^x\mathbf{S}' + \mathcal{O}({}^x\mathbf{S}'^3). \end{aligned} \quad (74)$$

Accordingly, a matrix element ${}^\phi H_{\mu\nu}$ is approximated as

$$\begin{aligned} {}^\phi H_{\mu\nu} \approx & {}^x H_{\mu\nu} - \frac{1}{2} \sum_{\lambda=1}^M ({}^x S'_{\mu\lambda} {}^x H_{\lambda\nu} + {}^x H_{\mu\lambda} {}^x S'_{\lambda\nu}) \\ & + \frac{1}{8} \sum_{\lambda=1}^M \sum_{\sigma=1}^M (3 {}^x S'_{\mu\lambda} {}^x S'_{\lambda\sigma} {}^x H_{\sigma\nu} + 3 {}^x H_{\mu\lambda} {}^x S'_{\lambda\sigma} {}^x S'_{\sigma\nu} + 2 {}^x S'_{\mu\lambda} {}^x H_{\lambda\sigma} {}^x S'_{\sigma\nu}). \end{aligned} \quad (75)$$

Gray and Stone showed¹⁹¹ that this power series expansion is nonconvergent in the general case. More specifically, the power series expansion fails to converge when the largest eigenvalue of ${}^x\mathbf{S}'$ exceeds 1.0¹⁹¹ which is often the case (e.g., it is 1.3 for methane and 2.1 for benzene when applying an ECP-3G basis set). Chandler and Grader¹²¹ and Neymeyer¹¹⁰⁻¹¹⁴ subsequently introduced alternative convergent power series expansions. These were, however, not applied to derive approximate orthogonalization corrections for the OM*x* models, nor for any other NDDO-SEMO model. The nonconvergence of Eq. (74) does not appear to be a problem in practice, which may be attributed to the fact that it was only taken as a guideline to develop parametric expressions. Eq. (74) is therefore not directly applied to carry out the basis transformation in the OM*x* models (recall that the exact transformation of ${}^x\mathbf{H}$ from the χ - to the ϕ -basis does not yield a useful NDDO-SEMO model).

Analogously to the MNDO model, different parametric expressions are applied for the evaluation of the matrix elements ${}^\phi H_{\mu\nu}^{\text{OM}x}$ depending on the number of atoms on which the corresponding basis functions χ are centered (one-center one-electron and two-center one-electron matrix elements).

5.2.1 One-Center One-Electron Matrix Elements

We first discuss how $\phi H_{\mu\nu}^{\text{OM}x}$ is determined when the corresponding basis functions χ are centered on the *same* atom, i.e, χ_μ^I and χ_ν^I are both centered on the atom I . In this case, the matrix elements $\phi H_{\mu\nu}^{\text{OM}x}$ are given by

$$\begin{aligned} \phi H_{\mu\nu}^{\text{OM}x} = & {}^x H_{\mu\nu}^{\text{OM}x} - \frac{1}{2} F_1^{Z_I} \sum_{\lambda=1}^M ({}^x S'_{\mu\lambda} \theta(\chi_\nu^I, \chi_\lambda^J) + \theta(\chi_\mu^I, \chi_\lambda^J) {}^x S'_{\lambda\nu}) \\ & + \frac{1}{8} F_2^{Z_I} \sum_{\lambda=1}^M {}^x S'_{\mu\lambda} {}^x S'_{\lambda\nu} (\eta(\chi_\mu^I, \chi_\lambda^J) + \eta(\chi_\nu^I, \chi_\lambda^J) - \eta(\chi_\lambda^J, \chi_\mu^I) - \eta(\chi_\lambda^J, \chi_\nu^I)), \end{aligned} \quad (76)$$

where $F_1^{Z_I}$ and $F_2^{Z_I}$ are element-dependent parameters. Additionally, Eq. (76) contains the functions $\theta(\chi_\nu^I, \chi_\lambda^J)$ and $\eta(\chi_\mu^I, \chi_\lambda^J)$ which we will specify in the following paragraphs. When comparing Eqs. (75) and (76), we notice several similarities and differences. Firstly, both equations start with the corresponding matrix element in the χ -basis. The second contribution to $\phi H_{\mu\nu}^{\text{OM}x}$ is similar to the second contribution to $\phi H_{\mu\nu}$. The analytical expression (Eq. (75)) does not contain the parameter $F_1^{Z_I}$ which implies that $F_1^{Z_I}$ should be close to one when the analytical expression is approximated (cf. Ref. 58). The function $\theta(\chi_\nu^I, \chi_\lambda^J)$ appears to model an entry in ${}^x \mathbf{H}$. More specifically, it models the matrix elements ${}^x H_{\mu\lambda}$ when χ_μ^I and χ_λ^J are centered on different atoms, i.e., $I \neq J$. This is apparent when studying ${}^x S'_{\mu\lambda}$ which is only different from zero when χ_μ^I and χ_λ^J are centered on different atoms due to the condition of local orthogonality and the way in which ${}^x \mathbf{S}'$ is constructed (Eq. (72)). In summary, the second contribution to Eq. (76) is identical to the analytical expression when $F_1^{Z_I} = 1$ and $\theta(\chi_\mu^I, \chi_\lambda^J) = {}^x H_{\mu\lambda}$. The relation of the third contribution to Eqs. (76) and (75) is harder to see. It includes the approximation that all four-center contributions are neglected, see Ref. 59 for a detailed derivation. Hence, it is impossible to establish a similar relationship between $F_2^{Z_I}$ and $\eta(\chi_\mu^I, \chi_\lambda^J)$ in the parametric expression and analogs in the analytical expression. In the OM3 model, $F_2^{Z_I} = 0$ whereas in the OM1 and OM2 models both orthogonalization corrections are considered.

We now examine how the contributions to $\phi H_{\mu\nu}^{\text{OM}x}$ are evaluated. Its first contribution, ${}^x H_{\mu\nu}^{\text{OM}x}$, on the right-hand side of Eq. (76) is given by¹⁵²

$$\begin{aligned} {}^x H_{\mu\nu}^{\text{OM}x} = & U_{l(\mu)l(\nu)}^{Z_I} + \sum_{\substack{J=1 \\ J \neq I}}^N \langle \chi_\mu^I | \text{ECP}_J | \chi_\nu^I \rangle - \sum_{\substack{J=1 \\ J \neq I}}^N \{ Q_J [\chi_\mu^I \chi_\nu^I | s^J s^J] \\ & - f_{IJ}^{\text{KO}} Q_J \langle \chi_\mu^I \chi_\nu^I | s^J s^J \rangle + f_{IJ}^{\text{KO}} \left\langle \chi_\mu^I \left| \frac{Q_J}{|\mathbf{r}_i - \bar{\mathbf{R}}_J|} \right| \chi_\nu^I \right\rangle \}, \end{aligned} \quad (77)$$

where the element- and orbital-type-dependent parameter $U_{l(\mu)l(\mu)}^{Z_I}$ replaces the calculation of $\langle \chi_\mu^I | -\frac{1}{2} \nabla^2 | \chi_\nu^I \rangle - \left\langle \chi_\mu^I \left| \frac{Q_I}{|\mathbf{r}_i - \tilde{\mathbf{R}}_I|} \right| \chi_\nu^I \right\rangle + \langle \chi_\mu^I | \text{ECP}_I | \chi_\nu^I \rangle$ (cf. the MNDO model). Kolb and Thiel explicitly stated that $U_{l(\mu)l(\mu)}^{Z_I}$ is also assumed to include all contributions from the core electrons.⁵⁸

The next term is the contribution from the ECP with all other atoms J . In the first OM x model, OM1, the contributions to the one-electron matrix are evaluated analytically as presented in Refs. 117, 192. The analytical results were then subjected to Klopman–Ohno scaling.⁵⁸ In the OM2 and OM3 models, the *ab initio* effective core potential in the χ -basis was substituted for a semiempirical one,^{59,60}

$$\begin{aligned} \langle \chi_\mu^I | \text{ECP}_K | \chi_\nu^J \rangle &\approx - \langle \chi_\mu^I | \omega^K \rangle \theta(\chi_\nu^J, \omega^K) - \theta(\chi_\mu^I, \omega^K) \langle \omega^K | \chi_\nu^J \rangle \\ &\quad - \langle \chi_\mu^I | \omega^K \rangle \langle \omega^K | \chi_\nu^J \rangle W^{Z(K)}. \end{aligned} \quad (78)$$

In this expression, we introduced an auxiliary set of basis functions $\omega = \{\omega^I\}$ (no additional subscript index is necessary because there is at most one additional s -type basis function per atom). Each basis function ω is characterized by an orbital exponent $\zeta_\omega^{Z_I}$. Note that an orbital ω^I is generally not locally orthogonal to χ_μ^I . An additional element-dependent parameter $W^{Z(K)}$ enters Eq. (78).

The last contribution to Eq. (77) describes the interaction of the charge distribution $\chi_\mu^I \chi_\nu^I$ with all other atomic nuclei $J \neq I$. It is composed of three contributions: The first one is identical to the one applied to describe this interaction in the MNDO model (Eq. (50)). As stated in Section 4.3.1, this expression is the result of an error compensation between the so-called penetration integrals (Eq. (51)) and the orthogonalization corrections. Because the OM x models explicitly consider orthogonalization corrections, also the penetration integrals must be considered which make up the last two terms (subjected to Klopman–Ohno scaling). If χ_μ^I and χ_ν^I are s -type orbitals, Eq. (77) will reduce to

$$\chi H_{\mu\nu}^{\text{OM}x} = U_{ss}^{Z_I} - \sum_{\substack{J=1 \\ J \neq I}}^N f_{IJ}^{\text{KO}} \left\langle s^I \left| \frac{Q_J}{|\mathbf{r}_i - \tilde{\mathbf{R}}_J|} \right| s^I \right\rangle + \sum_{\substack{J=1 \\ J \neq I}}^N f_{IJ}^{\text{KO}} \langle s^I | \text{ECP}_J | s^I \rangle, \quad (79)$$

because the first two remaining terms in Eq. (77) cancel out exactly,

$$\begin{aligned} Q_J [s^I s^I | s^J s^J] - f_{IJ}^{\text{KO}} Q_J \langle s^I s^I | s^J s^J \rangle &= Q_J [s^I s^I | s^J s^J] \\ - Q_J \frac{[s^I s^I | s^J s^J]}{\langle s^I s^I | s^J s^J \rangle} \langle s^I s^I | s^J s^J \rangle &= 0. \end{aligned} \quad (80)$$

If either χ_μ^I or χ_ν^I are not s -type orbitals, Eq. (80) will not hold true and we will have a contribution $Q_J ([\chi_\mu^I \chi_\nu^I | s^J s^J] - f_{IJ}^{\text{KO}} \langle \chi_\mu^I \chi_\nu^I | s^J s^J \rangle)$ to Eq. (77). Generally, however, the differences in the results of Eq. (77) and Eq. (79) are quite small.¹⁵¹

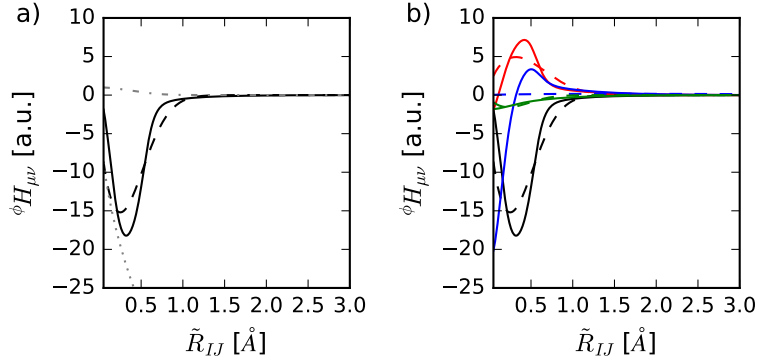


Figure 12: Dependence of $\phi H_{\mu\nu}$ (solid lines) and $\theta(\chi_\mu^I, \chi_\nu^J)$ (dashed lines) on the distance \tilde{R}_{IJ} in a C_2 molecule described in an OM2-3G basis ($\boldsymbol{\chi} = \{\chi_1^{C_1}, \chi_2^{C_1}, \chi_3^{C_1}, \chi_4^{C_1}, \chi_5^{C_2}, \chi_6^{C_2}, \chi_7^{C_2}, \chi_8^{C_2}\}$ where the first and fifth basis functions are $2s$, the second and sixth are $2p_x$, the third and seventh are $2p_y$, and the fourth and eighth are $2p_z$ basis functions). a) $\theta(s^{C_1}, s^{C_2})$ with the best-fit parameters $\beta_s^6 = -38.9$ a.u. and $a_s^6 = 1.0$ a.u. The contributions to $\theta(s^{C_1}, s^{C_2})$ are divided into the scaled square-root contributions (dashed gray line) and the Gaussian contribution (dashed-dotted gray line). b) $\theta(s^{C_1}, s^{C_2})$ with $\beta_s^6 = -38.9$ a.u. and $a_s^6 = 1.0$ a.u. (black lines), $\theta(s^{C_1}, p_z^{C_2})$ with $\beta_p^6 = \beta_p^6 = -11.2$ a.u. and $\alpha_p^6 = \alpha_p^6 = 0.6$ a.u. (red lines), $\theta(p_z^{C_1}, p_z^{C_2})$ with $\beta_p^6 = -0.2$ a.u. and $\alpha_p^6 = 0.1$ a.u. (blue lines), and $\theta(p_x^{C_1}, p_x^{C_2})$ with $\beta_p^6 = -4.2$ a.u. and $\alpha_p^6 = 1.2$ a.u. (green lines).

The function $\theta(\chi_\mu^I, \chi_\lambda^J)$,⁵⁸

$$\theta(\chi_\mu^I, \chi_\lambda^J) = (-1)^{l(\lambda)+m(\lambda)} \frac{b_{l(\mu)}^{Z_I} + b_{l(\lambda)}^{Z_J}}{2} \sqrt{\tilde{R}_{IJ}} \exp\left(- (a_{l(\mu)}^{Z_I} + a_{l(\lambda)}^{Z_J}) \tilde{R}_{IJ}^2\right), \quad (81)$$

consists of the product of a phase vector, $(-1)^{l(\lambda)+m(\lambda)}$, the scaled square-root of the interatomic distance \tilde{R}_{IJ} , and a Gaussian contribution depending on \tilde{R}_{IJ}^2 (see Figure 12). The function $\theta(\chi_\mu^I, \chi_\lambda^J)$ is evaluated in the same local coordinate system which is applied in MNDO-type methods (see Section 4.2) and have to be transformed accordingly. The scaling factor for the square-root of the interatomic distance \tilde{R}_{IJ} is determined from element- and orbital-type-dependent parameters $b_{l(\mu)}^{Z_I}$. The width of the Gaussian function

is determined by element- and orbital-type-dependent parameters $a_{l(\mu)}^{Z_I}$, it determines how fast the whole function approaches to zero. The parameters $a_{l(\mu)}^{Z_I}$ must be positive to obtain a sensible expression. Within OM x models, the parameters $b_{l(\mu)}^{Z_I}$ are unanimously negative. Hence, the phase vector determines the sign of $\theta(\chi_\mu^I, \chi_\lambda^J)$. Consequently, the sign of $\theta(\chi_\mu^I, \chi_\lambda^J)$ does not depend on \tilde{R}_{IJ} . The function $\theta(\chi_\nu^I, \chi_\lambda^J)$ was designed to emulate ${}^\phi H_{\mu\lambda}$.⁵⁸ The matrix element ${}^\phi H_{\mu\lambda}$, which the function $\theta(\chi_\mu^I, \chi_\lambda^J)$ is supposed to model, may, however, have a different sign for different \tilde{R}_{IJ} . In fact, Kolb and Thiel included an example where ${}^\phi H_{\mu\lambda}$ changes its sign for different \tilde{R}_{IJ} in Figure 2 of Ref. 58 (see also Figure 12 in the present work). Furthermore, it is interesting that no ECP is explicitly considered for the two-center one-electron matrix elements which is apparently assumed to be absorbed into Eq. (81).

Finally, we need to evaluate the function $\eta(\chi_\mu^I, \chi_\lambda^J)$ to assemble Eq. (76). It is evaluated similarly to the corresponding local one-electron matrix element in the MNDO model. The function $\eta(\chi_\mu^I, \chi_\lambda^J)$ is evaluated as¹⁵¹

$$\eta(\chi_\mu^I, \chi_\lambda^K) = U_{\mu\mu}^{Z_I} - Q_K [\chi_\mu^I \chi_\mu^I | s^K s^K] \quad (82)$$

(cf. Eq. (47)). Note that the order in which the basis functions are written in the function matters, i.e., $\eta(\chi_\mu^I, \chi_\lambda^K) \neq \eta(\chi_\lambda^K, \chi_\mu^I)$. The function $\eta(\chi_\mu^I, \chi_\lambda^J)$ is not rotationally invariant, so that the functions have to be averaged when χ_μ^I is a p -type basis function,¹⁵¹

$$\eta(p^I, \chi_\lambda^K) = \frac{1}{3} (\eta(p_x^I, \chi_\lambda^K) + \eta(p_y^I, \chi_\lambda^K) + \eta(p_z^I, \chi_\lambda^K)). \quad (83)$$

5.2.2 Two-Center One-Electron Matrix Elements

While Kolb and Thiel explicitly pointed out that $\theta(\chi_\mu^I, \chi_\lambda^J)$ is assumed to contain orthogonalization corrections,⁵⁸ it turned out that it cannot accomplish this fully.⁵⁹ As a remedy, Weber and Thiel⁵⁹ developed an orthogonalization correction for matrix elements ${}^\phi H_{\mu\nu}^{\text{OM}x}$ for which χ_μ^I and χ_ν^J are centered on different atoms,

$$\begin{aligned} {}^\phi H_{\mu\nu}^{\text{OM}x} = & \theta(\chi_\mu^I, \chi_\nu^J) - \frac{1}{2} \frac{G_1^{Z_I} + G_1^{Z_J}}{2} \sum_{\lambda=1}^M (1 - \delta_{IK})(1 - \delta_{JK}) ({}^x S'_{\mu\lambda} \theta(\chi_\nu^I, \chi_\lambda^K) \\ & + \theta(\chi_\nu^J, \chi_\lambda^K) {}^x S'_{\lambda\nu}) + \frac{1}{8} \frac{G_2^{Z_I} + G_2^{Z_J}}{2} \sum_{\lambda=1}^M (1 - \delta_{IK})(1 - \delta_{JK}) {}^x S'_{\mu\lambda} {}^x S'_{\lambda\nu} \\ & \times (\eta(\chi_\mu^I, \chi_\lambda^K) + \eta(\chi_\nu^J, \chi_\lambda^K) - \eta(\chi_\lambda^K, \chi_\mu^I) - \eta(\chi_\lambda^K, \chi_\nu^J)), \end{aligned} \quad (84)$$

which contains the element-dependent parameters $G_1^{Z_I}$ and $G_2^{Z_I}$. This equation significantly differs from the analytic expression for the transformation of the matrix elements (Eq. (75)). Most importantly, the corrections do *only* include terms with basis functions which are centered on a third atom ($K \neq I \neq J$; indicated by $(1 - \delta_{IK})(1 - \delta_{JK})$ in Eq. (84)). Other than that similar considerations apply as in the one-center case. The similarity of Eqs. (77) and (84) might imply that $F_1^{Z_I} \approx 2 \cdot G_1^{Z_I}$ and $F_2^{Z_I} \approx 2 \cdot G_2^{Z_I}$ which is, however, generally not the case.

In the earliest variant, OM1, $G_1^{Z_I} = 0$ and $G_2^{Z_I} = 0$, i.e., orthogonalization corrections are only considered when χ_μ^I and χ_ν^J are centered on a single atom. The latest version, OM3, sets $F_2^{Z_I} = 0$ and $G_2^{Z_I} = 0$. The OM2 model considers all orthogonalization corrections.

5.3 Empirical Scaling of the Core-Core Repulsion Energy

The contribution of each pairwise repulsion of atomic cores $I, J \neq I$ is scaled with the Klopman–Ohno factor f_{IJ}^{KO} ,^{58–60,152}

$$V_v^{\text{OM}x} = \sum_{I=1}^N \sum_{J>I}^N f_{IJ}^{\text{KO}} \frac{Q_I Q_J}{\tilde{R}_{IJ}}. \quad (85)$$

It is argued^{58–60,152} that the core-core repulsion energy needs to be reduced for small interatomic distances to ensure a balance within the model (ERIs and contributions to the core-electron attraction terms are also scaled with f_{IJ}^{KO}). In contrast to the MNDO-type core-core repulsion (Eqs. (54), (59), and (62)), Eq. (85) has a singularity for $\tilde{R}_{IJ} = 0$. When $\tilde{R}_{IJ} \rightarrow \infty$, $f_{IJ}^{\text{KO}} \rightarrow 1$, i.e., the core-core repulsion energy approximates the point-charge model asymptotically.

6 Other NDDO-SEMO models

Several other models, which have not found widespread popularity, introduce new conceptual ideas beyond the MNDO-type and OM x models. In the following sections, several of these ideas are reviewed and discussed without providing the complete formalism for these models. This list is by no means complete. We selected models which feature conceptually large differences to the introduced models, but are still built around the NDDO approximation. For other NDDO-SEMO models see also Refs. 104, 146–148, 185, 193–198.

6.1 The Nonorthogonalized Modified Neglect of Differential Overlap (NO-MNDO) Model

An obvious weakness of the MNDO model is the lack of explicit orthogonalization corrections to \mathbf{H} (Section 4.3). Sattelmeyer *et al.* claimed that this problem can be addressed by introducing the overlap matrix into the SCF equations⁶¹ and coined the name *Nonorthogonalized Modified Neglect of Differential Overlap* (NO-MNDO) model for this procedure.⁶¹ Let us neglect the presence of parameters for the moment and assume that all integrals are calculated analytically. Their suggestion then reads, in our notation,

$$({}^x\mathbf{H} + {}^x\mathbf{G}^{\text{NDDO}}) {}^x\mathbf{C} = {}^x\mathbf{S} {}^x\mathbf{C}\epsilon, \quad (86)$$

which can be reformulated to

$$({}^\phi\mathbf{H} + {}^x\mathbf{S}^{-\frac{1}{2}} {}^x\mathbf{G}^{\text{NDDO}} {}^x\mathbf{S}^{-\frac{1}{2}}) {}^\phi\mathbf{C} = {}^\phi\mathbf{C}\epsilon, \quad (87)$$

when applying Eq. (23). While it is obvious that the one-electron matrix is explicitly orthogonalized, a problem arises. The NDDO approximation emulates a basis transformation for \mathbf{G} (cf. Eq. (23)). The application of a matrix transformation to ${}^x\mathbf{G}^{\text{NDDO}}$ is therefore not sensible. When applying the matrix transformation again, we end up with a situation where

$${}^x\mathbf{S}^{-\frac{1}{2}} {}^x\mathbf{G}^{\text{NDDO}} {}^x\mathbf{S}^{-\frac{1}{2}} \not\approx {}^\phi\mathbf{G} \quad (88)$$

and

$${}^x\mathbf{S}^{-\frac{1}{2}} {}^x\mathbf{G}^{\text{NDDO}} {}^x\mathbf{S}^{-\frac{1}{2}} \not\approx {}^x\mathbf{G} \quad (89)$$

(see Figure 13).

According to Sattelmeyer *et al.*⁶¹ the NO-MNDO model appeared to significantly improve on the MNDO model. We speculate that the good performance of the NO-MNDO model might be due to a combination of two reasons: (i) The parameters in the NO-MNDO model might provide a sufficient flexibility to remedy the conceptual shortcomings and (ii) the explicit orthogonalization of ${}^x\mathbf{H}$ might outweigh the conceptual error to a certain extent. The improvements of NO-MNDO in areas which are typically associated with orthogonalization errors for MNDO⁶¹ (e.g., wrong barriers of rotations about single bonds) might be taken as an indicator for this statement.

In any case, it appears promising to attempt the construction of a similar (MNDO-type) model which does not share the conceptual difficulties of NO-MNDO. Without considering the parametrization, the corresponding SCF

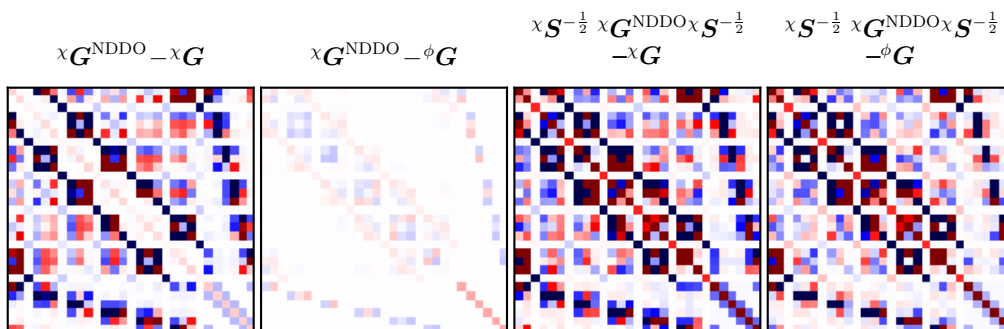


Figure 13: Graphical representation of $\chi\mathbf{G}^{\text{NDDO}}-\chi\mathbf{G}$ (left), $\chi\mathbf{G}^{\text{NDDO}}-\phi\mathbf{G}$ (middle left), $\chi\mathbf{S}^{-\frac{1}{2}}\chi\mathbf{G}^{\text{NDDO}}\chi\mathbf{S}^{-\frac{1}{2}}-\chi\mathbf{G}$ (middle right), and $\chi\mathbf{S}^{-\frac{1}{2}}\chi\mathbf{G}^{\text{NDDO}}\chi\mathbf{S}^{-\frac{1}{2}}-\phi\mathbf{G}$ (right) for a benzene molecule described in an MNDO-3G basis. The entries are colored according to their values from negative (blue) to zero (white) to positive (red).

equations might read,

$$\left(\chi\mathbf{S}^{-\frac{1}{2}}\chi\mathbf{H}\chi\mathbf{S}^{-\frac{1}{2}}+\chi\mathbf{G}^{\text{NDDO}}\right)\phi\mathbf{C}=\phi\mathbf{C}\epsilon. \quad (90)$$

It might be possible that such an attempt could result in a model which is more accurate than NO-MNDO, and hence, significantly more accurate than MNDO.

6.2 The Polarized Molecular Orbital (PMO x) Models

The *Polarized Molecular Orbital* (PMO x , $x = 1, 2$) models^{62–66} were developed in an attempt to provide a more accurate description of noncovalent interactions and polarization effects than possible with the standard NDDO-SEMO models. It is built upon the MNDO model, but features a key difference in its formalism: The PMO x models activate one s - and three p -type basis functions for hydrogen (compared to only one s -type basis function for MNDO). Truhlar and co-workers determined that the activation of diffuse p -type basis functions for hydrogen atoms is already sufficient to obtain a significant improvement in the description of polarization effects in *ab initio* studies.^{62–64} Similar results were also published before in a different context.^{199–201} Such a basis set, nevertheless, fulfills the condition of local orthogonality. The addition of p -type basis functions for hydrogen atoms was, furthermore, accompanied by changes to the parametric expressions applied to evaluate the one-electron matrix elements and the core-core repulsion energy.⁶⁵

6.3 The Machine Learning OM2 (ML-OM2) Model

Dral, von Lilienfeld, and Thiel suggested⁶⁷ to combine machine learning techniques with NDDO-SEMO models which resulted in the machine learning OM2 (ML-OM2) model. The formalism of the ML-OM2 model is identical to that of the OM2 model. It differs from the OM2 model only in the value of the parameter $(\zeta^6)^2$ with which the exponents of the primitive Gaussian functions of the ECP-3G basis functions for carbon are scaled.⁶⁷ Dral *et al.* applied⁶⁷ kernel ridge regression to predict $(\zeta^6)^2$ for individual molecules, i.e., $(\zeta^6)^2$ was not assumed to be a constant element-dependent parameter in ML-OM2. As a consequence, the resulting model offers a much greater flexibility. The mean absolute error in predicted atomization enthalpies could be reduced from 26.4 kJ mol⁻¹ with OM2 to 7.1 kJ mol⁻¹ with ML-OM2 for a test set of organic molecules.⁶⁷

6.4 The High-Performance Computer-Aided Drug Design (hpCADD) Model

Very recently, Thomas *et al.* introduced the *High-Performance Computer-Aided Drug Design* (hpCADD) model⁶⁸ which differs from an MNDO-type model in the dependence of the parameters. In the MNDO model, all parameters are element-dependent. Thomas *et al.* proposed to adopt the concept of ‘atom types’ (well-known for force fields) into an MNDO-type model, i.e., they proposed to make the parameters in the MNDO model *environment-dependent*.⁶⁸ E.g., hpCADD does not only comprise one parameter set for sulfur, but separate sets of parameters for a sulfur atom which is part of a π -system (such as the one in thiophene) and for a sulfur atom which is part of a thiol group.⁶⁸ Hence, this conceptually follows the introduction of *valence states* of atoms in molecules, which is known to advance parametrized concepts such as electronegativity.²⁰² We will come back to the advantages and disadvantages which are associated with such an approach in Section 7.3.

7 Implicit Description of Electron Correlation Effects through Parametrization

So far, we have discussed how NDDO-SEMO models approximate the SCF equations in the ϕ -basis (Eq. (9)). Historically, NDDO-SEMO models were developed to reproduce experimental data rather than, e.g., HF data.^{9, 50, 51, 127} Consequently, NDDO-SEMO models have to be able to capture electron correlation effects in some manner. The most popular way to describe electron

correlation effects is implicit, i.e., through the calibration of the parameters incorporated in the NDDO-SEMO model.

7.1 Parallels to Kohn–Sham Density-Functional Theory

A comparison to correlation functional derivations of KS-DFT is likely to highlight insufficiencies in the description of electron correlation in a parametrized single-determinant approach. The comparison of the elements of the Fock matrix for KS-DFT in the χ -basis,

$$\chi\mathbf{F}^{\text{KS-DFT}} = \chi\mathbf{H} + \chi\mathbf{J} + (1 - \Lambda)\chi\mathbf{K} + \Lambda\mathbf{V}^x + \mathbf{V}^c, \quad (91)$$

highlights the connection between KS-DFT and HF (through Λ). The parameter Λ quantifies the amount of exact (HF) exchange $\chi\mathbf{K}$. For $0 < \Lambda \leq 1$, we have a contribution of a (approximate) DFT contribution to the exchange potential, \mathbf{V}^x , to $\chi\mathbf{F}^{\text{KS-DFT}}$.²⁰³ Additionally, \mathbf{V}^c is the DFT description of the correlation potential. HF theory does not consider a correlation potential so that when $\Lambda = 0$ and no \mathbf{V}^c is considered then $\chi\mathbf{F}^{\text{KS-DFT}} = \chi\mathbf{F}^{\text{HF}}$.

Yang and co-workers classified the most severe drawbacks in KS-DFT at the example of fractional electrons and of fractional spins for the prototypical molecules H_2 and H_2^+ .^{203–206} The energy for a system with a fractional number of electrons (or a fractional spin) is given by the straight line connecting the energies for the system with integer electron numbers (or integer spins).^{203–206} Approximate density functionals and HF are not able to correctly reproduce this behavior which may be interpreted as the source of many failures of approximate KS-DFT and HF models (such as delocalization and static correlation errors).^{203–206}

We may also study NDDO-SEMO models in this respect for which we choose as an example an H_8 cube, whose structure is described in Ref. 206 (see Figure 14). Not surprisingly, the NDDO-SEMO models are not able to describe the discontinuities in the energy for integer electron numbers per hydrogen atom (see Figure 14). The NDDO-SEMO models can also not be reparametrized to yield such a behavior. We emphasize that the significance of this result is not the inability of NDDO-SEMO models to accurately describe H_8 with different electron numbers. Rather, it shows that NDDO-SEMO models fail to describe the quantum mechanical interaction of electrons in the same way as HF and approximate KS-DFT fail to do this. We may therefore take this failure as an indication that NDDO-SEMO models share the same systematic errors as approximate KS-DFT and HF models. Hence, these systematic errors *cannot* be alleviated through parametrization of the existing NDDO-SEMO models. However, these fundamental errors

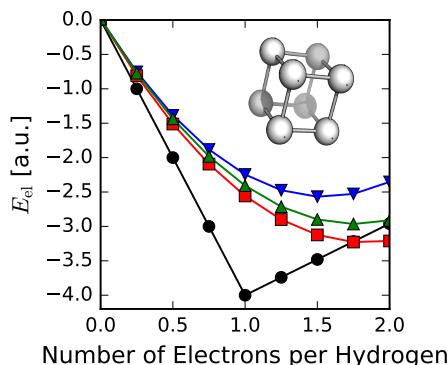


Figure 14: MNDO (red squares), AM1 (green triangles), and PM6 (blue triangles) electronic energies in a.u. for a closed-shell H_8 cube with an edge length of 1000 Å and 0, 2, 4, 6, 8, 10, 12, 14, and 16 electrons. The FCI reference energies (black circles) were taken from Ref. 206.

may not severely affect the equilibrium structures of organic molecules,²⁰³ but they will have a larger effect for non-equilibrium structures of organic molecules and for molecules with a more complicated electronic structure such as transition-metal complexes.²⁰³

7.2 NDDO-SEMO Models for Isolated Atoms

Historically, NDDO-SEMO models are built upon considerations for isolated atoms.^{8,183} Studying isolated atoms has two distinct advantages: (i) We do not have to consider orthogonalization effects ($\chi = \phi$ for an isolated atom) and (ii) the NDDO approximation is no approximation in this special case. The one-electron matrix elements ${}^\phi H_{\mu\nu} = {}^x H_{\mu\nu}$ are equal to the corresponding one-center parameters $U_{l(\mu)l(\nu)}^{Z_I}$. The one-center ERIs ($\gamma_{ss}^{Z_I}$, $\gamma_{pp}^{Z_I}$, $\gamma_{sp}^{Z_I}$, $\gamma_{pp'}^{Z_I}$, and $\tilde{\gamma}_{sp}^{Z_I}$, and if d -type orbitals are activated, the additional parameters specified in Section 4.5.1) will enter the two-electron matrix. For each element, the one-center parameters originally are calibrated^{144,183,207,208} with respect to reference electronic energies $E_{\text{el}}^{\text{ref}}$ for isolated atoms and monatomic ions (e.g., the one-center parameters for carbon (C) are calibrated with respect to $E_{\text{el}}^{\text{ref}}$ for C^{3+} ($n_v = 1$), C^{2+} ($n_v = 2$), C^+ ($n_v = 3$), C ($n_v = 4$), and C^- ($n_v = 5$) in Ref. 183). $E_{\text{el}}^{\text{ref}}$ may be approximately determined from atomic ionization energies,^{144,183,207,208} or, quite recently, from coupled cluster data.²⁰⁹ Refs. 183 and 209 showed that it is not possible to achieve a good agreement between $E_{\text{el}}^{\text{ref}}$ and $E_{\text{el}}^{\text{NDDO-SEMO}}$ with a single element-dependent parameter set for a range of monatomic ions. Margraf and co-workers, how-

ever, achieved²⁰⁹ a good agreement with the first ionization potentials and electron affinities for the neutral atoms.

Oleari *et al.*,¹⁸³ and subsequent studies,^{207–209} found that the one-center parameters vary in a remarkably regular manner with respect to Z_I (quadratic dependence of $U_{ss}^{Z_I}$, $U_{pp}^{Z_I}$, and $U_{dd}^{Z_I}$ on Z_I ²⁰⁹ and linear dependence for the one-center ERI parameters on Z_I ;²⁰⁹ see also Figure 15). In NDDO-SEMO models, the one-center parameters are, however, not determined with respect to data for atoms, but with respect to data for molecules. Interestingly, the regularity of the one-center parameters with respect to Z_I disappears for heavier elements ($Z_I > 23$) when taking molecular data as reference data (compare, e.g., the red squares (atomic data as reference data) and blue circles (molecular data as reference data) in Figure 15). We may take this as a direct and method-inherent hint that the description of transition-metal complexes will be more challenging than the description of organic compounds with NDDO-SEMO models.

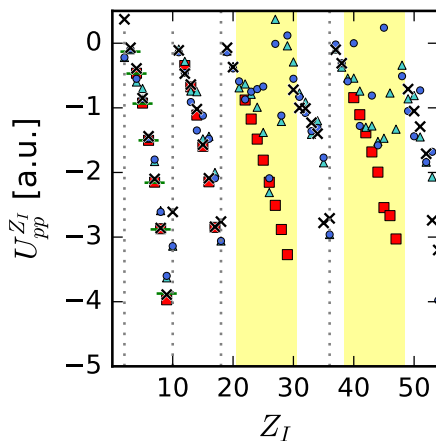


Figure 15: $U_{pp}^{Z_I}$ determined in a fit to *atomic* data in Refs. 183, 208 (red squares) and Ref. 209 (green dashes) and $U_{pp}^{Z_I}$ determined in a fit to *molecular* data for MNDO^{50,139} (black crosses), PM6⁵⁶ (light blue triangles), and PM7⁵⁷ (dark blue circles) for $Z_I = 2, 3, \dots, 54$. We highlight the transition metal blocks ($21 \leq Z_I \leq 30$, and $39 \leq Z_I \leq 48$) by a yellow background and we indicate Z_I of noble gases by vertical gray dashed lines.

7.3 General Parametrization Procedure

In general, parameters $\mathbf{p} = (p_1, p_2, \dots, p_p)^T$ are calibrated against a reference data set \mathcal{D} which comprises D data triples,

$$\mathcal{D} = \{(y_d, \mathbf{x}_d, w_d)\}, \quad \text{with } d = (1, 2, \dots, D), \quad (92)$$

consisting of (i) target observables y_d , (ii) input variables \mathbf{x}_d (e.g., atomic coordinates, charge, and spin multiplicity of a molecule), and (iii) weights w_d . Traditionally, the target observables are measured heats of formation $\Delta H_f^{298\text{K}}$ at 298 K,^{50,80,210} structural variables (bond distances or bond angles), dipole moments, and first vertical ionization potentials for a variety of molecules,^{50,56,57} or calculated electronic energy differences.^{211,212} The prediction of an observable by an NDDO-SEMO model, $f(\mathbf{x}_d, \mathbf{p})$, is determined by \mathbf{x}_d and \mathbf{p} . The parameter set \mathbf{p} is then calibrated through minimization of an error function \mathcal{E} which is evaluated from the sum of weighted square differences between y_d and $f(\mathbf{x}_d, \mathbf{p})$,^{50,56,57,152}

$$\mathcal{E} = \mathcal{E}_{\mathcal{D}}(\mathbf{p}) = \sum_{d=1}^D w_d [y_d - f(\mathbf{x}_d, \mathbf{p})]^2, \quad (93)$$

where w_d are the weights. The minimization of \mathcal{E} with respect to \mathbf{p} in a nonlinear ordinary least squares fit,

$$\frac{\partial \mathcal{E}_{\mathcal{D}}(\mathbf{p})}{\partial p_p} = 0, \quad \forall p_p \in \mathbf{p}, \quad (94)$$

yields an optimal parameter set $\mathbf{p}_{\mathcal{D}}$ with respect to the reference data set \mathcal{D} . Different optimization algorithms, e.g., the Levenberg–Marquardt algorithm,¹⁵² gradient-based methods,^{52,56,57} genetic algorithms,^{63,66,212–214} and line-search algorithms⁵⁰ can be straightforwardly applied for this task.

7.3.1 Applying Molecular Data Including Nuclear Effects as Reference Data

As we already noted, \mathcal{D} traditionally incorporates measured $\Delta H_f^{298\text{K}}$ for a variety of molecules.^{50,51,56,57} When applying an NDDO-SEMO model, $\Delta H_f^{298\text{K}}$ is usually predicted based on the electronic energies of the molecule and the constituent atoms, and the heats of formation of the atoms at 298 K, $\Delta H_{f,I}^{298\text{K}}$,^{50,80,210}

$$\Delta H_f^{298\text{K}} \approx E_{\text{el}}^{\{\tilde{\mathbf{R}}_I\}} + \sum_{I=1}^N \left(\Delta H_{f,I}^{298\text{K}} - E_{\text{el}}^{\tilde{\mathbf{R}}_I} \right). \quad (95)$$

The heat of formation of the atom at 298 K is taken from experimental data (for instance from Ref. 215). We can examine which approximations are included in Eq. (95) by comparing it with the standard expression to calculate $\Delta H_f^{298\text{K}}$ from first principles,²¹⁶

$$\Delta H_f^{298\text{K}} = E_{\text{el}}^{\{\tilde{\mathbf{R}}_I\}} + \text{ZPE} + H_{\text{rest}}(T) + \sum_{I=1}^N \left(\Delta H_{f,I}^{298\text{K}} - E_{\text{el}}^{\tilde{\mathbf{R}}_I} \right). \quad (96)$$

Compared to Eq. (95), Eq. (96) incorporates the zero-point energy (ZPE) and the temperature-dependent translational, rotational, and vibrational contributions (if coupling of degrees of freedom is neglected), $H_{\text{rest}}(T)$. Hence, the parameters of an NDDO-SEMO model must account for the neglect of ZPE and $H_{\text{rest}}(T)$ when calculating $\Delta H_f^{298\text{K}}$ according to Eq. (95). Consequently, an NDDO-SEMO electronic energy in a traditional parameterization *cannot* be considered a *pure* electronic energy. This is a very unsatisfactory situation from a theoretical point of view (as, e.g., also noted in Refs. 72,211,217). We would like to emphasize that, in principle, the standard protocol (Eq. (96)) and specialized approaches tailored toward SEMO models^{217,218} could be readily applied instead of Eq. (95).

Hicks and Thiel studied²¹¹ the severity of this conceptual inconsistency by reparametrizing MNDO with respect to electronic atomization energies ($\Delta E_{\text{el}}^{\text{at}}$),

$$\Delta E_{\text{el}}^{\text{at}} = E_{\text{el}}^{\{\tilde{\mathbf{R}}_I\}} - \sum_{I=1}^N E_{\text{el}}^{\tilde{\mathbf{R}}_I}. \quad (97)$$

Hicks and Thiel found²¹¹ that the errors between reference and predicted $\Delta H_f^{298\text{K}}$ and the errors between reference and predicted $\Delta E_{\text{el}}^{\text{at}}$ are similarly large. They therefore concluded²¹¹ that the errors are dominated by the error in the MNDO electronic energies rather than by the error caused by applying Eq. (95). Their study was, however, limited to 36 medium-sized hydrocarbon compounds. Later, it was found that the application of Eq. (95) in the parametrization process is the reason for poor results for very small (e.g., diatomic) and large compounds in comparison to medium-sized compounds^{96,219} (see, e.g., Figure 2 in Ref. 219). This is not surprising because \mathcal{D} is dominated by medium-sized organic compounds. The opinion that the most severe errors stem from the NDDO-SEMO model itself and not from the application of Eq. (95), however, persisted in the literature.²¹⁹

7.3.2 Dependence of $p_{\mathcal{D}}$ on \mathcal{D}

For the prediction of properties for molecules not included in \mathcal{D} , one needs to estimate the uncertainties of \mathbf{p} . We recently demonstrated^{220,221} how

to apply nonparametric bootstrapping^{222,223} in order to calibrate physicochemical property models with a limited amount of data and to determine the uncertainties of the incorporated parameters. Here, we re-optimize $\mathbf{p}^m = \{\beta_s^1, \beta_s^6, \beta_p^6\}$ for the MNDO model with respect to a model data set \mathcal{D}^m containing twelve measured ΔH_f^{298K} of hydrocarbon compounds (see Figure 16a). Starting from the MNDO values for \mathbf{p}^m , we determine the optimal parameter set $\mathbf{p}_{\mathcal{D}^m}^m$ by minimizing $\mathcal{E}_{\mathcal{D}^m}(\mathbf{p}^m)$ with the Nelder–Mead simplex algorithm. The application of nonparametric bootstrap sampling now enables the quantification of the dependence \mathbf{p}^m on the choice of \mathcal{D}^m . We generate $B = 1000$ bootstrap samples $\{\mathcal{D}_b^m\}$, $b = (1, 2, \dots, B)$ by drawing D elements with replacement at random from \mathcal{D}^m . For each bootstrap sample \mathcal{D}_b^m , we determine the optimal parameter set $\mathbf{p}_{\mathcal{D}_b^m}^m$ by minimizing $\mathcal{E}_{\mathcal{D}_b^m}(\mathbf{p}^m)$. We then determine the mean of the parameters $\bar{\mathbf{p}}_{\mathcal{D}^m}^m$ from all bootstrap samples,

$$\bar{\mathbf{p}}_{\mathcal{D}^m}^m = \frac{1}{B} \sum_{b=1}^B \mathbf{p}_{\mathcal{D}_b^m}^m. \quad (98)$$

Overall, $\bar{\mathbf{p}}_{\mathcal{D}^m}^m$ coincides nicely with $\mathbf{p}_{\mathcal{D}^m}^m$ and with the MNDO values. This means that we arrive at a very similar final parameter set, but we have gained significantly more knowledge from the parametrization procedure than from a fit to \mathcal{D}^m alone. Figure 16b shows the distribution of $\mathbf{p}_{\mathcal{D}_b^m}^m$ which we obtained for the B bootstrap samples $\{\mathcal{D}_b^m\}$. The parameters β_s^6 and β_p^6 differ

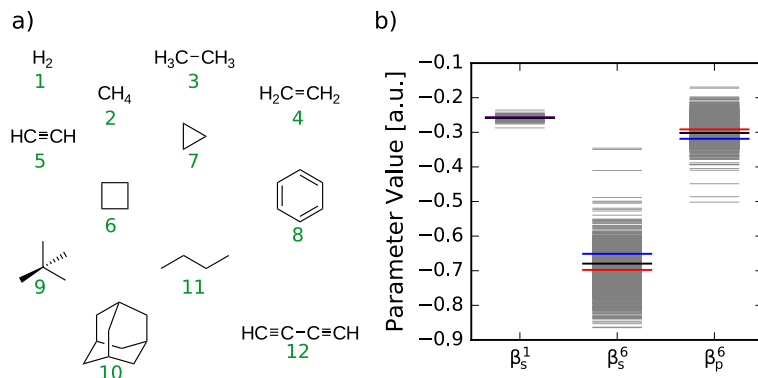


Figure 16: a) Model reference data set \mathcal{D}^m consisting of dihydrogen (1), methane (2), ethane (3), ethene (4), ethyne (5), cyclopropane (6), cyclobutane (7), benzene (8), neopentane (9), n-butane (10), adamantane (11), and 1,3-butadiene (12). b) MNDO parameter values (red lines), the $\mathbf{p}_{\mathcal{D}^m}^m$ values (blue lines), the B $\mathbf{p}_{\mathcal{D}_b^m}^m$ values (gray lines), and the $\bar{\mathbf{p}}_{\mathcal{D}^m}^m$ values (black lines) in a.u.

significantly when they are calibrated with respect to different \mathcal{D}_b^m (-0.87

a.u. $< \beta_s^6 < -0.33$ a.u. and -0.51 a.u. $< \beta_p^6 < -0.17$ a.u.). The parameter β_s^1 , by contrast, hardly varies for different \mathcal{D}_b^M (-0.29 a.u. $< \beta_s^1 < -0.24$ a.u.). Simply put, this means that we were not able to identify a single value for β_s^6 and β_p^6 which minimizes all different $\mathcal{E}_{\mathcal{D}_b^m}$. Rather, very different values for β_s^6 and β_p^6 are ideal to describe different \mathcal{D}_b^M . From the bootstrap samples, we can then also sample the model prediction uncertainty for the target property, ΔH_f^{298K} which yields very large 95% confidence intervals for all molecules in \mathcal{D}^m (> 20.0 kJ mol $^{-1}$, see Section 10.9).

The fact that there is no single transferable parameter set has been noted before.^{68,152,224} Scholten remarked that different parameter values are well-suited to describe different properties for the same set of reference molecules.¹⁵² The parametrization of the HpCADD model demonstrated that the parameters for hydrogen atoms vary by 406% when considering different environments.⁶⁸ Very recently, Oreluk *et al.* systematically assessed the variability of the PM7 parameters for a set of linear alkanes and came to the conclusion that no single set of parameters is consistent with the entire data set.²²⁴ Oreluk *et al.* propagated the uncertainties for the PM7 parameters to the prediction of heats of formations which then enables the attachment of an error bar to it.²²⁴

7.3.3 Insights from Benchmark Studies

Not surprisingly, NDDO-SEMO models are unable to describe systems with strong electron correlation. Such systems are, however, present in \mathcal{D} for some NDDO-SEMO models (see, e.g., the chromium dimer and CrO₃ which both exhibit a very strong multiconfigurational character²²⁵ are contained in the PM6 and PM7 reference data sets²²⁶). The inclusion of systems with strong electron correlation in \mathcal{D} may lead to a bias in \mathbf{p} which would at least partially explain the generally poor accuracy for transition-metal complexes. Despite significant efforts, it was not yet possible to create an NDDO-SEMO model which achieves a similar accuracy with respect to the reference data for transition-metal complexes as for organic compounds.^{56,57,227–231}

In this respect, we assess the performance of PM6 and PM7 for the WCCR10 set. The WCCR10 set²³³ contains ten ligand dissociation energies of large transition-metal complexes which feature different transition metals (Au, Ag, Pt, Ru, Cu, Pd) and a diverse selection of ligand environments. The PM6 and PM7 ligand dissociation energies deviate significantly (on average 130.6 kJ mol $^{-1}$ and 114.1 kJ mol $^{-1}$, respectively) from reference DLPNO-CCSD(T) ligand dissociation energies²³² (see Figure 17). While a deviation of PM6 and PM7 energies from DLPNO-CCSD(T) data is not particularly surprising, the severeness of the failure of PM6 and PM7 might be.

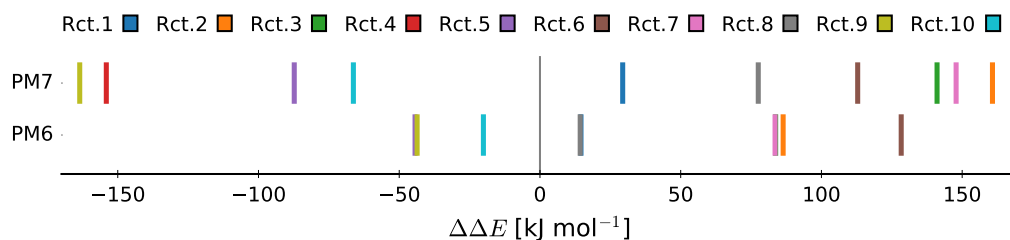


Figure 17: Deviation of electronic ligand dissociation energies ΔE in kJ mol^{-1} calculated with PM6 and PM7 from DLPNO-CCSD(T) energies²³² for the ten reactions in the WCCR10 set.²³³ We did not include $\Delta\Delta E = 786.8 \text{ kJ mol}^{-1}$ for reaction 4 for PM6 in this Figure.

The PM6 ligand dissociation energy for reaction 4, for instance, is strongly negative ($\Delta E = -579.8 \text{ kJ mol}^{-1}$).

Figure 18 shows that the PM7 structure of the charged product of reaction 1 is strongly distorted compared to the BP86/def2-QZVPP reference structure taken from Ref. 233 even though the deviation of the PM7 ligand dissociation energy from the DLPNO-CCSD(T) energy is only 29.4 kJ mol^{-1} for this reaction. In fact, the structures may be so severely distorted that a re-optimization with BP86/def2-QZVPP starting from the PM6 or PM7 optimized structures does not yield the original BP86/def2-QZVPP minimum-energy structures from which the PM6 and PM7 optimizations were started (e.g., reactant of reaction 9 in Figure 18). Great caution is therefore in order when applying NDDO-SEMO models to transition-metal complexes in general.

NDDO-SEMO models are mostly applied to study organic compounds which do not exhibit strong electron correlation. Recent benchmark studies show^{234,235} that OM x models with dispersion corrections are slightly superior to MNDO-type models. The performance of NDDO-SEMO models in extensive benchmark sets such as the GMTKN24 database²³⁴ is quite impressive considering their high computational efficiency (mean absolute deviation $< 33 \text{ kJ mol}^{-1}$ for OM3 at the GMTKN24 database²³⁴). Nevertheless, it is insightful to take a closer look at the distribution of the individual errors: It is not rare that a given NDDO-SEMO model either over- or underestimates relative electronic energies by over 80 kJ mol^{-1} (see, e.g., Figures 1–4 in Ref. 235). In special cases, the errors can be attributed to the insufficiency of the basis set (e.g., to explain the failure to describe nitro compounds²¹⁹) or to the absence of orthogonalization corrections in MNDO-type models (which is, e.g., assumed to be responsible for wrong rotation barriers²¹⁹). However,

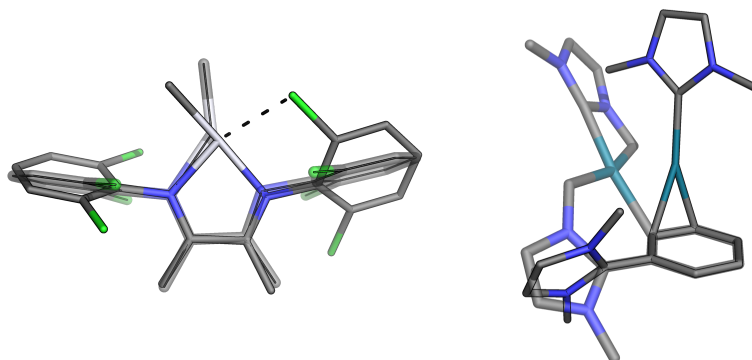


Figure 18: Overlay of the BP86/def2-QZVPP structure taken from Ref. 233 (solid) and the PM7 structure (translucent) of the charged product of reaction 1 (left) and of the reactant of reaction 9 (right) Element color code: carbon, gray; nitrogen, blue; chlorine, green; palladium, teal; platinum, silver. Hydrogen atoms are omitted for clarity.

it is basically impossible to rationalize why some error occurs in general due to the diversity of the approximations invoked in an NDDO-SEMO model.

7.3.4 Focused Reparameterization

A way to reduce the error is the restriction of the domain of applicability. Rossi and Truhlar proposed to adjust the parameters to describe specific reactions yielding specific reaction parameters.²¹² This approach has become more popular in recent years and parameters were adjusted to study specific compound classes and specific reactions (see, e.g., Refs. 67,236–244 and other references citing Ref. 212).

A focused reparameterization is, however, plagued by problems. Obviously, it cannot resolve systematic errors (cf. Section 7.1). Additionally, it may be difficult to curtail the domain of applicability adequately, i.e., to decide for a specific system whether it is similar enough to the ones for which it was parametrized. To define such a structure-based metric has been a long-standing goal in machine learning applied to chemistry²⁴⁵ and is related to the present problem. Strictly speaking, parameters are only valid for one arrangement of the atomic nuclei because they implicitly encode orthogonalization effects which, obviously, depend on the atomic nuclei. This statement is valid for all NDDO-SEMO models (even for the OM x models) because the parametric expressions are tuned to compensate for errors in $\phi\mathbf{G}$. Additionally, we might need different parameters for two atoms of the same element type in the same molecule (e.g., when they are encountered in

different local environments represented by different valence states). In the worst case, this means that we need to have separate parameters for every valence state of an atom in a molecule. It may be possible to define ‘atom types’ as proposed in Ref. 68. However, as a matter of principle it remains challenging to divide the atoms in a molecule into different atom types in a meaningful way. Moreover, when defining atom types, one obviously would inherit all of the problems associated with the definition of atom types from force-field development which does not appear particularly appealing for a method rooted in the first principles of quantum mechanics. The practical consequence of these considerations is that the number of parameters which we have to determine increases dramatically, e.g., in the case of MNDO with its six adjustable parameters per element to $6N$ parameters per molecule in the worst case which would bring SEMO models very close to machine-learning approaches. For standard static benchmark approaches that apply a fixed amount of pre-defined reference data, it is hardly imaginable how one could achieve a similar increase in the number of reference data so that we can determine \mathbf{p} in a well-defined manner (i.e., so that $D \gg p$).

7.4 Improving Parametric Functions

Contemporary NDDO-SEMO models have limitations which cannot be addressed by reparameterization and overcoming these limitations requires the adoption of novel parametric functions. Unfortunately, the NDDO approximation causes large and uncontrollable errors in the ERIs in the ϕ -basis and these errors propagate to all quantities calculated on the basis of the ERIs.^{104, 110–114, 116, 118–123} Contemporary NDDO-SEMO models counteract the errors by introducing parametric expressions to evaluate the one-electron matrix and the core-core repulsion energy, i.e., they rely on error cancellation.

This raises the question why one does not directly correct ${}^\phi\mathbf{G}$ or the ERIs in the ϕ -basis. A reason might be that the ERIs in the ϕ -basis, ${}^\phi\mathbf{G}$, and also ${}^x\mathbf{G}$ encode information on the whole molecule (cf. Eqs. (12), (15), and (17), respectively). By contrast, the contributions to ${}^x\mathbf{H}$ and V_v are straightforwardly transferable from molecule to molecule. It is therefore comparatively easy to develop transferable parametric expressions to model ${}^x\mathbf{H}$ and V_v on the examples of simple model systems (e.g., by considering diatomic systems). Unfortunately, approximating ${}^x\mathbf{H}$ and V_v well is not sufficient for the design of a reliable NDDO-SEMO model. Instead, the parametric expressions applied to approximate ${}^x\mathbf{H}$ and V_v need to be flexible enough to compensate for the errors in ${}^\phi\mathbf{G}$. Hence, we may anticipate that the improvement of the parametric expressions is as complicated as the direct correction for the error in ${}^\phi\mathbf{G}$.

We recently introduced¹¹⁶ a strategy to directly correct for the error caused by the NDDO approximation in $\phi\mathbf{G}$ which we call the correction inheritance for semiempirics (CISE) approach. We drew inspiration from the work carried out by Roby and Sinanoğlu who suggested¹⁰⁴ to scale ${}^x\mathbf{G}^{\text{NDDO}}$ with a scaling matrix $\mathbf{\Gamma}$ to obtain a better estimate for $\phi\mathbf{G}$,¹⁰⁴

$$\phi\mathbf{G} \approx \mathbf{\Gamma} {}^x\mathbf{G}^{\text{NDDO}}. \quad (99)$$

The goal of Roby and Sinanoğlu in 1969 was to speed up single-point HF calculations for a diverse set of small molecules, and hence, they attempted to define universal rules to assemble $\mathbf{\Gamma}$ which, not surprisingly, turned out to be impossible.¹⁰⁴ It is, however, possible to exactly determine $\mathbf{\Gamma}(\{\tilde{\mathbf{R}}_I^n\})$ for a given structure $\{\tilde{\mathbf{R}}_I^n\}$ from a reference self-consistent field (i.e., HF, KS-DFT, or general multi-configurational SCF) calculation (yielding the exact $\phi\mathbf{G}(\{\tilde{\mathbf{R}}_I^n\})$),

$$\mathbf{\Gamma}(\{\tilde{\mathbf{R}}_I^n\}) = \phi\mathbf{G}(\{\tilde{\mathbf{R}}_I^n\}) \cdot ({}^x\mathbf{G}^{\text{NDDO}}(\{\tilde{\mathbf{R}}_I^n\}))^{-1}. \quad (100)$$

Obviously, we will then not achieve a speed-up with respect to the reference calculation. We found¹¹⁶ that $\mathbf{\Gamma}(\{\tilde{\mathbf{R}}_I^n\})$ is transferable to a certain degree in a sequence of related structures, i.e., for two similar structures $\{\tilde{\mathbf{R}}_I^n\}$ and $\{\tilde{\mathbf{R}}_I^{(n+1)}\}$,

$$\phi\mathbf{G}(\{\tilde{\mathbf{R}}_I^{(n+1)}\}) \approx \mathbf{\Gamma}(\{\tilde{\mathbf{R}}_I^n\}) \cdot {}^x\mathbf{G}^{\text{NDDO}}(\{\tilde{\mathbf{R}}_I^{(n+1)}\}), \quad (101)$$

for which we achieved a speed-up at a negligible loss of accuracy. We also showed¹¹⁶ that a correction to ${}^x\mathbf{G}^{\text{NDDO}}(\{\tilde{\mathbf{R}}_I^{(n+1)}\})$ can be constructed in different ways, departing from a Roby–Sinanoğlu-type approach. We proposed¹¹⁶ to construct additive corrections $\mathbf{\Gamma}_J$ and $\mathbf{\Gamma}_K$ to the matrices ${}^x\mathbf{J}^{\text{NDDO}}$ and to ${}^x\mathbf{K}^{\text{NDDO}}$, respectively,

$$\begin{aligned} \phi\mathbf{G}(\{\tilde{\mathbf{R}}_I^{(n+1)}\}) &\approx \mathbf{\Gamma}_J(\{\tilde{\mathbf{R}}_I^n\}) + {}^x\mathbf{J}^{\text{NDDO}}(\{\tilde{\mathbf{R}}_I^{(n+1)}\}) \\ &+ \mathbf{\Gamma}_K(\{\tilde{\mathbf{R}}_I^n\}) + {}^x\mathbf{K}^{\text{NDDO}}(\{\tilde{\mathbf{R}}_I^{(n+1)}\}). \end{aligned} \quad (102)$$

The CISE approach has a potential for application whenever we are interested in obtaining electronic energies for sequences of related structures, e.g., in the context of kinetic modeling,^{246–249} in real-time^{35,36,38} and automated^{250–256} reaction-mechanism explorations, or in reaction and first-principles^{257–259} molecular dynamics simulations. The CISE approach differs conceptually from the existing NDDO-SEMO models insofar as that no determination of parameters in a statistical calibration is required. Instead, we maintain complete error control on the resulting model because we could

straightforwardly determine $\Gamma(\{\tilde{\mathbf{R}}_I^{(n+1)}\})$ for a given molecule with nuclear coordinates $\{\tilde{\mathbf{R}}_I^{(n+1)}\}$. By contrast, we cannot straightforwardly determine the best $\mathbf{p}(\{\tilde{\mathbf{R}}_I^{(n+1)}\})$ for the molecule $n + 1$ for contemporary NDDO-SEMO models.

8 Explicit Description of Electron Correlation Effects

The last question which we address in this work is whether one could, in principle, obtain FCI quality results in a given one-electron basis when applying an NDDO-SEMO reference wave function. It was suggested that all of the developed wave function methods can be (and many have been^{73,260-270}) straightforwardly applied after carrying out an NDDO-SEMO calculation which then essentially substitutes the HF calculation. It is, however, important to recognize that the NDDO approximation affects the ERIs over the molecular orbitals,

$$\begin{aligned} \langle \psi_i \psi_j | \psi_k \psi_l \rangle &= \sum_{\mu=1}^M \sum_{\nu=1}^M \sum_{\lambda=1}^M \sum_{\sigma=1}^M \phi C_{\mu i} \phi C_{\nu j} \langle \phi_\mu \phi_\nu | \phi_\lambda \phi_\sigma \rangle \phi C_{\lambda k} \phi C_{\sigma l} \\ &\approx \sum_{\mu=1}^M \sum_{\nu=1}^M \sum_{\lambda=1}^M \sum_{\sigma=1}^M \phi C_{\mu i} \phi C_{\nu j} \delta_{IJ} \delta_{KL} \langle \chi_\mu^I \chi_\nu^J | \chi_\lambda^K \chi_\sigma^L \rangle \phi C_{\lambda k} \phi C_{\sigma l}. \end{aligned} \tag{103}$$

Previous results by Thiel and co-workers and Clark and co-workers showed that the correlation energy calculated with single-reference perturbation theories evaluated for an NDDO-SEMO reference is about one order of magnitude too small,^{73,261,262} which was also corroborated by our recent results.¹¹⁶ If we do not explicitly correct for the errors caused by the NDDO approximation, we will not be able to adequately capture dynamic electron correlation effects and we must rely on the proper calibration of the parameters to achieve this.

It is no surprise that single-determinantal NDDO-SEMO models do not adequately capture static electron correlation effects and that static electron correlation effects have to be considered explicitly.^{260,271} Static electron correlation effects may be described through a multi-reference configuration interaction (MR-CI) procedure (including single and double excitations) using the graphical unitary group approach (GUGA).²⁶³⁻²⁶⁷ Another approach is the application of an unrestricted natural orbital complete active space

(UNO-CAS) or configuration interaction (UNO-CI) ansatz.²⁶⁹ Such methods are usually applied to describe excited states and the dynamics of excited states. Note that all NDDO-SEMO models apply a valence-shell minimal basis sets which prevents a description of Rydberg states.⁵⁰ Usually, MNDO-type models tend to underestimate excited-state energies due to the symmetric splitting of bonding and antibonding orbitals (see also Section 4.3), whereas OM*x* models showed an overall good performance.^{260, 272, 273}

An open question in the NDDO-SEMO/MR-CI approaches is whether contributions to the correlation energy may be doubly counted. We may draw the parallel to KS-DFT as it was combined with MR-CI where a similar issue arises.^{274, 275} The main problem of KS-DFT/MR-CI is the double counting of the correlation energy which can be alleviated through the introduction of empirical parameters.^{274, 275} Similar measures have apparently not been taken when combining NDDO-SEMO models with MR-CI approaches. Recent benchmarks show, however, that double counting and the error caused by the NDDO approximation in the ERIs over molecular orbitals appear not to be an issue in practice.²⁷³

9 The Future of NDDO-SEMO Models

The success of NDDO-SEMO models is largely based on the effectiveness with which they allow one to solve the SCF equations. Contemporary NDDO-SEMO models yield electronic energies about three orders of magnitude faster than HF or KS-DFT models.⁴¹ The acceleration is largely due to the NDDO approximation which drastically reduces the number of ERIs to be computed and processed in the course of a calculation. The price to pay for the acceleration are significant errors in the ERIs in the Löwdin orthogonalized basis. As a consequence, the NDDO approximation must be tied to many other approximations in the one-electron matrix and in the core-core repulsion energy to define a meaningful NDDO-SEMO model. In this work, we presented a comprehensive overview of the parametric expressions applied in the MNDO-type (MNDO, MNDO/d, AM1, PM3, PM6, PM7, and RM1) and OM*x* models.

We outlined the systematic limitations which NDDO-SEMO model face. First, severe limitations are caused by the application of a small basis set. The drastic restriction of the basis set size will, in general, prohibit the determination of accurate relative electronic energies, force constants, and polarizabilities. The increase of the basis set size is, however, challenging within the framework of contemporary NDDO-SEMO models for practical reasons. Second, systematic errors are caused by the adoption of a parametrized mean-

field framework. The examination of the parallels to KS-DFT revealed that NDDO-SEMO models fail to describe the general behavior of electronic energy as a function of the electron number, in the same way as in HF and KS-DFT models. We may therefore anticipate that NDDO-SEMO models will be plagued by the same difficulties in describing electron correlation, irrespective of their specific parametrization.

In general, the parameters of NDDO-SEMO models are calibrated with respect to experimental reference data. When calibrating the parameters, one first encounters difficulties associated with the current practice of calculating heats of formation which leads to a contamination of the parameters with nuclear-motion contributions. Consequently, the electronic energy calculated with an NDDO-SEMO model cannot be considered a pure electronic energy which, however, does not appear to have severe practical consequences. This conceptual inconsistency could simply be alleviated by adjusting the parametrization procedure. Recent benchmark studies^{234, 235} showed that NDDO-SEMO models are notoriously unreliable. Large errors are observed^{234, 235} for molecules which do not show any apparent strong electron correlation. This may be partially explained by the fact that it is highly unlikely that there is a single parameter set which is suited to describe all molecules. We believe that bootstrap sampling^{220–222, 249, 276} offers an interesting insight into the parameterization of NDDO-SEMO models. When recalibrating a selection of parameters of the MNDO model in this work, we discovered that the parameters have to adopt significantly different values to describe different molecules well.

We briefly reviewed our recent proposal for system-focused NDDO-SEMO models that yield accurate results for structures related to a reference structure. Our CISE approach has the advantage that we are able to determine the parametrization of a corrective matrix directly for a given structure from a reference calculation. We, hence, do not have to apply a statistical procedure to calibrate parameters. This convenience obviously comes at the cost that the approach is restricted to the investigation of sequences of related structures which, however, are key areas of application for NDDO-SEMO models (e.g., structure optimization, Born–Oppenheim molecular dynamics, and real-time reactivity exploration).

To conclude this overview, we would like to stress that the age of NDDO-SEMO models is far from being over. Although we pointed out several (conceptual and practical) difficulties, we want to highlight again that contemporary NDDO-SEMO models achieve, overall, a remarkably high accuracy with respect to experimental data. To make NDDO-SEMO models useful for predictive work, we, however, have to know when, and why, they fail. This may, for instance, be achieved through statistical learning models.^{277, 278}

Acknowledgements

This work was supported by the Schweizerischer Nationalfonds. We are grateful to Professor Tim Clark for drawing our attention to the undocumented 6 kcal/mol correction in MOPAC and for providing information on AM1* that allowed us to implement this approach. The authors thank Professors Walter Thiel, Alexander A. Voityuk, and Jens Spanget-Larsen for helpful discussions.

10 Appendix

10.1 Computational Methodology

We implemented the MNDO(/d), AM1(/d), PM3, PM6, OM1, OM2, and OM3 models in our cross-platform quantum chemistry package SCINE.²⁷⁹ This new module of SCINE, SCINESEMO, will be made available on our Web page and can be applied as a stand-alone SEMO program or within the SCINE framework.

We evaluated ERIs in the χ -basis with PYSCF (version 1.4).^{280,281} The ERIs in the χ -basis were transformed to the corresponding ERIs in the ϕ -basis with the AO2MO integral transformation module of PYSCF.

Lastly, we evaluated heat of formations at 298 K with MOPAC 2016¹⁷⁸ in the course of the re-optimization of the parameters. We specified nonstandard parameters given in Table 10 through the keyword ‘EXTERNAL’.

10.2 Basic Specifications

The MNDO-type models, MNDO,⁵⁰ MNDO/d,^{53,54} AM1,⁵¹ PM3,⁵² RM1,⁵⁵ PM6,⁵⁶ and PM7 are freely available in the MOPAC program.¹⁷⁸ Throughout this work, MOPAC served as our reference implementation for these NDDO-SEMO models because the parameters for the PM x ^{52,56,57} and RM1⁵⁵ models and for many elements for the MNDO(/d) and AM1 models¹³⁹ were determined with MOPAC.

In this work, we uncovered inconsistencies in the equations which we found implemented in many programs, also in MOPAC. Note that it is not easily possible altering the implementation because the parameterization of the NDDO-SEMO models was carried out with a specific set of equations. Instead, one would have to determine a new set of parameters when implementing another set of equations. Implementations of MNDO-type models are also available in other programs. If one wishes to check if an MNDO

model is implemented in the same way as in MOPAC, one can compare the parameter values and the values of the one- and two-center ERIs to the ones provided by MOPAC when invoking the keyword `Hcore`.

The parameters for the OMx models were determined with the (not freely available) MNDO2005 program.²⁸² We verified our implementation of the OMx models by comparison to numerical data provided in Refs. 58–60, 151, 152, 235.

A calculation with an NDDO-SEMO model requires the specification of the number of explicitly considered electrons n_v , of the basis functions which are activated, and of a set of parameters for every element in the system of interest. We specify these quantities in Table 1 for the MNDO,⁵⁰ MNDO/d,^{53,54} AM1,⁵¹ AM1*,^{51,167–169,171–176,283–285} PM3,⁵² RM1,⁵⁵ PM6,⁵⁶ PM7,⁵⁷ OM1,⁵⁸ OM2,⁵⁹ and OM3⁶⁰ models.

Table 1: Nuclear charge Z , number of explicitly considered electrons n_v , and type of basis functions activated for each element ($1 \leq Z \leq 57$ and $71 \leq Z \leq 83$) in semiempirical models.

Element	Availability of Parameters	Z	n_v	Basis Functions
H	MNDO(/d), AM1, AM1*, PM3, PM6, PM7, RM1, OM1, OM2, OM3	1	1	1s
He	MNDO(/d), AM1, PM3, PM6, PM7	2	2	1s, 2p
Li	MNDO(/d), AM1, PM3, PM6, PM7	3	1	2s, 2p
Be	MNDO(/d), AM1, PM3, PM6, PM7	4	2	2s, 2p
B	MNDO(/d), AM1*, PM3, PM6, PM7	5	3	2s, 2p
C	MNDO(/d), AM1, AM1*, PM3, PM6, PM7, RM1, OM1, OM2, OM3	6	4	2s, 2p
N	MNDO(/d), AM1, AM1*, PM3, PM6, PM7, RM1, OM1, OM2, OM3	7	5	2s, 2p
O	MNDO(/d), AM1, AM1*, PM3, PM6, PM7, RM1, OM1, OM2, OM3	8	6	2s, 2p
F	MNDO(/d), AM1, AM1*, PM3, PM6, PM7, RM1, OM1, OM2, OM3	9	7	2s, 2p
Ne	MNDO(/d), AM1, PM3, PM6, PM7	10	6	2p, 3s
Na	MNDO(/d), AM1, PM3, PM6, PM7	11	1	3s, 3p
Mg	MNDO(/d), AM1, PM3, PM6, PM7	12	2	3s, 3p
Al	MNDO, AM1, PM3	13	3	3s, 3p
	MNDO/d, AM1*, PM6, PM7	13	3	3s, 3p, 3d
Si	MNDO, AM1, PM3	14	4	3s, 3p
	MNDO/d, AM1*, PM6, PM7	14	4	3s, 3p, 3d

Element	Availability of Parameters	Z	n_v	Basis Functions
P	MNDO, AM1, PM3, RM1	15	5	$3s, 3p$
	MNDO/d, AM1*, PM6, PM7	15	5	$3s, 3p, 3d$
S	MNDO, AM1, PM3, RM1	16	6	$3s, 3p$
	MNDO/d, AM1*, PM6, PM7	16	6	$3s, 3p, 3d$
Cl	MNDO, AM1, PM3, RM1	17	7	$3s, 3p$
	MNDO/d, AM1*, PM6, PM7	17	7	$3s, 3p, 3d$
Ar	MNDO, AM1, PM3, PM6, PM7	18	6	$3p, 4s$
K	MNDO, AM1, PM3, PM6, PM7	19	1	$4s, 4p$
Ca	MNDO, AM1, PM3, PM6, PM7	20	2	$4s, 4p$
Sc	PM6, PM7	21	3	$3d, 4s, 4p$
Ti	AM1*, PM6, PM7	22	4	$3d, 4s, 4p$
V	AM1*, PM6, PM7	23	5	$3d, 4s, 4p$
Cr	AM1*, PM6, PM7	24	6	$3d, 4s, 4p$
Mn	AM1*, PM6, PM7	25	7	$3d, 4s, 4p$
Fe	AM1*, PM6, PM7	26	8	$3d, 4s, 4p$
Co	AM1*, PM6, PM7	27	9	$3d, 4s, 4p$
Ni	AM1*, PM6, PM7	28	10	$3d, 4s, 4p$
Cu	AM1*, PM6, PM7	29	11	$3d, 4s, 4p$
Zn	MNDO, AM1, PM3, PM6, PM7	30	2	$4s, 4p$
	AM1*	30	12	$3d, 4s, 4p$
Ga	MNDO, AM1, PM3, PM6, PM7	31	3	$4s, 4p$
Ge	MNDO, AM1, PM3, PM6, PM7	32	4	$4s, 4p$
As	MNDO, AM1, PM3	33	5	$4s, 4p$
	PM6, PM7	33	5	$4s, 4p, 4d$
Se	MNDO, AM1, PM3, PM6, PM7	34	6	$4s, 4p, 4d$
Br	MNDO, AM1, PM3, RM1	35	7	$4s, 4p$
	MNDO/d, AM1*, PM6, PM7	35	7	$4s, 4p, 4d$
Kr	MNDO, AM1, PM3, PM6, PM7	36	6	$4p, 5s$
Rb	MNDO, AM1, PM3, PM6, PM7	37	1	$5s, 5p$
Sr	MNDO, AM1, PM3, PM6, PM7	38	2	$5s, 5p$
Y	PM6, PM7	39	3	$4d, 5s, 5p$
Zr	AM1*, PM6, PM7	40	4	$4d, 5s, 5p$
Nb	PM6, PM7	41	5	$4d, 5s, 5p$
Mo	AM1*, PM6, PM7, AM1	42	6	$4d, 5s, 5p$
Tc	PM6, PM7	43	7	$4d, 5s, 5p$
Ru	PM6, PM7	44	8	$4d, 5s, 5p$
Rh	PM6, PM7	45	9	$4d, 5s, 5p$
Pd	AM1*, PM6, PM7	46	10	$4d, 5s, 5p$
Ag	AM1*, PM6, PM7	47	11	$4d, 5s, 5p$

Element	Availability of Parameters	Z	n_v	Basis Functions
Cd	MNDO/d, PM3, PM6, PM7	48	2	$5s, 5p$
In	MNDO, AM1, PM3, PM6, PM7	49	3	$5s, 5p$
Sn	MNDO, AM1, PM3, PM6, PM7	50	4	$5s, 5p$
Sb	MNDO, AM1, PM3	51	5	$5s, 5p$
	PM6, PM7	51	5	$5s, 5p, 5d$
Te	MNDO, AM1, PM3, PM6, PM7	52	6	$5s, 5p, 5d$
I	MNDO, AM1, PM3, RM1	53	7	$5s, 5p$
	MNDO/d, AM1*, PM6, PM7	53	7	$5s, 5p, 5d$
Xe	MNDO, AM1, PM3, PM6, PM7	54	6	$5p, 6s$
Cs	MNDO, AM1, PM3, PM6, PM7	55	1	$6s, 6p$
Ba	MNDO, AM1, PM3, PM6, PM7	56	2	$6s, 6p$
La	PM6, PM7	57	3	$5d, 6s, 6p$
Lu	PM6, PM7	71	3	$5d, 6s, 6p$
Hf	PM6, PM7	72	4	$5d, 6s, 6p$
Ta	PM6, PM7	73	5	$5d, 6s, 6p$
W	PM6, PM7	74	6	$5d, 6s, 6p$
Re	PM6, PM7	75	7	$5d, 6s, 6p$
Os	PM6, PM7	76	8	$5d, 6s, 6p$
Ir	PM6, PM7	77	9	$5d, 6s, 6p$
Pt	PM6, PM7	78	10	$5d, 6s, 6p$
Au	AM1*, PM6, PM7	79	11	$5d, 6s, 6p$
Hg	MNDO(/d), AM1, PM3, PM6, PM7	80	2	$6s, 6p$
Tl	MNDO, AM1, PM3, PM6	81	3	$6s, 6p$
	PM7	81	3	$6s, 6p, 6d$
Pb	MNDO, AM1, PM3, PM6, PM7	82	4	$6s, 6p$
Bi	MNDO, AM1, PM3, PM6	83	5	$6s, 6p$
	PM7	83	5	$6s, 6p, 6d$

While we mostly adhered to the original parameter abbreviations, we chose to re-name several parameters to avoid confusion with other quantities. The NDDO-SEMO models were developed independently of each other, and hence, they also sometimes apply different parameter names. We indicate in Tables 2 and 3 how the parameter abbreviations introduced in the main text relate to the ones chosen in several popular publications.

Table 2: Relation of the parameter abbreviations introduced in the main text for MNDO-type models to the ones chosen in several popular publications.

Main Text	MOPAC ¹⁷⁸	MNDO ⁵⁰	AM1 ⁵¹	AM1* ^{168,169}	MNDO/d ^{53,54}	PM6, ⁵⁶ PM7 ⁵⁷
U_{ss}	USS	U_{ss}	U_{ss}	U_{ss}	U_{ss}	U_{ss}
U_{pp}	UPP	U_{pp}	U_{pp}	U_{pp}	U_{pp}	U_{pp}
U_{dd}	UDD	—	—	U_{dd}	U_{dd}	U_{dd}
ζ_s	ZS	ζ	ζ_s	ζ_s	ζ_s	ζ_s
ζ_p	ZP	ζ	ζ_p	ζ_p	ζ_p	ζ_p
ζ_d	ZD	—	—	ζ_d	ζ_d	ζ_d
β_s	BETAS	β_s	β_s	β_s	β_s	β_s
β_p	BETAP	β_p	β_p	β_p	β_p	β_p
β_d	BETAD	—	—	β_d	β_d	β_d
γ_{ss}	GSS	g_{ss}	g_{ss}	g_{ss}	g_{ss}	g_{ss}
γ_{pp}	GPP	g_{pp}	g_{pp}	g_{pp}	g_{pp}	g_{pp}
γ_{sp}	GSP	g_{sp}	g_{sp}	g_{sp}	—	g_{sp}
γ_{pp}'	GP2	g_{p2}	g_{p2}	g_{p2}	—	g_{p2}
$\tilde{\gamma}_{sp}$	HSP	h_{sp}	h_{sp}	h_{sp}	—	h_{sp}
ζ_s'	ZSN	—	—	z_{sn}	$\tilde{\zeta}_s$	z_{sn}
ζ_p'	ZPN	—	—	z_{pn}	$\tilde{\zeta}_p$	z_{pn}
ζ_d'	ZDN	—	—	z_{dn}	$\tilde{\zeta}_d$	z_{dn}
ϑ	P09	—	—	$\rho(\text{core})$	q_{core}	$\rho(\text{core})$
K_a	FN1a	—	K_a	—	—	a
L_a	FN2a	—	L_a	—	—	b
M_a	FN3a	—	M_a	—	—	c
α	ALP	α	α	—	α	—
α'	ALPB	—	—	α_{ij}	—	α
x	XFAC	—	—	δ_{ij}	—	χ

Table 3: Relation of the parameter abbreviations introduced in the main text for OM x models to the ones chosen in several popular publications.

Main Text	OM1 ⁵⁸	OM2 ⁵⁹	OM3 ⁶⁰
U_{ss}	U_{ss}	U_{ss}	U_{ss}
U_{pp}	U_{pp}	U_{pp}	U_{pp}
Scaling factor	ζ	ζ	ζ
Scaling factor for core orbitals	—	ζ_α	ζ_α
$b_{l(\mu)}$	$\beta_{l(\mu)}$	$\beta_{l(\mu)}$	$\beta_{l(\mu)}$
$a_{l(\mu)}$	$\alpha_{l(\mu)}$	$\alpha_{l(\mu)}$	$\alpha_{l(\mu)}$
W	—	$F_{\alpha\alpha}$	$F_{\alpha\alpha}$
F_1	γ_1	F_1	F_1
F_2	γ_2	F_2	—
G_1	—	G_1	G_1
G_2	—	G_2	—

Furthermore, Thiel and co-workers denote $\theta(\chi_\mu^I, \chi_\lambda^J)$ with $\beta_{\mu\lambda}$ in Refs. 58–60, 152 and $\eta(\chi_\mu^I, \chi_\lambda^J)$ is denoted as⁵⁸ $H_{\mu\mu}^{IJ}$ or as^{59,60,152} $H_{\mu\mu,J}^{\text{loc}}$.

10.3 Parametrization of One-Center ERIs

The one-center ERI $\langle p^I p^I | p^I p^I \rangle$ is calculated from γ_{pp}^{ZI} and $\gamma_{pp'}^{ZI}$ with Eq. (37). A practical issue with Eq. (37) arises when $\gamma_{pp}^{ZI} < \gamma_{pp'}^{ZI}$ so that $\langle p^I p^I | p^I p^I \rangle$ is negative. In this case, it will not be possible to determine a parameter necessary to calculate the distance D_Q in the quadrupole moments according to Eq. (113) because the applied numerical procedure will not converge. The search for the parameter value was terminated after 5 iterations in MOPAC²⁸⁶ even if it had not converged yet which is likely the reason why this failure has not been detected yet.

This is not a practical issue in the original MNDO model,⁵⁰ in the original MNDO/d model,⁵³ in the original AM1 model,⁵¹ the RM1 model,⁵⁵ or the OM*x* models.^{58–60}

In the following, we list the elements and NDDO-SEMO models for which we encountered negative $\langle p^I p^I | p^I p^I \rangle$ in MOPAC:

- MNDO — Ga, Sr, Xe, Ba, and Tl¹³⁹
- AM1 — Li, Be, Mg, Ga, Sr, Sb, Xe, Ba, and Tl¹³⁹
- PM3 — Be,⁵² Mg,²⁸⁷ Rb,¹³⁹ Sr,¹³⁹ Xe, Cs,¹³⁹ Ba,¹³⁹ Hg,²⁸⁷ and Tl²⁸⁷
- PM6 — He, Be, F, Ne, Na, Mg, Ar, K, Ca, Ga, Kr, Sr, In, Xe, Hg, and Tl⁵⁶
- PM7 — He, B, Be, F, Ne, Na, Mg, Ar, K, Ca, Ga, Kr, Sr, In, Xe, Hg, and Pb⁵⁷

10.4 Evaluation of Two-Center ERIs in MNDO-type Models with an *s, p* basis set

The two-center ERIs $\langle \chi_\mu^I \chi_\nu^I | \chi_\lambda^J \chi_\sigma^J \rangle$, $I \neq J$ can be interpreted as the electrostatic interaction between a charge distribution $\chi_\mu^I \chi_\nu^I$ centered on atom *I* and a charge distribution $\chi_\lambda^J \chi_\sigma^J$ centered on atom *J*. The different possible charge distributions $\chi_\mu^I \chi_\nu^I$ in the *s, p* minimal valence-shell basis are listed in Table 4. Each charge distribution is approximately represented as a truncated classical multipole expansion of $T_{\mu\nu}$ multipoles $\Theta_t^{\mu\nu}$, $t = (1, 2, \dots, T_{\mu\nu})$.⁴⁹

The two-center ERI is then approximated as the electrostatic interaction energy $U(\Theta_t^{\mu\nu}, \Theta_s^{\lambda\sigma})$ of the $T_{\mu\nu}$ multipoles $\Theta_t^{\mu\nu}$ specified for $\chi_\mu^I \chi_\nu^I$ with the $T_{\lambda\sigma}$ multipoles $\Theta_s^{\lambda\sigma}$ specified for $\chi_\lambda^J \chi_\sigma^J$,

$$\langle \chi_\mu^I \chi_\nu^I | \chi_\lambda^J \chi_\sigma^J \rangle \approx \sum_{t=1}^{T_{\mu\nu}} \sum_{s=1}^{T_{\lambda\sigma}} U(\Theta_t^{\mu\nu}, \Theta_s^{\lambda\sigma}). \quad (104)$$

The multipoles $\Theta_t^{\mu\nu}$ may be a monopole q^I , a dipole $\mu_{x,y,z}^I$, a linear quadrupole $Q_{xx,yy,zz}^I$, and a square quadrupole $Q_{xy,xz,yz}^I$ (see also Figure 3 in the main text). Table 4 indicates which multipoles $\Theta_t^{\mu\nu}$ appear in the multipole expansion for the charge distribution $\chi_\mu^I \chi_\nu^I$.

Table 4: Number of multipoles $T_{\mu\nu}$ and types of multipoles applied to represent the charge distribution $\chi_\mu^I \chi_\nu^I$ in an s, p basis.

Charge Distribution	$T_{\mu\nu}$	Multipoles
$s^I s^I$	1	q^I
$p_x^I p_x^I$	2	q^I, Q_{xx}^I
$p_y^I p_y^I$	2	q^I, Q_{yy}^I
$p_z^I p_z^I$	2	q^I, Q_{zz}^I
$s^I p_x^I$	1	μ_x^I
$s^I p_y^I$	1	μ_y^I
$s^I p_z^I$	1	μ_z^I
$p_x^I p_y^I$	1	Q_{xy}^I
$p_x^I p_z^I$	1	Q_{xz}^I
$p_y^I p_z^I$	1	Q_{yz}^I

The specification of the positions of the point charges which make up the dipoles and the quadrupoles necessitates the specification of $D_{\mu,sp}$ and $D_{Q,pp}$ (see also Figure 3 in the main text). In the main text, we denoted $D_{\mu,sp}$ and $D_{Q,pp}$ as D_μ and D_Q , respectively, to keep the notation uncluttered. When an s, p, d basis set is considered (see Section 10.5), we need to specify additional subscript identifiers indicating which kind of charge distribution is approximated. The distances $D_{\mu,sp}$ and $D_{Q,pp}$ between the point charges are chosen such that the multipole moment of the point charge configuration approximates the one of the corresponding charge distribution.⁴⁹ We first need to introduce the function $A(\chi_\mu^I, \chi_\nu^I, a)$,⁵³

$$A(\chi_\mu^I, \chi_\nu^I, a) = (2\zeta_\mu)^{n_\mu + \frac{1}{2}} (2\zeta_\nu)^{n_\nu + \frac{1}{2}} (\zeta_\mu + \zeta_\nu)^{-n_\mu - n_\nu - a - 1} [(2n_\mu)! (2n_\nu)!]^{-\frac{1}{2}} (n_\mu + n_\nu + a)!, \quad (105)$$

where ζ_μ is the orbital exponent of χ_μ^I , n_μ is the principal quantum number associated with χ_μ^I , and a characterizes the angular momentum of the multipole ($a \in \{0, 1, 2, \dots\}$). The distances $D_{\mu,sp}$ and $D_{Q,pp}$ are then given by^{49,53}

$$D_{\mu,sp} = 3^{-\frac{1}{2}} A(\chi_\mu^I, \chi_\nu^I, 1) \quad (106)$$

and

$$D_{Q,pp} = 5^{-\frac{1}{2}} \sqrt{A(\chi_\mu^I, \chi_\nu^I, 2)}, \quad (107)$$

respectively. The implementation of the formulae to calculate $D_{\mu,sp}$ and $D_{Q,pp}$ can be verified by comparison of $D_{\mu,sp}$ and $D_{Q,pp}$ to DD2 and DD3, respectively, which MOPAC provides when specifying the keyword HCORE.

When comparing our implementation to MOPAC, we noticed that the MNDO-type models, in which s - and p -type basis functions with different principal quantum numbers ($n_s \neq n_p$) are activated for an atom (i.e., for He, Ne, Ar, Kr, and Xe; see Table 1), do not actually apply the different principal quantum numbers to evaluate $D_{\mu,sp}$ and $D_{Q,pp}$. Instead, only the lower principal quantum number is applied.

With the help of $D_{\mu,sp}$ and $D_{Q,pp}$, we can specify the positions and charges of the C individual point charges q_c , $c = (1, 2, \dots, C)$ of the multipoles relative to the atom I on which the charge distribution $\chi_\mu^I \chi_\nu^I$ is centered (see Table 5).

Table 5: Specification of the position $\mathbf{r}_c = (r_{c,x}, r_{c,y}, r_{c,z})$ of the C point charges q_c , $c = (1, 2, \dots, C)$ chosen to represent a specific multipole (Table 4). The total number of point charges C is given in brackets after the specification of the multipole. The positions \mathbf{r}_c are given in relation to the origin of the local coordinate system (Section 10.6). The charges q_c are given in atomic units, i.e., as multiples of the elementary charge.

Multipole	$r_{c,x}$	$r_{c,y}$	$r_{c,z}$	q_c
q ($C = 1$)	0.0	0.0	0.0	+1.00
μ_x ($C = 2$)	$-D_{\mu,sp}$	0.0	0.0	-0.50
	$+D_{\mu,sp}$	0.0	0.0	+0.50
μ_y ($C = 2$)	0.0	$-D_{\mu,sp}$	0.0	-0.50
	0.0	$+D_{\mu,sp}$	0.0	+0.50
μ_z ($C = 2$)	0.0	0.0	$-D_{\mu,sp}$	-0.50
	0.0	0.0	$+D_{\mu,sp}$	+0.50
Q_{xx} ($C = 3$)	$-2D_{Q,pp}$	0.0	0.0	+0.25
	$+2D_{Q,pp}$	0.0	0.0	+0.25
	0.0	0.0	0.0	-0.50

Multipole	$r_{c,x}$	$r_{c,y}$	$r_{c,z}$	q_c
$Q_{yy} (C = 3)$	0.0	$-2D_{Q,pp}$	0.0	+0.25
	0.0	$+2D_{Q,pp}$	0.0	+0.25
	0.0	0.0	0.0	-0.50
$Q_{zz} (C = 3)$	0.0	0.0	$-2D_{Q,pp}$	+0.25
	0.0	0.0	$+2D_{Q,pp}$	+0.25
	0.0	0.0	0.0	-0.50
$Q_{xy} (C = 4)$	$+D_{Q,pp}$	$+D_{Q,pp}$	0.0	+0.25
	$-D_{Q,pp}$	$-D_{Q,pp}$	0.0	+0.25
	$+D_{Q,pp}$	$-D_{Q,pp}$	0.0	-0.25
	$-D_{Q,pp}$	$+D_{Q,pp}$	0.0	-0.25
$Q_{xz} (C = 4)$	$+D_{Q,pp}$	0.0	$+D_{Q,pp}$	+0.25
	$-D_{Q,pp}$	0.0	$-D_{Q,pp}$	+0.25
	$+D_{Q,pp}$	0.0	$-D_{Q,pp}$	-0.25
	$-D_{Q,pp}$	0.0	$+D_{Q,pp}$	-0.25
$Q_{yz} (C = 4)$	0.0	$+D_{Q,pp}$	$+D_{Q,pp}$	+0.25
	0.0	$-D_{Q,pp}$	$-D_{Q,pp}$	+0.25
	0.0	$+D_{Q,pp}$	$-D_{Q,pp}$	-0.25
	0.0	$-D_{Q,pp}$	$+D_{Q,pp}$	-0.25

After the specification of the position and value of the point charges, we can straightforwardly assess the electrostatic potential energy $U(\Theta_t^{\mu\nu}, \Theta_s^{\lambda\sigma})$ of the interaction of the C_t and C_s point charges making up $\Theta_t^{\mu\nu}$ and $\Theta_s^{\lambda\sigma}$, respectively (in atomic units),

$$U(\Theta_t^{\mu\nu}, \Theta_s^{\lambda\sigma}) = \sum_{c=1}^{C_t} \sum_{d=1}^{C_s} \frac{q_c^I q_d^J}{|\mathbf{r}_c^I - \mathbf{r}_d^J|}. \quad (108)$$

As stated in the main text, this interaction is not calculated analytically, but within the empirical Klopman approximation.^{49,50,141} The Klopman approximation is introduced to be able to recover the respective one-center ERIs $\langle \chi_\mu^I \chi_\nu^I | \chi_\lambda^J \chi_\sigma^J \rangle$ in the limit $\tilde{R}_{IJ} = 0$. In general, this means that the denominator in Eq. (108) is modified in such a way that we obtain the correct one-center limit,

$$U(\Theta_t^{\mu\nu}, \Theta_s^{\lambda\sigma}) = \sum_{c=1}^{C_t} \sum_{d=1}^{C_s} \frac{q_c^I q_d^J}{\sqrt{|\mathbf{r}_c^I - \mathbf{r}_d^J|^2 + (\vartheta_c^I(\chi_\mu^I \chi_\nu^I) + \vartheta_d^J(\chi_\lambda^J \chi_\sigma^J))^2}}. \quad (109)$$

The term ϑ_c^I depends on the multipole to which the point charge q_c belongs (see Table 5). If q_c is part of a monopole q^I representing the charge distribution $s^I s^I$, $\vartheta_{q,ss}^I$ is applied in Eq. (109). The four terms $\vartheta_{q,ss}^I$, $\vartheta_{q,pp}^I$, $\vartheta_{\mu,sp}^I$, and $\vartheta_{Q,pp}^I$ are calculated with reference to the one-center ERIs $\gamma_{ss}^{Z_I}$, $\tilde{\gamma}_{sp}^{Z_I}$, $\gamma_{pp}^{Z_I}$, and $\gamma_{pp'}^{Z_I}$,⁴⁹

$$\vartheta_{q,ss}^I = \frac{1}{2\gamma_{ss}}, \quad (110)$$

$$\vartheta_{q,pp}^I = \vartheta_{q,ss}^I, \quad (111)$$

$$(\vartheta_{\mu,sp}^I)^{-1} - \left[(\vartheta_{\mu,sp}^I)^2 + (D_{\mu,sp})^2 \right]^{-\frac{1}{2}} = \frac{4}{3} \tilde{\gamma}_{sp}, \quad (112)$$

and

$$(\vartheta_{Q,pp}^I)^{-1} - 2 \left[(\vartheta_{Q,pp}^I)^2 + (D_{Q,pp})^2 \right]^{-\frac{1}{2}} + \left[(\vartheta_{Q,pp}^I)^2 + 2(D_{Q,pp})^2 \right]^{-\frac{1}{2}} = \frac{24}{25} \langle p^I p'^I | p^I p'^I \rangle, \quad (113)$$

The parameters cannot be calculated analytically, but have to be determined in an iterative numerical procedure. The values for $\vartheta_{q,ss}^I$, $\vartheta_{q,pp}^I$, $\vartheta_{\mu,sp}^I$, and $\vartheta_{Q,pp}^I$ can be compared to those provided for P01, P07, P02, and P03, respectively, when specifying the keyword `Hcore` in MOPAC.

The implementation of the procedure to calculate the two-center ERIs can be compared to the implementation in MOPAC when specifying the keyword `Hcore` for the calculation of the electronic energy of a diatomic molecule which is aligned along the z -axis. The values of the two-center ERIs are then listed under `TWO-ELECTRON MATRIX IN HCORE` (note that these values really are the values for the ERIs and not the two-electron matrix entries). The first one hundred entries are the one-center ERIs for the first atom (i.e., γ_{ss} , γ_{sp} , γ_{pp} , $\gamma_{pp'}$, $\tilde{\gamma}_{sp}$, $\tilde{\gamma}_{pp'}$, and zeros). The next one hundred entries are the two-center ERIs which arise between the first and the second atom. The order in which the two-center ERIs are given is described in Ref. 288 and is also given in the following:

$$\begin{aligned} & \langle ss|ss \rangle \langle ss|sp_x \rangle \langle ss|p_x p_x \rangle \langle ss|sp_y \rangle \langle ss|p_x p_y \rangle \langle ss|p_y p_y \rangle \langle ss|sp_z \rangle \langle ss|p_x p_z \rangle \langle ss|p_y p_z \rangle \\ & \langle ss|p_z p_z \rangle \langle sp_x|ss \rangle \langle sp_x|sp_x \rangle \langle sp_x|p_x p_x \rangle \langle sp_x|sp_y \rangle \langle sp_x|p_x p_y \rangle \langle sp_x|p_y p_y \rangle \langle sp_x|sp_z \rangle \\ & \langle sp_x|p_x p_z \rangle \langle sp_x|p_y p_z \rangle \langle sp_x|p_z p_z \rangle \langle p_x p_x|ss \rangle \langle p_x p_x|sp_x \rangle \langle p_x p_x|p_x p_x \rangle \langle p_x p_x|sp_y \rangle \\ & \langle p_x p_x|p_x p_y \rangle \langle p_x p_x|p_y p_y \rangle \langle p_x p_x|sp_z \rangle \langle p_x p_x|p_x p_z \rangle \langle p_x p_x|p_y p_z \rangle \langle p_x p_x|p_z p_z \rangle \langle sp_y|ss \rangle \\ & \langle sp_y|sp_x \rangle \langle sp_y|p_x p_x \rangle \langle sp_y|sp_y \rangle \langle sp_y|p_x p_y \rangle \langle sp_y|p_y p_y \rangle \langle sp_y|sp_z \rangle \langle sp_y|p_x p_z \rangle \langle sp_y|p_y p_z \rangle \\ & \langle sp_y|p_z p_z \rangle \langle p_x p_y|ss \rangle \langle p_x p_y|sp_x \rangle \langle p_x p_y|p_x p_x \rangle \langle p_x p_y|sp_y \rangle \langle p_x p_y|p_x p_y \rangle \langle p_x p_y|p_y p_y \rangle \\ & \langle p_x p_y|sp_z \rangle \langle p_x p_y|p_x p_z \rangle \langle p_x p_y|p_y p_z \rangle \langle p_x p_y|p_z p_z \rangle \langle p_y p_y|ss \rangle \langle p_y p_y|sp_x \rangle \langle p_y p_y|p_x p_x \rangle \\ & \langle p_y p_y|sp_y \rangle \langle p_y p_y|p_x p_y \rangle \langle p_y p_y|p_y p_y \rangle \langle p_y p_y|sp_z \rangle \langle p_y p_y|p_x p_z \rangle \langle p_y p_y|p_y p_z \rangle \langle p_y p_y|p_z p_z \rangle \\ & \langle sp_z|ss \rangle \langle sp_z|sp_x \rangle \langle sp_z|p_x p_x \rangle \langle sp_z|sp_y \rangle \langle sp_z|p_x p_y \rangle \langle sp_z|p_y p_y \rangle \langle sp_z|sp_z \rangle \langle sp_z|p_x p_z \rangle \\ & \langle sp_z|p_y p_z \rangle \langle sp_z|p_z p_z \rangle \langle p_x p_z|ss \rangle \langle p_x p_z|sp_x \rangle \langle p_x p_z|p_x p_x \rangle \langle p_x p_z|sp_y \rangle \langle p_x p_z|p_x p_y \rangle \end{aligned}$$

$$\begin{aligned}
& \langle p_x p_z | p_y p_y \rangle \langle p_x p_z | s p_z \rangle \langle p_x p_z | p_x p_z \rangle \langle p_x p_z | p_y p_z \rangle \langle p_x p_z | p_z p_z \rangle \langle p_y p_z | s s \rangle \langle p_y p_z | s p_x \rangle \\
& \langle p_y p_z | p_x p_x \rangle \langle p_y p_z | s p_y \rangle \langle p_y p_z | p_x p_y \rangle \langle p_y p_z | p_y p_y \rangle \langle p_y p_z | s p_z \rangle \langle p_y p_z | p_x p_z \rangle \langle p_y p_z | p_y p_z \rangle \\
& \langle p_y p_z | p_z p_z \rangle \langle p_z p_z | s s \rangle \langle p_z p_z | s p_x \rangle \langle p_z p_z | p_x p_x \rangle \langle p_z p_z | s p_y \rangle \langle p_z p_z | p_x p_y \rangle \langle p_z p_z | p_y p_y \rangle \\
& \langle p_z p_z | s p_z \rangle \langle p_z p_z | p_x p_z \rangle \langle p_z p_z | p_y p_z \rangle \langle p_z p_z | p_z p_z \rangle
\end{aligned}$$

10.5 MNDO-type Models with an s, p, d basis set

10.5.1 Evaluation of One-Center ERIs

The one-center ERIs $\langle \chi_\mu^I \chi_\nu^I | \chi_\lambda^I \chi_\sigma^I \rangle$ will be calculated analytically if s -, p -, and d -type basis functions are activated for the atom I . For this purpose, the one-center ERIs are re-written as⁸³

$$\begin{aligned}
\langle \chi_\mu^I \chi_\nu^I | \chi_\lambda^I \chi_\sigma^I \rangle &= \sum_{k=0}^{\infty} C^k(l(\mu)m(\mu), l(\nu)m(\nu)) C^k(l(\sigma)m(\sigma), l(\lambda)m(\lambda)) \\
&\times R^k(\chi_\mu^I, \chi_\nu^I, \chi_\lambda^I, \chi_\sigma^I),
\end{aligned} \tag{114}$$

where $C^k(l(\mu)m(\mu), l(\nu)m(\nu))$ denotes the so-called angular coefficients and $R^k(\chi_\mu^I, \chi_\nu^I, \chi_\lambda^I, \chi_\sigma^I)$ the radial integrals. The radial integrals $R^k(\chi_\mu^I, \chi_\nu^I, \chi_\lambda^I, \chi_\sigma^I)$ are calculated as follows (Eq. (3) in Ref. 85),

$$\begin{aligned}
R^k(\chi_\mu^I, \chi_\nu^I, \chi_\lambda^I, \chi_\sigma^I) &= \frac{(2\zeta'_\lambda)^{n_\lambda+1/2} (2\zeta'_\sigma)^{n_\sigma+1/2} (2\zeta'_\mu)^{n_\mu+1/2} (2\zeta'_\nu)^{n_\nu+1/2}}{\sqrt{(2n_\lambda)!(2n_\sigma)!} \sqrt{(2n_\mu)!(2n_\nu)!}} \\
&\times \frac{(n_\sigma + n_\lambda + k)!}{(\zeta'_\sigma + \zeta'_\lambda)^{n_\sigma+n_\lambda+k+1}} \left\{ \frac{(n_\mu + n_\nu - k - 1)!}{(\zeta'_\mu + \zeta'_\nu)^{n_\mu+n_\nu-k}} \right. \\
&- \sum_{k'=1}^{n_\sigma+n_\lambda+k+1} \frac{(\zeta'_\sigma + \zeta'_\lambda)^{n_\sigma+n_\lambda+k-k'+1}}{(n_\sigma + n_\lambda + k - k' + 1)! [\zeta'_\mu + \zeta'_\nu + \zeta'_\lambda + \zeta'_\sigma]^{n_\mu+n_\nu+n_\lambda+n_\sigma-k'+1}} \frac{[n_\mu + n_\nu + n_\lambda + n_\sigma - k']!}{[\zeta'_\mu + \zeta'_\nu + \zeta'_\lambda + \zeta'_\sigma]^{n_\mu+n_\nu+n_\lambda+n_\sigma-k'+1}} \\
&+ \sum_{k'=1}^{n_\lambda+n_\sigma-k} \left[\frac{(\zeta'_\lambda + \zeta'_\sigma)^{n_\lambda+n_\sigma+k-k'+1} (n_\lambda + n_\sigma - k - 1)!}{(n_\lambda + n_\sigma + k)! (n_\lambda + n_\sigma - k - k')!} \right. \\
&\left. \left. \times \frac{[n_\mu + n_\nu + n_\lambda + n_\sigma - k']!}{[\zeta'_\mu + \zeta'_\nu + \zeta'_\lambda + \zeta'_\sigma]^{n_\mu+n_\nu+n_\lambda+n_\sigma-k'+1}} \right] \right\},
\end{aligned} \tag{115}$$

where ζ'_μ is the auxiliary orbital exponent and n_μ the principal quantum number associated with the basis function χ_μ^I .

Pelikán and Nagy determined⁸⁴ the values of the 58 unique nonzero one-center ERIs $\langle \chi_\mu^I \chi_\nu^I | \chi_\lambda^I \chi_\sigma^I \rangle$ in terms of $R^k(\chi_\mu^I, \chi_\nu^I, \chi_\lambda^I, \chi_\sigma^I)$ by explicitly evaluating Eq. (114). For this purpose, they used the angular coefficients $C^k(l(\mu)m(\mu), l(\nu)m(\nu))$ which are presented in Table 1 on pp. 178–179

in Ref. 83. In their work, the term $R^k(\chi_\mu^I, \chi_\nu^I, \chi_\lambda^I, \chi_\sigma^I)$ is also denoted as $R_{l(\mu)l(\nu)l(\lambda)l(\sigma)}^k$. It is customary^{83,84} to introduce the quantities $F_{l(\mu)l(\nu)}^k$,

$$F_{l(\mu)l(\nu)}^k \equiv R_{l(\mu)l(\mu)l(\nu)l(\nu)}^k, \quad (116)$$

and $G_{l(\mu)l(\nu)}^k$,

$$G_{l(\mu)l(\nu)}^k \equiv R_{l(\mu)l(\nu)l(\mu)l(\nu)}^k, \quad (117)$$

to simplify the notation. The formulae for the one-center ERIs are presented in Table 2 of Ref. 84, but some contain typographical mistakes which we clarify here (corrected formulae are indicated by an asterisk appended to the equation number); for the 58 one-center ERIs, they read in our notation:

$$\langle s^I s^I | s^I s^I \rangle = F_{ss}^0 \quad (118)$$

$$\langle s^I s^I | p_x^I p_x^I \rangle = \langle s^I s^I | p_y^I p_y^I \rangle = \langle s^I s^I | p_z^I p_z^I \rangle = F_{sp}^0 \quad (119)$$

$$\langle s^I p_x^I | s^I p_x^I \rangle = \langle s^I p_y^I | s^I p_y^I \rangle = \langle s^I p_z^I | s^I p_z^I \rangle = \frac{1}{3} G_{sp}^1 \quad (120)$$

$$\langle p_x^I p_x^I | p_x^I p_x^I \rangle = \langle p_y^I p_y^I | p_y^I p_y^I \rangle = \langle p_z^I p_z^I | p_z^I p_z^I \rangle = F_{pp}^0 + \frac{4}{25} F_{pp}^2 \quad (121)$$

$$\langle p_x^I p_x^I | p_y^I p_y^I \rangle = \langle p_x^I p_x^I | p_z^I p_z^I \rangle = \langle p_y^I p_y^I | p_z^I p_z^I \rangle = F_{pp}^0 - \frac{2}{25} F_{pp}^2 \quad (122)$$

$$\langle p_x^I p_y^I | p_x^I p_y^I \rangle = \langle p_x^I p_z^I | p_x^I p_z^I \rangle = \langle p_y^I p_z^I | p_y^I p_z^I \rangle = \frac{3}{25} F_{pp}^2 \quad (123)$$

$$\langle p_x^I d_{z^2}^I | p_x^I d_{z^2}^I \rangle = \langle p_y^I d_{z^2}^I | p_y^I d_{z^2}^I \rangle = \frac{1}{15} G_{pd}^1 + \frac{18}{245} G_{pd}^3 \quad (124)$$

$$\langle p_x^I d_{z^2}^I | p_x^I d_{x^2-y^2}^I \rangle = \langle p_x^I d_{z^2}^I | p_y^I d_{xy}^I \rangle = \langle p_x^I d_{xy}^I | d_{z^2}^I p_y^I \rangle = -\frac{\sqrt{3}}{15} G_{pd}^1 - \frac{\sqrt{27}}{245} G_{pd}^3 \quad (125)$$

$$\langle p_x^I d_{x^2-y^2}^I | p_y^I d_{xy}^I \rangle = \frac{1}{5} G_{pd}^1 - \frac{21}{245} G_{pd}^3 \quad (126)$$

$$\langle p_x^I d_{xy}^I | p_y^I d_{x^2-y^2}^I \rangle = -\frac{1}{5} G_{pd}^1 + \frac{21}{245} G_{pd}^3 \quad (127)$$

$$\langle p_x^I p_x^I | d_{z^2}^I d_{z^2}^I \rangle = \langle p_y^I p_y^I | d_{z^2}^I d_{z^2}^I \rangle = F_{pd}^0 - \frac{2}{35} F_{pd}^2 \quad (128)$$

$$\langle p_x^I p_x^I | d_{z^2}^I d_{x^2-y^2}^I \rangle = \langle p_x^I p_y^I | d_{z^2}^I d_{xy}^I \rangle = -\frac{\sqrt{12}}{35} F_{pd}^2 \quad (129)$$

$$\langle p_y^I d_{z^2}^I | p_y^I d_{x^2-y^2}^I \rangle = \frac{\sqrt{3}}{15} G_{pd}^1 + \frac{\sqrt{27}}{245} G_{pd}^3 \quad (130)$$

$$\langle p_z^I d_{z^2}^I | p_z^I d_{z^2}^I \rangle = \frac{4}{15} G_{pd}^1 + \frac{27}{245} G_{pd}^3 \quad (131)$$

$$\begin{aligned} \langle p_z^I d_{x^2-y^2}^I | p_z^I d_{x^2-y^2}^I \rangle &= \langle p_z^I d_{xy}^I | p_z^I d_{xy}^I \rangle = \langle p_x^I d_{yz}^I | p_x^I d_{yz}^I \rangle = \langle p_y^I d_{xz}^I | p_y^I d_{xz}^I \rangle \\ &= \langle p_z^I d_{x^2-y^2}^I | p_x^I d_{xz}^I \rangle = \langle p_z^I d_{xy}^I | p_x^I d_{yz}^I \rangle = \langle p_z^I d_{xy}^I | p_y^I d_{xz}^I \rangle = \langle p_x^I d_{yz}^I | p_y^I d_{xz}^I \rangle \quad (132) \\ &= \frac{3}{49} G_{pd}^3 \end{aligned}$$

$$\begin{aligned} \langle p_z^I d_{xz}^I | p_z^I d_{xz}^I \rangle &= \langle p_z^I d_{yz}^I | p_z^I d_{yz}^I \rangle = \langle p_x^I d_{xy}^I | p_x^I d_{xy}^I \rangle = \langle p_x^I d_{x^2-y^2}^I | p_x^I d_{x^2-y^2}^I \rangle \\ &= \langle p_x^I d_{xz}^I | p_x^I d_{xz}^I \rangle = \langle p_y^I d_{xy}^I | p_y^I d_{xy}^I \rangle = \langle p_y^I d_{yz}^I | p_y^I d_{yz}^I \rangle = \langle p_y^I d_{x^2-y^2}^I | p_y^I d_{x^2-y^2}^I \rangle \\ &= \frac{1}{5} G_{pd}^1 + \frac{24}{245} G_{pd}^3 \quad (133) \end{aligned}$$

$$\langle p_z^I d_{z^2}^I | p_x^I d_{xz}^I \rangle = \langle p_z^I d_{z^2}^I | p_y^I d_{yz}^I \rangle = \frac{\sqrt{12}}{15} G_{pd}^1 - \frac{\sqrt{243}}{245} G_{pd}^3 \quad (134^*)$$

$$\begin{aligned} \langle p_z^I d_{xz}^I | p_x^I d_{x^2-y^2}^I \rangle &= \langle p_z^I d_{yz}^I | p_x^I d_{xy}^I \rangle = \langle p_z^I d_{xz}^I | p_y^I d_{xy}^I \rangle = \langle p_x^I d_{xz}^I | p_y^I d_{yz}^I \rangle \\ &= \frac{1}{5} G_{pd}^1 - \frac{6}{245} G_{pd}^3 \quad (135) \end{aligned}$$

$$\langle p_z^I d_{x^2-y^2}^I | p_y^I d_{yz}^I \rangle = -\frac{3}{49} G_{pd}^3 \quad (136)$$

$$\langle p_z^I d_{yz}^I | p_y^I d_{z^2}^I \rangle = \langle p_z^I d_{xz}^I | p_x^I d_{z^2}^I \rangle = -\frac{\sqrt{3}}{15} G_{pd}^1 + \frac{\sqrt{432}}{245} G_{pd}^3 \quad (137)$$

$$\langle p_z^I d_{yz}^I | p_y^I d_{x^2-y^2}^I \rangle = -\frac{1}{5} G_{pd}^1 + \frac{6}{245} G_{pd}^3 \quad (138)$$

$$\langle p_z^I p_z^I | d_{z^2}^I d_{z^2}^I \rangle = F_{pd}^0 + \frac{4}{35} F_{pd}^2 \quad (139)$$

$$\langle p_z^I p_x^I | d_{z^2}^I d_{xz}^I \rangle = \langle p_z^I p_y^I | d_{z^2}^I d_{yz}^I \rangle = \frac{\sqrt{3}}{35} F_{pd}^2 \quad (140)$$

$$\begin{aligned} \langle p_z^I p_z^I | d_{x^2-y^2}^I d_{x^2-y^2}^I \rangle &= \langle p_z^I p_z^I | d_{xy}^I d_{xy}^I \rangle = \langle p_x^I p_x^I | d_{yz}^I d_{yz}^I \rangle = \langle p_y^I p_y^I | d_{xz}^I d_{xz}^I \rangle \\ &= F_{pd}^0 - \frac{4}{35} F_{pd}^2 \quad (141) \end{aligned}$$

$$\langle p_z^I p_x^I | d_{x^2-y^2}^I d_{xz}^I \rangle = \langle p_z^I p_x^I | d_{xy}^I d_{yz}^I \rangle = \langle p_z^I p_y^I | d_{xy}^I d_{xz}^I \rangle = \langle p_x^I p_y^I | d_{xz}^I d_{yz}^I \rangle = \frac{3}{35} F_{pd}^2 \quad (142)$$

$$\langle p_z^I p_y^I | d_{x^2-y^2}^I d_{yz}^I \rangle = -\frac{3}{35} F_{pd}^2 \quad (143)$$

$$\begin{aligned}
\langle p_z^I p_z^I | d_{xz}^I d_{xz}^I \rangle &= \langle p_z^I p_z^I | d_{yz}^I d_{yz}^I \rangle = \langle p_x^I p_x^I | d_{xy}^I d_{xy}^I \rangle = \langle p_x^I p_x^I | d_{x^2-y^2}^I d_{x^2-y^2}^I \rangle \\
&= \langle p_x^I p_x^I | d_{xz}^I d_{xz}^I \rangle = \langle p_y^I p_y^I | d_{xy}^I d_{xy}^I \rangle = \langle p_y^I p_y^I | d_{yz}^I d_{yz}^I \rangle = \langle p_y^I p_y^I | d_{x^2-y^2}^I d_{x^2-y^2}^I \rangle \\
&= F_{pd}^0 + \frac{2}{35} F_{pd}^2
\end{aligned} \tag{144}$$

$$\langle p_y^I p_y^I | d_{z^2}^I d_{x^2-y^2}^I \rangle = \frac{\sqrt{12}}{35} F_{pd}^2 \tag{145}$$

$$\begin{aligned}
\langle s^I d_{z^2}^I | s^I d_{z^2}^I \rangle &= \langle s^I d_{x^2-y^2}^I | s^I d_{x^2-y^2}^I \rangle = \langle s^I d_{xy}^I | s^I d_{xy}^I \rangle = \langle s^I d_{xz}^I | s^I d_{xz}^I \rangle \\
&= \langle s^I d_{yz}^I | s^I d_{yz}^I \rangle = \frac{1}{5} G_{sd}^2
\end{aligned} \tag{146}$$

$$\begin{aligned}
\langle s^I s^I | d_{z^2}^I d_{z^2}^I \rangle &= \langle s^I s^I | d_{x^2-y^2}^I d_{x^2-y^2}^I \rangle = \langle s^I s^I | d_{xy}^I d_{xy}^I \rangle = \langle s^I s^I | d_{xz}^I d_{xz}^I \rangle \\
&= \langle s^I s^I | d_{yz}^I d_{yz}^I \rangle = F_{sd}^0
\end{aligned} \tag{147}$$

$$\begin{aligned}
\langle d_{z^2}^I d_{z^2}^I | d_{z^2}^I d_{z^2}^I \rangle &= \langle d_{x^2-y^2}^I d_{x^2-y^2}^I | d_{x^2-y^2}^I d_{x^2-y^2}^I \rangle = \langle d_{xy}^I d_{xy}^I | d_{xy}^I d_{xy}^I \rangle \\
&= \langle d_{xz}^I d_{xz}^I | d_{xz}^I d_{xz}^I \rangle = \langle d_{yz}^I d_{yz}^I | d_{yz}^I d_{yz}^I \rangle = F_{dd}^0 + \frac{4}{49} F_{dd}^2 + \frac{36}{441} F_{dd}^4
\end{aligned} \tag{148}$$

$$\langle d_{z^2}^I d_{x^2-y^2}^I | d_{z^2}^I d_{x^2-y^2}^I \rangle = \langle d_{z^2}^I d_{xy}^I | d_{z^2}^I d_{xy}^I \rangle = \frac{4}{49} F_{dd}^2 + \frac{15}{441} F_{dd}^4 \tag{149}$$

$$\langle d_{z^2}^I d_{xz}^I | d_{z^2}^I d_{xz}^I \rangle = \langle d_{z^2}^I d_{yz}^I | d_{z^2}^I d_{yz}^I \rangle = \frac{1}{49} F_{dd}^2 + \frac{30}{441} F_{dd}^4 \tag{150}$$

$$\langle d_{z^2}^I d_{z^2}^I | d_{x^2-y^2}^I d_{x^2-y^2}^I \rangle = \langle d_{z^2}^I d_{z^2}^I | d_{xy}^I d_{xy}^I \rangle = F_{dd}^0 - \frac{4}{49} F_{dd}^2 + \frac{6}{441} F_{dd}^4 \tag{151}$$

$$\langle d_{z^2}^I d_{xz}^I | d_{x^2-y^2}^I d_{xz}^I \rangle = \langle d_{z^2}^I d_{xz}^I | d_{xy}^I d_{yz}^I \rangle = \langle d_{z^2}^I d_{yz}^I | d_{xy}^I d_{xz}^I \rangle = \frac{\sqrt{3}}{49} F_{dd}^2 - \frac{\sqrt{75}}{441} F_{dd}^4 \tag{152}$$

$$\langle d_{z^2}^I d_{yz}^I | d_{x^2-y^2}^I d_{yz}^I \rangle = -\frac{\sqrt{3}}{49} F_{dd}^2 + \frac{\sqrt{75}}{441} F_{dd}^4 \tag{153}$$

$$\langle d_{z^2}^I d_{z^2}^I | d_{xz}^I d_{xz}^I \rangle = \langle d_{z^2}^I d_{z^2}^I | d_{yz}^I d_{yz}^I \rangle = F_{dd}^0 + \frac{2}{49} F_{dd}^2 - \frac{24}{441} F_{dd}^4 \tag{154}$$

$$\langle d_{z^2}^I d_{x^2-y^2}^I | d_{xz}^I d_{xz}^I \rangle = \langle d_{z^2}^I d_{xy}^I | d_{xz}^I d_{yz}^I \rangle = -\frac{\sqrt{12}}{49} F_{dd}^2 + \frac{\sqrt{300}}{441} F_{dd}^4 \tag{155}$$

$$\langle d_{z^2}^I d_{x^2-y^2}^I | d_{yz}^I d_{yz}^I \rangle = \frac{\sqrt{12}}{49} F_{dd}^2 - \frac{\sqrt{300}}{441} F_{dd}^4 \tag{156}$$

$$\langle d_{x^2-y^2}^I d_{xy}^I | d_{x^2-y^2}^I d_{xy}^I \rangle = \frac{35}{441} F_{dd}^4 \tag{157}$$

$$\begin{aligned}
\langle d_{xy}^I d_{xz}^I | d_{xy}^I d_{xz}^I \rangle &= \langle d_{xy}^I d_{yz}^I | d_{xy}^I d_{yz}^I \rangle = \langle d_{xz}^I d_{yz}^I | d_{xz}^I d_{yz}^I \rangle = \langle d_{x^2-y^2}^I d_{xz}^I | d_{x^2-y^2}^I d_{xz}^I \rangle \\
&= \langle d_{x^2-y^2}^I d_{yz}^I | d_{x^2-y^2}^I d_{yz}^I \rangle = \frac{3}{49} F_{dd}^2 + \frac{20}{441} F_{dd}^4
\end{aligned} \tag{158}$$

$$\langle d_{x^2-y^2}^I d_{x^2-y^2}^I | d_{xy}^I d_{xy}^I \rangle = F_{dd}^0 + \frac{4}{49} F_{dd}^2 - \frac{34}{441} F_{dd}^4 \quad (159)$$

$$\langle d_{x^2-y^2}^I d_{xz}^I | d_{xy}^I d_{yz}^I \rangle = \frac{3}{49} F_{dd}^2 - \frac{15}{441} F_{dd}^4 \quad (160)$$

$$\langle d_{x^2-y^2}^I d_{yz}^I | d_{xy}^I d_{xz}^I \rangle = -\frac{3}{49} F_{dd}^2 + \frac{15}{441} F_{dd}^4 \quad (161)$$

$$\begin{aligned} \langle d_{xy}^I d_{xy}^I | d_{xz}^I d_{xz}^I \rangle &= \langle d_{xy}^I d_{xy}^I | d_{yz}^I d_{yz}^I \rangle = \langle d_{xz}^I d_{xz}^I | d_{yz}^I d_{yz}^I \rangle = \langle d_{x^2-y^2}^I d_{x^2-y^2}^I | d_{xz}^I d_{xz}^I \rangle \\ &= \langle d_{x^2-y^2}^I d_{x^2-y^2}^I | d_{yz}^I d_{yz}^I \rangle = F_{dd}^0 - \frac{2}{49} F_{dd}^2 - \frac{4}{441} F_{dd}^4 \end{aligned} \quad (162)$$

$$\langle s^I d_{z^2}^I | d_{z^2}^I d_{z^2}^I \rangle = \frac{2}{\sqrt{245}} R_{sddd}^2 \quad (163)$$

$$\begin{aligned} \langle s^I d_{x^2-y^2}^I | d_{z^2}^I d_{x^2-y^2}^I \rangle &= \langle s^I d_{xy}^I | d_{z^2}^I d_{xy}^I \rangle = \langle s^I d_{z^2}^I | d_{x^2-y^2}^I d_{x^2-y^2}^I \rangle = \langle s^I d_{z^2}^I | d_{xy}^I d_{xy}^I \rangle \\ &= -\frac{2}{\sqrt{245}} R_{sddd}^2 \end{aligned} \quad (164)$$

$$\langle s^I d_{xz}^I | d_{z^2}^I d_{xz}^I \rangle = \langle s^I d_{yz}^I | d_{z^2}^I d_{yz}^I \rangle = \langle s^I d_{z^2}^I | d_{xz}^I d_{xz}^I \rangle = \langle s^I d_{z^2}^I | d_{yz}^I d_{yz}^I \rangle = \frac{1}{\sqrt{245}} R_{sddd}^2 \quad (165)$$

$$\begin{aligned} \langle s^I d_{xz}^I | d_{x^2-y^2}^I d_{xz}^I \rangle &= \langle s^I d_{xz}^I | d_{xy}^I d_{yz}^I \rangle = \langle s^I d_{yz}^I | d_{xy}^I d_{xz}^I \rangle = \langle s^I d_{xy}^I | d_{xz}^I d_{yz}^I \rangle \\ &= \langle s^I d_{x^2-y^2}^I | d_{xz}^I d_{xz}^I \rangle = \frac{\sqrt{3}}{\sqrt{245}} R_{sddd}^2 \end{aligned} \quad (166)$$

$$\langle s^I d_{yz}^I | d_{x^2-y^2}^I d_{yz}^I \rangle = \langle s^I d_{x^2-y^2}^I | d_{yz}^I d_{yz}^I \rangle = -\frac{\sqrt{3}}{\sqrt{245}} R_{sddd}^2 \quad (167)$$

$$\langle s^I d_{z^2}^I | p_x^I p_x^I \rangle = \langle s^I d_{z^2}^I | p_y^I p_y^I \rangle = -\frac{1}{\sqrt{125}} R_{sdpp}^2 \quad (168^*)$$

$$\langle s^I p_y^I | p_y^I d_{x^2-y^2}^I \rangle = -\frac{\sqrt{3}}{\sqrt{45}} R_{sppd}^1 \quad (169)$$

$$\langle p_y^I p_y^I | s^I d_{x^2-y^2}^I \rangle = -\frac{\sqrt{3}}{\sqrt{125}} R_{sdpp}^2 \quad (170^*)$$

$$\langle p_z^I s^I | p_z^I d_{z^2}^I \rangle = \frac{2}{\sqrt{45}} R_{sppd}^1 \quad (171^*)$$

$$\begin{aligned} \langle p_z^I s^I | p_x^I d_{xz}^I \rangle &= \langle p_z^I d_{xz}^I | p_x^I s^I \rangle = \langle p_z^I s^I | p_y^I d_{yz}^I \rangle = \langle p_z^I d_{yz}^I | p_y^I s^I \rangle = \langle p_x^I s^I | p_x^I d_{x^2-y^2}^I \rangle \\ &= \langle p_x^I s^I | p_y^I d_{xy}^I \rangle = \langle p_x^I d_{xy}^I | s^I p_y^I \rangle = \frac{\sqrt{3}}{\sqrt{45}} R_{sppd}^1 \end{aligned} \quad (172)$$

$$\langle p_z^I p_z^I | s^I d_{z^2}^I \rangle = \frac{2}{\sqrt{125}} R_{sdpp}^2 \quad (173^*)$$

$$\langle p_z^I p_x^I | s^I d_{xz}^I \rangle = \langle p_z^I p_y^I | s^I d_{yz}^I \rangle = \langle p_x^I p_x^I | s^I d_{x^2-y^2}^I \rangle = \langle p_x^I p_y^I | s^I d_{xy}^I \rangle = \frac{\sqrt{3}}{\sqrt{125}} R_{sdpp}^2 \quad (174^*)$$

$$\langle p_x^I s^I | p_x^I d_{z^2}^I \rangle = \langle p_y^I s^I | p_y^I d_{z^2}^I \rangle = -\frac{1}{\sqrt{45}} R_{sppd}^1 \quad (175)$$

The typographical mistakes in Ref. 84 which we corrected here can be summarized as follows:

- The factor 12 has to be substituted for $\sqrt{12}$ in Eq. (17) of Ref. 84, see Eq. (134*).
- The radial integral R_{sppd}^2 has to be replaced by R_{sdpp}^2 in Eqs. (51), (53), (56), and (57) of Ref. 84, see Eqs. (168*), (170*), (173*), and (174*), respectively.
- R_{spdd}^1 has to be replaced for R_{sppd}^1 in Eq. (54) of Ref. 84, see Eq. (171*).

The implementation of the erroneous equations would affect all MNDO-type models which activate d -type basis functions (i.e., MNDO/d, AM1, PM6, and PM7). Specifically, the one-center ERIs $\langle p_z^I d_{z^2}^I | p_x^I d_{xz}^I \rangle$, $\langle p_z^I d_{z^2}^I | p_y^I d_{yz}^I \rangle$, $\langle s^I d_{z^2}^I | p_x^I p_x^I \rangle$, $\langle s^I d_{z^2}^I | p_y^I p_y^I \rangle$, $\langle p_y^I p_y^I | s^I d_{x^2-y^2}^I \rangle$, $\langle p_z^I s^I | p_z^I d_{z^2}^I \rangle$, $\langle p_z^I p_z^I | s^I d_{z^2}^I \rangle$, $\langle p_z^I p_x^I | s^I d_{xz}^I \rangle$, $\langle p_z^I p_y^I | s^I d_{yz}^I \rangle$, $\langle p_x^I p_x^I | s^I d_{x^2-y^2}^I \rangle$, and $\langle p_x^I p_y^I | s^I d_{xy}^I \rangle$ would then be erroneous.

One can then find 2025 values for the one-center ERIs (their order is detailed in Ref. 288) listed under **TWO-ELECTRON MATRIX IN HCore** in the output when carrying out a calculation with MOPAC and invoking the keyword **Hcore**.

10.5.2 Evaluation of Two-Center ERIs

Conceptually, the calculation of the two-center ERIs in the s, p, d basis is similar to the one in the s, p basis.^{53,54} If at least *one* of the basis functions contributing to a two-center ERI is a d -type basis function, the following equations are applied instead of the ones specified in Section 10.4.

To fully describe the point charge interactions when a d -type orbital is involved in a two-center ERI, Thiel and Voityuk specified an additional point charge configuration $\tilde{Q}_{xy,yz,xz}$ (see Figure 19). Within an s, p, d -orbital basis, many more combinations of charge distributions are now possible^{53,54} than

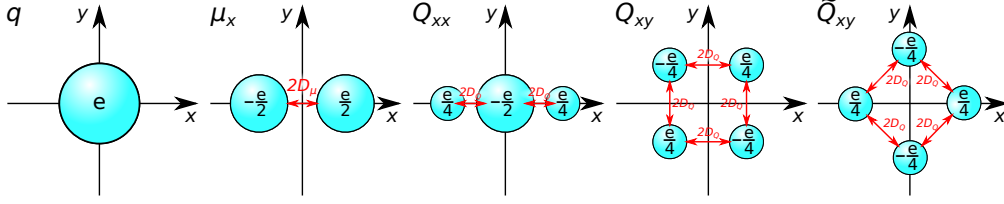


Figure 19: Illustration of the configuration of point charges (blue spheres) for the monopole q , the dipole μ_x , the linear quadrupole Q_{xx} , the square quadrupole Q_{xy} , and the quadrupole $\tilde{Q}_{xy,xz,yz}$. The charge for each point charge is given in units of the elementary charge. The point charges in μ_x are $2D_\mu$ apart and the ones in Q_{xx} , Q_{xy} , and \tilde{Q}_{xy} are $2D_Q$ apart.

in the s, p basis (see Table 6). These multipoles are applied when at least one d -type orbital is involved.

Table 6: Specification of multipoles which are applied to represent the possible charge distributions $\chi_\mu^I \chi_\nu^J$ in an s, p, d basis set in a truncated multipole expansion. We indicate the center of the multipole by a superscript atom index.

Charge Distribution	$T_{\mu\nu}$	Multipoles
$s^I s^I$	1	q^I
$p_x^I p_x^I$	3	$q^I, -\frac{2}{3} \left(\tilde{Q}_{zx}^I - \frac{1}{2} \tilde{Q}_{xy}^I \right), \tilde{Q}_{xy}^I$
$p_y^I p_y^I$	3	$q^I, -\frac{2}{3} \left(\tilde{Q}_{zx}^I - \frac{1}{2} \tilde{Q}_{xy}^I \right), -\tilde{Q}_{xy}^I$
$p_z^I p_z^I$	2	$q^I, \frac{4}{3} \left(\tilde{Q}_{zx}^I - \frac{1}{2} \tilde{Q}_{xy}^I \right)$
$s^I p_x^I$	1	μ_x^I
$s^I p_y^I$	1	μ_y^I
$s^I p_z^I$	1	μ_z^I
$p_x^I p_y^I$	1	Q_{xy}^I
$p_x^I p_z^I$	1	Q_{xz}^I
$p_y^I p_z^I$	1	Q_{yz}^I
$s^I d_{z^2}^I$	1	$\sqrt{\frac{4}{3}} \left(\tilde{Q}_{zx}^I - \frac{1}{2} \tilde{Q}_{xy}^I \right)$
$s^I d_{xz}^I$	1	Q_{xz}^I
$s^I d_{yz}^I$	1	Q_{yz}^I
$s^I d_{x^2-y^2}^I$	1	\tilde{Q}_{xy}^I
$s^I d_{xy}^I$	1	Q_{xy}^I
$p_x^I d_{z^2}^I$	1	$-\sqrt{\frac{1}{3}} \mu_x^I$

Charge Distribution	$T_{\mu\nu}$	Multipoles
$p_x^I d_{xz}^I$	1	μ_z^I
$p_x^I d_{yz}^I$	0	—
$p_x^I d_{x^2-y^2}^I$	1	μ_x^I
$p_x^I d_{xy}^I$	1	μ_y^I
$p_y^I d_{z^2}^I$	1	$-\sqrt{\frac{1}{3}}\mu_y^I$
$p_y^I d_{xz}^I$	0	—
$p_y^I d_{yz}^I$	1	μ_z^I
$p_y^I d_{x^2-y^2}^I$	1	$-\mu_y^I$
$p_y^I d_{xy}^I$	1	μ_x^I
$p_z^I d_{z^2}^I$	1	$\sqrt{\frac{4}{3}}\mu_z^I$
$p_z^I d_{xz}^I$	1	μ_x^I
$p_z^I d_{yz}^I$	1	μ_y^I
$p_z^I d_{x^2-y^2}^I$	0	—
$p_z^I d_{xy}^I$	0	—
$d_{z^2}^I d_{z^2}^I$	2	$q^I, \frac{4}{3} \left(\tilde{Q}_{zx}^I - \frac{1}{2} \tilde{Q}_{xy}^I \right)$
$d_{z^2}^I d_{xz}^I$	1	$\sqrt{\frac{1}{3}}Q_{xz}^I$
$d_{z^2}^I d_{yz}^I$	1	$\sqrt{\frac{1}{3}}Q_{yz}^I$
$d_{z^2}^I d_{x^2-y^2}^I$	1	$-\sqrt{\frac{4}{3}}\tilde{Q}_{xy}^I$
$d_{z^2}^I d_{xy}^I$	1	$-\sqrt{\frac{4}{3}}Q_{xy}^I$
$d_{xz}^I d_{xz}^I$	3	$q^I, \frac{2}{3} \left(\tilde{Q}_{zx}^I - \frac{1}{2} \tilde{Q}_{xy}^I \right), \tilde{Q}_{xy}^I$
$d_{xz}^I d_{yz}^I$	1	Q_{xy}^I
$d_{xz}^I d_{x^2-y^2}^I$	1	Q_{xz}^I
$d_{xz}^I d_{xy}^I$	1	Q_{yz}^I
$d_{yz}^I d_{yz}^I$	3	$q^I, \frac{2}{3} \left(\tilde{Q}_{zx}^I - \frac{1}{2} \tilde{Q}_{xy}^I \right), -\tilde{Q}_{xy}^I$
$d_{yz}^I d_{x^2-y^2}^I$	1	$-Q_{yz}^I$
$d_{yz}^I d_{xy}^I$	1	Q_{xz}^I
$d_{x^2-y^2}^I d_{x^2-y^2}^I$	2	$q^I, -\frac{4}{3} \left(\tilde{Q}_{zx}^I - \frac{1}{2} \tilde{Q}_{xy}^I \right)$
$d_{x^2-y^2}^I d_{xy}^I$	0	—
$d_{xy}^I d_{xy}^I$	2	$q^I, -\frac{4}{3} \left(\tilde{Q}_{zx}^I - \frac{1}{2} \tilde{Q}_{xy}^I \right)$

For the charge distributions $p_x^I d_{yz}^I$, $p_y^I d_{xz}^I$, $p_z^I d_{x^2-y^2}^I$, $p_z^I d_{xy}^I$, and $d_{x^2-y^2}^I d_{xy}^I$ no multipoles (i.e., $T_{\mu\nu} = 0$ in Table 6) are specified. This is due to the fact

that octopole (or higher) moments are neglected.⁵³ As a consequence, all two-center ERIs which involve at least one of these charge distributions are exactly zero for all \tilde{R}_{IJ} .

Note how the multipoles specified for the charge distributions $p_x^I p_x^I$, $p_y^I p_y^I$, and $p_z^I p_z^I$ are different than the ones specified in Table 4 which means that the representation of $p_x^I p_x^I$, $p_y^I p_y^I$, and $p_z^I p_z^I$ differs depending on whether the second charge distribution contains a d -type orbital or not.

Additionally, we are now in a situation where a dipole moment μ_x^I is applied to describe different charge distributions, e.g., $s^I p_x^I$ and $p_x^I d_{x^2-y^2}^I$. As a consequence, we need to specify different distances for the multipoles which appear in the multipole expansions describing a charge distribution. In addition to $D_{\mu, sd}$ and $D_{Q, pp}$, we must define the distances $D_{\mu, pd}$, $D_{Q, sd}$, and $Q_{\mu, dd}$. These distances are again defined with respect to $A(\chi_\mu^I, \chi_\nu^I, a)$ (Eq. (105)),⁵³

$$D_{\mu, pd} = 5^{-\frac{1}{2}} A(\chi_\mu^I, \chi_\nu^I, 1), \quad (176)$$

$$D_{Q, sd} = 15^{-\frac{1}{4}} \sqrt{A(\chi_\mu^I, \chi_\nu^I, 2)}, \quad (177)$$

and

$$D_{Q, dd} = 7^{-\frac{1}{2}} \sqrt{A(\chi_\mu^I, \chi_\nu^I, 2)}. \quad (178)$$

The implementation of the formulae to calculate $D_{\mu, pd}$, $D_{Q, sd}$, and $D_{Q, dd}$ can be verified by comparison to the respective values supplied by MOPAC¹⁷⁸ when specifying the keyword HCORE. For each element, the value tabulated as DD2 corresponds to $D_{\mu, sp}$, DD3 to $D_{Q, pp}$, DD4 to $D_{Q, sd}$, DD5 to $D_{\mu, pd}$, and DD6 to $D_{Q, dd}$.

The positions of the point charges arising for a monopole q , a dipole $\mu_{x,y,z}$, a linear quadrupole $Q_{xx,yy,zz}$, and a square quadrupole $Q_{xy,yz,zz}$ are listed in Table 5. The positions of the point charges for the quadrupole $\tilde{Q}_{xy,xz,yz}$ relative to atom I on which the charge distribution $\chi_\mu^I \chi_\nu^I$ is centered are given in Table 7.

Table 7: Specification of the position ($\mathbf{r}_C = (r_{C,x}, r_{C,y}, r_{C,z})$) of the C point charges chosen to represent a specific multipole (Table 4). The number of point charges is given in brackets after the specification of the multipole moment. The positions \mathbf{r}_c are given in relation to the origin of the local coordinate system (Section 10.6). The charges q_C are given in atomic units.

Multipole	$r_{C,x}$	$r_{C,y}$	$r_{C,z}$	q_C
\tilde{Q}_{xy} ($C = 4$)	$+\sqrt{2}D_{Q,pp}$	0.0	0.0	+0.25
	$-\sqrt{2}D_{Q,pp}$	0.0	0.0	+0.25

Multipole	$r_{C,x}$	$r_{C,y}$	$r_{C,z}$	q_C
	0.0	$-\sqrt{2}D_{Q,pp}$	0.0	-0.25
	0.0	$+\sqrt{2}D_{Q,pp}$	0.0	-0.25
\tilde{Q}_{xz} ($C = 4$)	$+\sqrt{2}D_{Q,pp}$	0.0	0.0	+0.25
	$-\sqrt{2}D_{Q,pp}$	0.0	0.0	+0.25
	0.0	0.0	$-\sqrt{2}D_{Q,pp}$	-0.25
	0.0	0.0	$+\sqrt{2}D_{Q,pp}$	-0.25
\tilde{Q}_{yz} ($C = 4$)	0.0	$+\sqrt{2}D_{Q,pp}$	0.0	+0.25
	0.0	$-\sqrt{2}D_{Q,pp}$	0.0	+0.25
	0.0	0.0	$-\sqrt{2}D_{Q,pp}$	-0.25
	0.0	0.0	$+\sqrt{2}D_{Q,pp}$	-0.25

Now we can again straightforwardly apply Eq. (109) after specifying $\vartheta_{q,ss}^I$, $\vartheta_{q,pp}^I$, $\vartheta_{\mu,pp}^I$, $\vartheta_{\mu,dd}^I$, $\vartheta_{\mu,sp}^I$, $\vartheta_{\mu,pd}^I$, $\vartheta_{Q,pp}^I$, $\vartheta_{Q,sp}^I$, and $\vartheta_{Q,dd}^I$. The additive terms $\vartheta_{q,ss}^I$, $\vartheta_{q,pp}^I$, $\vartheta_{q,ss}^I$, $\vartheta_{\mu,pp}^I$, and $\vartheta_{Q,pp}^I$, are determined numerically from Eqs. (110), (111), (112), and (113), respectively. The other terms are determined from the following equations,^{53,54}

$$\vartheta_{q,dd}^I = \frac{1}{2F_{dd}^0}, \quad (179)$$

$$(\vartheta_{\mu,pd}^I)^{-1} - [(\vartheta_{\mu,pd}^I)^2 + (D_{\mu,pd})^2]^{-\frac{1}{2}} = \frac{16}{15}G_{pd}^1, \quad (180)$$

$$(\vartheta_{Q,sd}^I)^{-1} - 2 [(\vartheta_{Q,sd}^I)^2 + (D_{Q,sd})^2]^{-\frac{1}{2}} + [(\vartheta_{Q,sd}^I)^2 + 2(D_{Q,sd})^2]^{-\frac{1}{2}} = \frac{8}{5}G_{sd}^2, \quad (181)$$

and

$$(\vartheta_{Q,dd}^I)^{-1} - 2 [(\vartheta_{Q,dd}^I)^2 + (D_{Q,dd})^2]^{-\frac{1}{2}} + [(\vartheta_{Q,dd}^I)^2 + 2(D_{Q,dd})^2]^{-\frac{1}{2}} = \frac{24}{49}F_{dd}^2. \quad (182)$$

The values for $\vartheta_{q,ss}^I$, $\vartheta_{q,pp}^I$, $\vartheta_{q,dd}^I$, $\vartheta_{\mu,sp}^I$, $\vartheta_{\mu,pd}^I$, $\vartheta_{Q,pp}^I$, $\vartheta_{Q,sd}^I$, and $\vartheta_{Q,dd}^I$ can be verified against the values for P01, P07, P08, P02, P05, P03, P04, and P06, respectively, when specifying the keyword `Hcore` in MOPAC.

In Ref. 53, M_{20} is defined as

$$M_{20} = \tilde{Q}_{zx} - \frac{1}{2}\tilde{Q}_{xy}. \quad (183)$$

Hence, the interaction of two multipoles M_{20} is calculated to be

$$[M_{20}, M_{20}] = [\tilde{Q}_{zx}, \tilde{Q}_{zx}] - \frac{1}{2}[\tilde{Q}_{zx}, \tilde{Q}_{xy}] - \frac{1}{2}[\tilde{Q}_{xy}, \tilde{Q}_{zx}] + \frac{1}{4}[\tilde{Q}_{xy}, \tilde{Q}_{xy}]. \quad (184)$$

This formulae can be simplified to

$$[M_{20}, M_{20}] = [\tilde{Q}_{zx}, \tilde{Q}_{zx}] + \frac{3}{4}[\tilde{Q}_{xy}, \tilde{Q}_{xy}]. \quad (185)$$

when inserting

$$[\tilde{Q}_{zx}, \tilde{Q}_{xy}] = -\frac{1}{2}[\tilde{Q}_{xy}, \tilde{Q}_{xy}]. \quad (186)$$

Note that Ref. 53 appears to contain a misprint because it specifies that $[\tilde{Q}_{zx}, \tilde{Q}_{xy}] = 0$. Apparently, MOPAC implements a different formula,

$$[M_{20}, M_{20}] = [\tilde{Q}_{zx}, \tilde{Q}_{zx}] - \frac{1}{4}[\tilde{Q}_{xy}, \tilde{Q}_{xy}] \quad (187)$$

which is derivable when one defines

$$M_{20} = \tilde{Q}_{zx} + \frac{1}{2}\tilde{Q}_{xy}. \quad (188)$$

The values of two-center ERIs that involve at least one of the following charge distributions, $p_z^I p_z^I$, $p_x^I p_x^I$, $p_y^I p_y^I$, $s^I d_{z^2}^I$, $d_{xy}^I d_{xy}^I$, $d_{xz}^I d_{xz}^I$, $d_{yz}^I d_{yz}^I$, $d_{z^2}^I d_{z^2}^I$, and $d_{x^2-y^2}^I d_{x^2-y^2}^I$, differ when either Eq. (187) or Eq. (185) is applied. We illustrate this for the example of a Br—Cl molecule with an internuclear distance of 0.4 Å (see Table 8). Note that it is not easily possible to switch

Table 8: Value of selected two-center ERIs with PM6 parameters in eV obtained with MOPAC, with Eq. (187) in SCINE,²⁷⁹ and with Eq. (185) in SCINE.

ERI	MOPAC	Eq. (187) in SCINE	Eq. (185) in SCINE
$\langle d_{z^2}^I d_{z^2}^I d_{xz}^J d_{xz}^J \rangle$	20.798	20.798	21.401
$\langle d_{z^2}^I d_{z^2}^I d_{z^2}^J d_{z^2}^J \rangle$	21.475	21.475	22.681
$\langle p_x^I p_x^I d_{yz}^J d_{yz}^J \rangle$	10.833	10.833	10.497
$\langle p_y^I p_y^I s^J d_{z^2}^J \rangle$	-0.021	-0.021	-0.071

between Eq. (187) and Eq. (185). The parameters elements appear to have been determined with an implementation of Eq. (187), and hence, the parameters cannot simply be transferred to a program implementing Eq. (185). Instead, one would have to determine a new set of parameters when implementing the other equation (Eq. (185)).

The implementation of the procedure to calculate those two-center ERIs can be compared to the implementation in MOPAC when invoking the keyword `Hcore` for a calculation of the electronic energy for a diatomic molecule which is aligned along the z -axis (for which s -, p -, and d -type basis functions are activated). The values of the two-center ERIs are then listed under

text. A local coordinate system is defined for each pair of atoms I and $J \neq I$ which are positioned at $\tilde{\mathbf{R}}_I = (\tilde{R}_{I,x}, \tilde{R}_{I,y}, \tilde{R}_{I,z})$ and $\tilde{\mathbf{R}}_J = (\tilde{R}_{J,x}, \tilde{R}_{J,y}, \tilde{R}_{J,z})$, respectively. The standard basis $\mathbf{x}^{\text{loc}}, \mathbf{y}^{\text{loc}}, \mathbf{z}^{\text{loc}}$ of the local coordinate system can then be determined, e.g., as described in Ref. 86 or in Ref. 289. The first unit vector \mathbf{z}^{loc} is defined as the normalized vector connecting $\tilde{\mathbf{R}}_I$ and $\tilde{\mathbf{R}}_J$,

$$\mathbf{z}^{\text{loc}} = \frac{\tilde{\mathbf{R}}_I - \tilde{\mathbf{R}}_J}{|\tilde{\mathbf{R}}_I - \tilde{\mathbf{R}}_J|} = (z_x^{\text{loc}}, z_y^{\text{loc}}, z_z^{\text{loc}}). \quad (189)$$

The vector \mathbf{z}^{loc} can be applied to construct a perpendicular vector \mathbf{y}^{loc} ,

$$\mathbf{y}^{\text{loc}} = \frac{1}{\sqrt{z_x^{\text{loc}2} + z_y^{\text{loc}2}}}(z_y^{\text{loc}}, -z_x^{\text{loc}}, 0). \quad (190)$$

The cross product of \mathbf{z}^{loc} and \mathbf{y}^{loc} yields \mathbf{x}^{loc} ,

$$\mathbf{x}^{\text{loc}} = \mathbf{z}^{\text{loc}} \times \mathbf{y}^{\text{loc}}. \quad (191)$$

We can then construct the rotation matrices which transform the results from the local to the global coordinate system.⁸⁶

The implementation of the transformation procedure can be compared to the implementation in MOPAC when invoking the keyword `Hcore` the calculation of the electronic energy of a diatomic molecule which is *not* aligned along the z -axis. The one hundred first to two hundredth entry listed under `TWO-ELECTRON MATRIX IN Hcore` are the transformed two-center ERIs.

10.7 Modification to the PM6 Core-Core Repulsion Energy

For certain element pairs, a scaling factor different from f_{IJ}^{PM6} (Eq. (62) in the main text) is applied in the PM6 model.⁵⁶ The scaling function $f'_{IJ}{}^{\text{PM6}}$ to calculate the core-core repulsion energy between two carbon atoms is given by

$$\begin{aligned} f'_{IJ}{}^{\text{PM6}} = & 1 + 2x^{Z_I, Z_J} \exp\left(-\alpha^{Z_I, Z_J} \left(\tilde{R}_{IJ} + 0.0003\text{\AA}^{-5} \tilde{R}_{IJ}^6\right)\right) \\ & + 9.28 \exp\left(-5.98\text{\AA}^{-1} \tilde{R}_{IJ}\right) + K^{Z_I} \exp\left(-L^{Z_I} \left(\tilde{R}_{IJ} - M^{Z_I}\right)^2\right) \\ & + K^{Z_J} \exp\left(-L^{Z_J} \left(\tilde{R}_{IJ} - M^{Z_J}\right)^2\right). \end{aligned} \quad (192)$$

For N–H and O–H interactions, the scaling function $f_{IJ}''^{\text{PM6}}$ reads,

$$f_{IJ}''^{\text{PM6}} = 1 + 2x^{Z_I, Z_J} \exp\left(-\alpha^{Z_I, Z_J} \text{\AA}^{-1} \tilde{R}_{IJ}^2\right) + K^{Z_I} \exp\left(-L^{Z_I} \left(\tilde{R}_{IJ} - M^{Z_I}\right)^2\right) \\ + K^{Z_J} \exp\left(-L^{Z_J} \left(\tilde{R}_{IJ} - M^{Z_J}\right)^2\right). \quad (193)$$

Note that MOPAC applies this equation not only for N–H and O–H interactions, but also for C–H interactions, which, however, is not the intended use according to the original publication in Ref. 56. The scaling function $f_{IJ}'''^{\text{PM6}}$ for Si–O interactions is given by

$$f_{IJ}'''^{\text{PM6}} = 1 + 2x^{Z_I, Z_J} \exp\left(-\alpha^{Z_I, Z_J} \left(\tilde{R}_{IJ} + 0.0003 \text{\AA}^{-5} \tilde{R}_{IJ}^6\right)\right) \\ - 0.0007 \exp\left(-\text{\AA}^{-2} \left(\tilde{R}_{IJ} - 2.9 \text{\AA}\right)^2\right) \\ + K^{Z_I} \exp\left(-L^{Z_I} \left(\tilde{R}_{IJ} - M^{Z_I}\right)^2\right) + K^{Z_J} \exp\left(-L^{Z_J} \left(\tilde{R}_{IJ} - M^{Z_J}\right)^2\right). \quad (194)$$

As there exists no theoretical foundation for the introduction of the modified expressions to calculate the core-core repulsion energy, we do not know why the application of these modified scaling factors yield a better agreement with experimental data.

10.8 Constraints on Parameters

During the parameter optimization, certain constraints have to be imposed on the parameter values to keep the parametric expressions sensible from a physical point of view. Several parameters, for instance, determine the sign of an exponential functions which depends on the internuclear distance \tilde{R}_{IJ} . The sign of the argument of the exponential function must be negative so that it does not become infinite for large \tilde{R}_{IJ} which means that $\zeta_{l(\mu)}^{Z_I} > 0$, $\zeta'_{l(\mu)}^{Z_I} > 0$, $\alpha^{Z_I} > 0$, $\alpha^{Z_I, Z_J} > 0$, $a_{l(\mu)}^{Z_I} + a_{l(\lambda)}^{Z_J} > 0$, and $L_a^{Z_I} > 0$. Furthermore, the scaling factors for the core-core repulsion must not become negative (which would correspond to an attractive interaction between two cores), i.e., x^{Z_I, Z_J} and $K_a^{Z_I}$ have to be constrained such that the scaling factors are positive. These constraints are fulfilled by all NDDO-SEMO models. To our understanding, it is not simply possible to constrain the values of the other parameters in a meaningful way.

Interestingly, the parameters appear to vary regularly with the atomic number for lighter elements. Dewar and Thiel noted that the MNDO parameters change in a remarkably regular manner with the atomic number of hydrogen, carbon, nitrogen, and oxygen⁵⁰ (see also Figure 20). This regular behavior is so pronounced that it was, for example, possible to estimate the parameters for fluorine to good accuracy based on the ones for hydrogen, carbon, nitrogen, and oxygen.²⁹⁰ Dewar and co-workers remarked that this ‘suggest[s] that the MNDO method as a whole is suitably self-consistent’.²⁹⁰ For heavier elements, the regularity is lost (e.g., for the second transition-metal block). Additionally, one can also see that the parameters also vary significantly between the different NDDO-SEMO models.

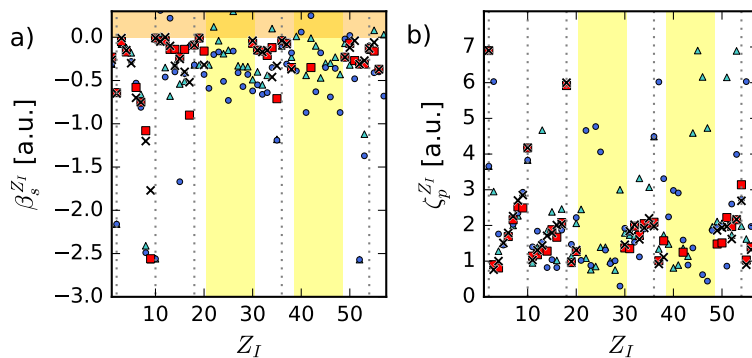


Figure 20: Variation of a) $\beta_s^{Z_I}$ and b) $\zeta_p^{Z_I}$ in a.u. with the atomic number Z_I in a range of $Z_I = 1-57$: MNDO values^{50,139} (black crosses) PM6 values⁵⁶ (light blue triangles), PM7 values⁵⁷ (dark blue circles), and AM1 values^{51,139} (red squares). We highlight the transition metal blocks ($21 \leq Z_I \leq 30$ and $39 \leq Z_I \leq 48$) by a yellow background and indicate Z_I of rare gases by gray dashed lines. The orange area marks the parameter values for which $\beta_s^{Z_I} > 0$.

10.9 Parametrization of the MNDO Model

For this work, we re-optimized the $\beta_{i(\mu)}^{Z_I}$ parameters in the MNDO model for carbon and hydrogen. The applied reference data set \mathcal{D}^m contains 12 heats of formation at 298 K ($\Delta H_f^{298\text{K}}$) of hydrocarbon compounds which are also present in the original reference data set of MNDO⁵⁰ (see Table 9).

Table 9: Reference data set \mathcal{D}^m consisting of $\Delta H_f^{298\text{K}}$ (and the standard deviation of $\Delta H_f^{298\text{K}}$) for twelve compounds in kJ mol⁻¹.

Compound	$\Delta H_f^{298\text{K}}$	Ref.
dihydrogen	0.0 ± 0.0	—
methane	-76.3 ± 0.3	291
ethane	-84.0 ± 0.4	291
ethene	52.4 ± 0.5	291
ethyne	227.4 ± 0.8	291
cyclopropane	53.5 ± 0.6	292
cyclobutane	3.0 ± 0.1	293
benzene	49.0 ± 0.9	294
neopentane	-167.9 ± 0.6	295
n-butane	-125.6 ± 0.7	296
adamantane	-192.5 ± 0.4	297
1,3-butadiene	455.8 ± 2.0	298

We list the values for the parameters β_s^1 , β_s^6 , and β_p^6 which are applied within MNDO⁵⁰ and which we obtained in our parametrizations in Table 10. We supply the parameter files which can be read in through the keyword `External` in MOPAC to reproduce our results with standard software.

Table 10: Values for the parameters β_s^1 , β_s^6 , and β_p^6 which are applied within MNDO⁵⁰ and which we obtained in our parametrizations in a.u.

Parametrization	β_s^1	β_s^6	β_p^6
MNDO	-0.26	-0.70	-0.29
$\mathbf{p}_{\mathcal{D}^m}^m$	-0.26	-0.65	-0.32
$\bar{\mathbf{p}}_{\mathcal{D}^m}^m$	-0.26	-0.68	-0.30

The results for $\Delta H_f^{298\text{K}}$ obtained with the MNDO values, the $\mathbf{p}_{\mathcal{D}^m}^m$ values, and the $\bar{\mathbf{p}}_{\mathcal{D}_b^m}^m$ values for β_s^1 , β_s^6 , and β_p^6 are given in Table 11 and illustrated in Figure 21.

Table 11: $\Delta H_f^{298\text{K}}$ obtained with the original MNDO values, the $\mathbf{p}_{\mathcal{D}^m}^m$ values, and the bootstrapped minimum, mean, and maximum $\bar{\mathbf{p}}_{\mathcal{D}_b^m}^m$ values for β_s^1 , β_s^6 , and β_p^6 in kJ mol^{-1} .

Compound	MNDO	$\mathbf{p}_{\mathcal{D}^m}^m$	$\bar{\mathbf{p}}_{\mathcal{D}_b^m}^m$		
			Min.	Mean	Max.
dihydrogen	11.2	9.5	-19.9	6.4	30.1
methane	-48.3	-54.1	-83.2	-57.2	-30.0
ethane	-79.5	-95.6	-119.6	-95.2	-68.5
ethene	65.6	62.5	29.8	58.4	86.7
ethyne	245.7	247.1	213.3	243.7	268.3
cyclopropane	55.9	36.9	18.6	39.7	58.6
cyclobutane	-13.0	-50.3	-76.0	-38.9	3.3
benzene	91.7	64.7	20.6	74.9	145.0
neopentane	-86.5	-131.3	-166.2	-121.8	-78.3
n-butane	-116.3	-152.5	-182.6	-145.5	-109.8
adamantane	-76.2	-181.0	-266.6	-137.7	36.5
1,3-butadyne	432.7	435.6	369.1	432.9	491.5

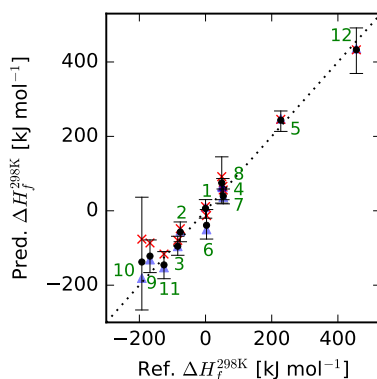


Figure 21: Comparison of the reference ΔH_f^{298K} with the predicted values for ΔH_f^{298K} in kJ mol^{-1} . ΔH_f^{298K} was predicted with the MNDO values for \mathbf{p}^m (red crosses), the $\mathbf{p}_{\mathcal{D}^m}^m$ values (blue triangles), and the $\bar{\mathbf{p}}_{\mathcal{D}_b^m}^m$ values (black circles). We provide the 95% confidence interval for the bootstrapped ΔH_f^{298K} (gray bars). The uncertainties for the experimental data are too small to be visible in this figure. It is denoted for each datapoint in green font to which entry in \mathcal{D}^m it belongs (cf. Figure 16 in the main text).

References

- [1] Hückel, E. Quantentheoretische Beiträge zum Benzolproblem, *Z. Physik* **1931**, 70, 204–286.
- [2] Parr, R. G. A Method for Estimating Electronic Repulsion Integrals Over LCAO MO'S in Complex Unsaturated Molecules, *J. Chem. Phys.* **1952**, 20, 1499–1499.
- [3] Pople, J. A. Electron Interaction in Unsaturated Hydrocarbons, *Trans. Faraday Soc.* **1953**, 49, 1375–1385.
- [4] Pariser, R.; Parr, R. G. A Semi-Empirical Theory of the Electronic Spectra and Electronic Structure of Complex Unsaturated Molecules. I., *J. Chem. Phys.* **1953**, 21, 466–471.
- [5] Pariser, R.; Parr, R. G. A Semi-Empirical Theory of the Electronic Spectra and Electronic Structure of Complex Unsaturated Molecules. II, *J. Chem. Phys.* **1953**, 21, 767–776.
- [6] Parr, R. G. Three Remarks on Molecular Orbital Theory of Complex Molecules, *J. Chem. Phys.* **1960**, 33, 1184–1199.

- [7] Ohno, K. Some Remarks on the Pariser-Parr-Pople Method, *Theor. Chim. Acta* **1964**, *2*, 219–227.
- [8] Pople, J. A.; Santry, D. P.; Segal, G. A. Approximate Self-Consistent Molecular Orbital Theory. I. Invariant Procedures, *J. Chem. Phys.* **1965**, *43*, 129–135.
- [9] Dewar, M. J. S. *The Molecular Orbital Theory of Organic Chemistry*; McGraw-Hill Book Co.: New York, 1969.
- [10] Pople, J. A.; Beveridge, D. L. *Approximate Molecular Orbital Theory*; McGraw-Hill Book Co.: New York, 1970.
- [11] Dykstra, C.; Frenking, G.; Kim, K.; Scuseria, G. *Theory and Applications of Computational Chemistry: The First Forty Years*; Elsevier: Amsterdam, 2005.
- [12] Kohn, W.; Sham, L. J. Self-Consistent Equations Including Exchange and Correlation Effects, *Phys. Rev.* **1965**, *140*, 1133–1138.
- [13] Čížek, J. On the Correlation Problem in Atomic and Molecular Systems. Calculation of Wavefunction Components in Ursell-Type Expansion Using Quantum-Field Theoretical Methods, *J. Chem. Phys.* **1966**, *45*, 4256–4266.
- [14] Akimov, A. V.; Prezhdo, O. V. Large-Scale Computations in Chemistry: A Bird’s Eye View of a Vibrant Field, *Chem. Rev.* **2015**, *115*, 5797–5890.
- [15] Senn, H. M.; Thiel, W. QM/MM Methods for Biological Systems, *Top. Curr. Chem.* **2006**, *268*, 173–290.
- [16] Alexandrova, A. N.; Röthlisberger, D.; Baker, D.; Jorgensen, W. L. Catalytic Mechanism and Performance of Computationally Designed Enzymes for Kemp Elimination, *J. Am. Chem. Soc.* **2008**, *130*, 15907–15915.
- [17] Senn, H. M.; Thiel, W. QM/MM Methods for Biomolecular Systems, *Angew. Chem. Int. Ed.* **2009**, *48*, 1198–1229.
- [18] Alexandrova, A. N.; Jorgensen, W. L. Origin of the Activity Drop with the E50D Variant of Catalytic Antibody 34E4 for Kemp Elimination, *J. Phys. Chem. B* **2009**, *113*, 497–504.

- [19] Stewart, J. J. P. Application of the PM6 Method to Modeling Proteins, *J. Mol. Model.* **2009**, *15*, 765–805.
- [20] Acevedo, O.; Jorgensen, W. L. Advances in Quantum and Molecular Mechanical (QM/MM) Simulations for Organic and Enzymatic Reactions, *Acc. Chem. Res.* **2010**, *43*, 142–151.
- [21] Doron, D.; Major, D. T.; Kohen, A.; Thiel, W.; Wu, X. Hybrid Quantum and Classical Simulations of the Dihydrofolate Reductase Catalyzed Hydride Transfer Reaction on an Accurate Semi-Empirical Potential Energy Surface, *J. Chem. Theory Comput.* **2011**, *7*, 3420–3437.
- [22] Polyak, I.; Reetz, M. T.; Thiel, W. Quantum Mechanical/Molecular Mechanical Study on the Mechanism of the Enzymatic Baeyer–Villiger Reaction, *J. Am. Chem. Soc.* **2012**, *134*, 2732–2741.
- [23] B. Gerber, R.; Shemesh, D.; E. Varner, M.; Kalinowski, J.; Hirschberg, B. Ab Initio and Semi-Empirical Molecular Dynamics Simulations of Chemical Reactions in Isolated Molecules and in Clusters, *Phys. Chem. Chem. Phys.* **2014**, *16*, 9760–9775.
- [24] Weber, V.; Laino, T.; Pozdneev, A.; Fedulova, I.; Curioni, A. Semiempirical Molecular Dynamics (SEMD) I: Midpoint-Based Parallel Sparse Matrix–Matrix Multiplication Algorithm for Matrices with Decay, *J. Chem. Theory Comput.* **2015**, *11*, 3145–3152.
- [25] Husch, T.; Yilmazer, N. D.; Balducci, A.; Korth, M. Large-Scale Virtual High-Throughput Screening for the Identification of New Battery Electrolyte Solvents: Computing Infrastructure and Collective Properties, *Phys. Chem. Chem. Phys.* **2015**, *17*, 3394–3401.
- [26] Husch, T.; Korth, M. Charting the Known Chemical Space for Non-Aqueous Lithium–air Battery Electrolyte Solvents, *Phys. Chem. Chem. Phys.* **2015**, *17*, 22596–22603.
- [27] Lepšík, M.; Řezáč, J.; Kolář, M.; Pecina, A.; Hobza, P.; Fanfrlík, J. The Semiempirical Quantum Mechanical Scoring Function for In Silico Drug Design, *ChemPlusChem* **2013**, *78*, 921–931.
- [28] Brahmshatriya, S. P.; Dobes, P.; Fanfrlík, J.; Rezac, J.; Paruch, K.; Bronowska, A.; Lepšík, M.; Hobza, P. Quantum Mechanical Scoring:

Structural and Energetic Insights into Cyclin-Dependent Kinase 2 Inhibition by Pyrazolo[1,5-a]Pyrimidines, *Curr. Comput. Aided Drug Des.* **2013**, *9*, 118–129.

- [29] Yilmazer, N. D.; Korth, M. Enhanced Semiempirical QM Methods for Biomolecular Interactions, *Comput. Struct. Biotechnol. J.* **2015**, *13*, 169–175.
- [30] Vorlová, B.; Nachtigallová, D.; Jirásková-Vaníčková, J.; Ajani, H.; Jansa, P.; Řezáč, J.; Fanfrlík, J.; Otyepka, M.; Hobza, P.; Konvalinka, J.; Lepšík, M. Malonate-Based Inhibitors of Mammalian Serine Racemase: Kinetic Characterization and Structure-Based Computational Study, *Eur. J. Med. Chem.* **2015**, *89*, 189–197.
- [31] Yilmazer, N. D.; Korth, M. Prospects of Applying Enhanced Semi-Empirical QM Methods for Virtual Drug Design, *Curr. Med. Chem.* **2016**, *23*, 2101–2111.
- [32] Sulimov, A. V.; Kutov, D. C.; Katkova, E. V.; Ilin, I. S.; Sulimov, V. B. New generation of docking programs: Supercomputer validation of force fields and quantum-chemical methods for docking, *J. Mol. Graph. Model.* **2017**, *78*, 139–147.
- [33] Marti, K. H.; Reiher, M. Haptic quantum chemistry, *J. Comput. Chem.* **2009**, *30*, 2010–2020.
- [34] Haag, M. P.; Marti, K. H.; Reiher, M. Generation of Potential Energy Surfaces in High Dimensions and Their Haptic Exploration, *ChemPhysChem* **2011**, *12*, 3204–3213.
- [35] Haag, M. P.; Reiher, M. Real-Time Quantum Chemistry, *Int. J. Quantum Chem.* **2013**, *113*, 8–20.
- [36] Haag, M. P.; Vaucher, A. C.; Bosson, M.; Redon, S.; Reiher, M. Interactive Chemical Reactivity Exploration, *ChemPhysChem* **2014**, *15*, 3301–3319.
- [37] Haag, M. P.; Reiher, M. Studying chemical reactivity in a virtual environment, *Faraday Discuss.* **2014**, *169*, 89–118.
- [38] Vaucher, A. C.; Haag, M. P.; Reiher, M. Real-Time Feedback from Iterative Electronic Structure Calculations, *J. Comput. Chem.* **2016**, *37*, 805–812.

- [39] Mühlbach, A. H.; Vaucher, A. C.; Reiher, M. Accelerating Wave Function Convergence in Interactive Quantum Chemical Reactivity Studies, *J. Chem. Theory Comput.* **2016**, *12*, 1228–1235.
- [40] Heuer, M. A.; Vaucher, A. C.; Haag, M. P.; Reiher, M. Integrated Reaction Path Processing from Sampled Structure Sequences, *J. Chem. Theory Comput.* **2018**, *14*, 2052–2062.
- [41] Thiel, W. Semiempirical Quantum-Chemical Methods, *WIREs Comput. Mol. Sci.* **2014**, *4*, 145–157.
- [42] Elstner, M.; Frauenheim Th.; Kaxiras E.; Seifert G.; Suhai S., A Self-Consistent Charge Density-Functional Based Tight-Binding Scheme for Large Biomolecules, *Physica Status Solidi B* **2000**, *217*, 357–376.
- [43] Gaus, M.; Cui, Q.; Elstner, M. DFTB3: Extension of the Self-Consistent-Charge Density-Functional Tight-Binding Method (SCC-DFTB), *J. Chem. Theory Comput.* **2011**, *7*, 931–948.
- [44] Seifert, G.; Joswig, J.-O. Density-Functional Tight Binding—an Approximate Density-Functional Theory Method, *WIREs Comput. Mol. Sci.* **2012**, *2*, 456–465.
- [45] Elstner, M.; Seifert, G. Density Functional Tight Binding, *Phil. Trans. R. Soc. A* **2014**, *372*, 20120483.
- [46] Grimme, S.; Bannwarth, C.; Shushkov, P. A Robust and Accurate Tight-Binding Quantum Chemical Method for Structures, Vibrational Frequencies, and Noncovalent Interactions of Large Molecular Systems Parametrized for All spd-Block Elements ($Z = 1-86$), *J. Chem. Theory Comput.* **2017**, *13*, 1989–2009.
- [47] Bursch, M.; Hansen, A.; Grimme, S. Fast and Reasonable Geometry Optimization of Lanthanoid Complexes with an Extended Tight Binding Quantum Chemical Method, *Inorg. Chem.* **2017**, *56*, 12485–12491.
- [48] Krishnapriyan, A.; Yang, P.; Niklasson, A. M. N.; Cawkwell, M. J. Numerical Optimization of Density Functional Tight Binding Models: Application to Molecules Containing Carbon, Hydrogen, Nitrogen, and Oxygen, *J. Chem. Theory Comput.* **2017**, *13*, 6191–6200.
- [49] Dewar, M. J. S.; Thiel, W. A Semiempirical Model for the Two-Center Repulsion Integrals in the NDDO Approximation, *Theor. Chim. Acta* **1976**, *46*, 89–104.

- [50] Dewar, M. J. S.; Thiel, W. Ground States of Molecules. 38. The MNDO Method. Approximations and Parameters, *J. Am. Chem. Soc.* **1977**, *99*, 4899–4907.
- [51] Dewar, M. J. S.; Zoebisch, E. G.; Healy, E. F.; Stewart, J. J. P. Development and Use of Quantum Mechanical Molecular Models. 76. AM1: A New General Purpose Quantum Mechanical Molecular Model, *J. Am. Chem. Soc.* **1985**, *107*, 3902–3909.
- [52] Stewart, J. J. P. Optimization of Parameters for Semiempirical Methods I. Method, *J. Comput. Chem.* **1989**, *10*, 209–220.
- [53] Thiel, W.; Voityuk, A. A. Extension of the MNDO Formalism To d-Orbitals: Integral Approximations and Preliminary Numerical Results, *Theor. Chim. Acta* **1991**, *81*, 391–404.
- [54] Thiel, W.; Voityuk, A. A. Erratum: Extension of the MNDO Formalism To d-Orbitals: Integral Approximations and Preliminary Numerical Results, *Theor. Chim. Acta* **1996**, *93*, 315.
- [55] Rocha, G. B.; Freire, R. O.; Simas, A. M.; Stewart, J. J. P. RM1: A Reparameterization of AM1 for H, C, N, O, P, S, F, Cl, Br, and I, *J. Comput. Chem.* **2006**, *27*, 1101–1111.
- [56] Stewart, J. J. P. Optimization of Parameters for Semiempirical Methods V: Modification of NDDO Approximations and Application to 70 Elements, *J. Mol. Model.* **2007**, *13*, 1173–1213.
- [57] Stewart, J. J. P. Optimization of Parameters for Semiempirical Methods VI: More Modifications to the NDDO Approximations and Re-Optimization of Parameters, *J. Mol. Model.* **2012**, *19*, 1–32.
- [58] Kolb, M.; Thiel, W. Beyond the MNDO Model: Methodical Considerations and Numerical Results, *J. Comput. Chem.* **1993**, *14*, 775–789.
- [59] Weber, W.; Thiel, W. Orthogonalization Corrections for Semiempirical Methods, *Theor. Chem. Acc.* **2000**, *103*, 495–506.
- [60] Dral, P. O.; Wu, X.; Spörkel, L.; Koslowski, A.; Weber, W.; Steiger, R.; Scholten, M.; Thiel, W. Semiempirical Quantum-Chemical Orthogonalization-Corrected Methods: Theory, Implementation, and Parameters, *J. Chem. Theory Comput.* **2016**, *12*, 1082–1096.

- [61] Sattelmeyer, K. W.; Tubert-Brohman, I.; Jorgensen, W. L. NO-MNDO: Reintroduction of the Overlap Matrix into MNDO, *J. Chem. Theory Comput.* **2006**, *2*, 413–419.
- [62] Fiedler, L.; Gao, J.; Truhlar, D. G. Polarized Molecular Orbital Model Chemistry. 1. Ab Initio Foundations, *J. Chem. Theory Comput.* **2011**, *7*, 852–856.
- [63] Zhang, P.; Fiedler, L.; Leverentz, H. R.; Truhlar, D. G.; Gao, J. Polarized Molecular Orbital Model Chemistry. 2. The PMO Method, *J. Chem. Theory Comput.* **2011**, *7*, 857–867.
- [64] Zhang, P.; Fiedler, L.; Leverentz, H. R.; Truhlar, D. G.; Gao, J. Erratum: “Polarized Molecular Orbital Chemistry. 2. The PMO Method”, *J. Chem. Theory Comput.* **2012**, *8*, 2983.
- [65] Isegawa, M.; Fiedler, L.; Leverentz, H. R.; Wang, Y.; Nachimuthu, S.; Gao, J.; Truhlar, D. G. Polarized Molecular Orbital Model Chemistry 3. The PMO Method Extended to Organic Chemistry, *J. Chem. Theory Comput.* **2013**, *9*, 33–45.
- [66] Fiedler, L.; Leverentz, H. R.; Nachimuthu, S.; Friedrich, J.; Truhlar, D. G. Nitrogen and Sulfur Compounds in Atmospheric Aerosols: A New Parametrization of Polarized Molecular Orbital Model Chemistry and Its Validation against Converged CCSD(T) Calculations for Large Clusters, *J. Chem. Theory Comput.* **2014**, *10*, 3129–3139.
- [67] Dral, P. O.; von Lilienfeld, O. A.; Thiel, W. Machine Learning of Parameters for Accurate Semiempirical Quantum Chemical Calculations, *J. Chem. Theory Comput.* **2015**, *11*, 2120–2125.
- [68] Thomas, H. B.; Hennemann, M.; Kibies, P.; Hoffgaard, F.; Güssregen, S.; Hessler, G.; Kast, S. M.; Clark, T. The hpCADD NDDO Hamiltonian: Parametrization, *J. Chem. Inf. Model.* **2017**, *57*, 1907–1922.
- [69] Citation analysis of Refs.50–53,55–60, <https://scholar.google.com>, (Accessed: 25. April 2018).
- [70] Dewar, M. J. S. Development and status of MINDO/3 and MNDO, *J. Mol. Struct.* **1983**, *100*, 41–50.
- [71] Dewar, M. J. S. The Semiempirical Approach to Chemistry, *Int. J. Quantum Chem.* **1992**, *44*, 427–447.

- [72] Thiel, W. Semiempirical Methods: Current Status and Perspectives, *Tetrahedron* **1988**, *44*, 7393–7408.
- [73] Clark, T. Semiempirical Molecular Orbital Theory: Facts, Myths and Legends. In *Recent Experimental and Computational Advances in Molecular Spectroscopy*, Vol. 406; Fausto, R., Ed.; Springer: Dordrecht, 1993.
- [74] Thiel, W. Perspectives on Semiempirical Molecular Orbital Theory, *Adv. Chem. Phys.* **1996**, *93*, 703–757.
- [75] Thiel, W. Thermochemistry from Semiempirical Molecular Orbital Theory. In *Computational Thermochemistry: Prediction and Estimation of Molecular Thermodynamics*, Vol. 677; Irikura, K. K.; Frurip, D. J., Eds.; American Chemical Society: Washington, DC, 1998.
- [76] Clark, T. Quo Vadis Semiempirical MO-Theory?, *J. Mol. Struct. Theochem* **2000**, *530*, 1–10.
- [77] Bredow, T.; Jug, K. Theory and Range of Modern Semiempirical Molecular Orbital Methods, *Theor. Chem. Acc.* **2004**, *113*, 1–14.
- [78] Stewart, J. P. P. Semiempirical Molecular Orbital Methods. In *Reviews in Computational Chemistry*; Lipkowitz, K. B.; Boyd, D. B., Eds.; John Wiley & Sons: New York, 2007.
- [79] Clark, T.; Stewart, J. J. P. MNDO-Like Semiempirical Molecular Orbital Theory and Its Application to Large Systems. In *Computational Methods for Large Systems: Electronic Structure Approaches for Biotechnology and Nanotechnology*; Reimers, J. R., Ed.; John Wiley & Sons: New York, 2011.
- [80] Jug, K. *Zweihundert Jahre Entwicklung der Theoretischen Chemie im deutschsprachigen Raum*; Springer: Berlin, 2015, pp. 135-164.
- [81] Lewars, E. G. *Introduction to the Theory and Applications of Molecular and Quantum Mechanics*; Springer: Cham, 2016, pp. 391–444.
- [82] Bredow, T.; Jug, K. Semiempirical Molecular Orbital Methods. In *Handbook of Solid State Chemistry*; Dronskowski, R.; Kikkawa, S.; Stein, A., Eds.; John Wiley & Sons: New York, 2017.
- [83] Condon, E. U.; Shortley, G. H. *The Theory of Atomic Spectra*; Cambridge University Press: Cambridge, 1959, pp. 174–177.

- [84] Pelikán, P.; Turi Nagi, L. Expression of monocentric repulsion integrals on the basis of s,p,d atomic orbitals, *Chem. Pap.* **1974**, *28*, 594–598.
- [85] Kumar, A.; Mishra, P. C. Evaluation of one-centre electron interaction integrals over slater type atomic orbitals, *Pramana* **1987**, *29*, 385–390.
- [86] Glaeske, H.-J.; Reinhold, J.; Volkmer, P. *Quantenchemie - Ein Lehrgang. Band 5: Ausgewählte mathematische Methoden der Chemie*; VEB Deutscher Verlag der Wissenschaften: Leipzig, 1987, pp. 607–609.
- [87] Řezáč, J.; Fanfrlík, J.; Salahub, D.; Hobza, P. Semiempirical Quantum Chemical PM6 Method Augmented by Dispersion and H-Bonding Correction Terms Reliably Describes Various Types of Noncovalent Complexes, *J. Chem. Theory Comput.* **2009**, *5*, 1749–1760.
- [88] Korth, M.; Pitonak, M.; Rezac, J.; Hobza, P. A Transferable H-Bonding Correction for Semiempirical Quantum-Chemical Methods, *J. Chem. Theory Comput.* **2010**, *6*, 344–352.
- [89] Korth, M. Third-Generation Hydrogen-Bonding Corrections for Semiempirical QM Methods and Force Fields, *J. Chem. Theory Comput.* **2010**, *6*, 3808–3816.
- [90] Řezáč, J.; Hobza, P. Advanced Corrections of Hydrogen Bonding and Dispersion for Semiempirical Quantum Mechanical Methods, *J. Chem. Theory Comput.* **2012**, *8*, 141–151.
- [91] Brahmshatriya, P. S.; Dobes, P.; Fanfrlík, J.; Rezac, J.; Paruch, K.; Bronowska, A.; Lepsík, M.; Hobza, P. Quantum Mechanical Scoring: Structural and Energetic Insights into Cyclin-Dependent Kinase 2 Inhibition by Pyrazolo[1,5-a]Pyrimidines, *Curr. Comput. Aided Drug Des.* **2013**, *9*, 118–129.
- [92] Kromann, J. C.; Christensen, A. S.; Steinmann, C.; Korth, M.; Jensen, J. H. A Third-Generation Dispersion and Third-Generation Hydrogen Bonding Corrected PM6 Method: PM6-D3H+, *PeerJ* **2014**, *2*, e449.
- [93] Vorlová, B.; Nachtigallová, D.; Jirásková-Vaníčková, J.; Ajani, H.; Jansa, P.; Řezáč, J.; Fanfrlík, J.; Otyepka, M.; Hobza, P.; Konvalinka, J.; Lepšík, M. Malonate-Based Inhibitors of Mammalian Serine Racemase: Kinetic Characterization and Structure-Based Computational Study, *Eur. J. Med. Chem.* **2015**, *89*, 189–197.

- [94] Tuttle, T.; Thiel, W. OMx-D: Semiempirical Methods with Orthogonalization and Dispersion Corrections. Implementation and Biochemical Application, *Phys. Chem. Chem. Phys.* **2008**, *10*, 2159–2166.
- [95] Řezáč, J.; Hobza, P. A Halogen-Bonding Correction for the Semiempirical PM6 Method, *Chem. Phys. Lett.* **2011**, *506*, 286–289.
- [96] Repasky, M. P.; Chandrasekhar, J.; Jorgensen, W. L. PDDG/PM3 and PDDG/MNDO: Improved Semiempirical Methods, *J. Comput. Chem.* **2002**, *23*, 1601–1622.
- [97] Tubert-Brohman, I.; Guimaraes, C. R. W.; Repasky, M. P.; Jorgensen, W. L. Extension of the PDDG/PM3 and PDDG/MNDO Semiempirical Molecular Orbital Methods to the Halogens, *J. Comput. Chem.* **2004**, *25*, 138–150.
- [98] Christensen, A. S.; Kubař, T.; Cui, Q.; Elstner, M. Semiempirical Quantum Mechanical Methods for Noncovalent Interactions for Chemical and Biochemical Applications, *Chem. Rev.* **2016**, *116*, 5301–5337.
- [99] Szabo, A.; Ostlund, N. S. *Modern Quantum Chemistry: Introduction to Advanced Electronic Structure Theory*; Dover Publications: New York, 1996.
- [100] Helgaker, T.; Jorgensen, P.; Olsen, J. *Molecular Electronic-Structure Theory*; John Wiley & Sons: Chichester, 2012.
- [101] Löwdin, P.-O. On the Nonorthogonality Problem, *Adv. Quantum Chem.* **1970**, *5*, 185–199.
- [102] Fischer-Hjalmars, I. Zero Differential Overlap in ϕ -Electron Theories, *Adv. Quantum Chem.* **1966**, *2*, 25–46.
- [103] Cook, D. B.; Hollis, P. C.; McWeeny, R. Approximate Ab Initio Calculations on Polyatomic Molecules, *Mol. Phys.* **1967**, *13*, 553–571.
- [104] Roby, K. R.; Sinanoğlu, O. On the Performance and Parameter Problems of Approximate Molecular Orbital Theory, with Comparative Calculations on the Carbon Monoxide Molecule, *Int. J. Quantum Chem.* **1969**, *3*, 223–236.
- [105] Roby, K. R. On the Justifiability of Neglect of Differential Overlap Molecular Orbital Methods, *Chem. Phys. Lett.* **1971**, *11*, 6–10.

- [106] Roby, K. R. Fundamentals of an Orthonormal Basis Set Molecular Orbital Theory, *Chem. Phys. Lett.* **1972**, *12*, 579–582.
- [107] Brown, R. D.; Burden, F. R.; Williams, G. R.; Phillips, L. F. Simplified Ab-Initio Calculations on Hydrogen-Containing Molecules, *Theor. Chim. Acta* **1971**, *21*, 205–210.
- [108] Brown, R. D.; Burton, P. G. ‘Balance’ and Predictive Capability in Approximate Molecular Orbital Theory, *Chem. Phys. Lett.* **1973**, *20*, 45–49.
- [109] Weinhold, F.; Carpenter, J. E. A Collection of Papers Presented at the First World Congress of Theoretical Chemists: Some Remarks on Nonorthogonal Orbitals in Quantum Chemistry, *J. Mol. Struct. Theochem* **1988**, *165*, 189–202.
- [110] Neymeyr, K.; Seelig, F. F. “Neglect of Diatomic Differential Overlap” in Nonempirical Quantum Chemical Orbital Theories. I. On the Justification of the Neglect of Diatomic Differential Overlap Approximation, *Int. J. Quantum Chem.* **1995**, *53*, 515–518.
- [111] Neymeyr, K.; Seelig, F. F. “Neglect of Diatomic Differential Overlap” in Nonempirical Quantum Chemical Orbital Theories. II. A Polynomial Expansion for $\Delta^{-1/2}$ in Terms of Legendre and Chebyshev Polynomials, *Int. J. Quantum Chem.* **1995**, *53*, 519–535.
- [112] Neymeyr, K.; Engel, K. “Neglect of Diatomic Differential Overlap” in Nonempirical Quantum Chemical Orbital Theories. III. On the Spectrum of the Overlap Matrix for Diatomic Molecules over Locally Orthogonalized Basis Functions, *Int. J. Quantum Chem.* **1995**, *53*, 537–540.
- [113] Neymeyr, K. “Neglect of Diatomic Differential Overlap” in Nonempirical Quantum Chemical Orbital Theories. IV. An Examination of the Justification of the Neglect of Diatomic Differential Overlap (NDDO) Approximation, *Int. J. Quantum Chem.* **1995**, *53*, 541–552.
- [114] Neymeyr, K. “Neglect of Diatomic Differential Overlap” in Nonempirical Quantum Chemical Orbital Theories. V. A Calculus of Error Concerning the Justification of the Neglect of Diatomic Differential Overlap (NDDO) Approximation, *Int. J. Quantum Chem.* **1995**, *53*, 553–568.

- [115] Koch, W. Neglect of Diatomic Differential Overlap (NDDO) in Non-Empirical Quantum Chemical Orbital Theories, *Z. Naturforsch. A* **1993**, *48*, 819–828.
- [116] Husch, T.; Reiher, M. Comprehensive analysis of the neglect of diatomic differential overlap approximation, *J. Chem. Theory Comput.* **2018**, submitted, [arXiv: 1806.05615].
- [117] Stevens, W. J.; Basch, H.; Krauss, M. Compact Effective Potentials and Efficient Shared-exponent Basis Sets for the First- and Second-row Atoms, *J. Chem. Phys.* **1984**, *81*, 6026–6033.
- [118] Sustmann, R.; Williams, J. E.; Dewar, M. J. S.; Allen, L. C.; von Rague Schleyer, P. Molecular Orbital Calculations on Carbonium Ions. II. Methyl, Ethyl, and Vinyl Cations. The Series $C_3H_7^+$, *J. Am. Chem. Soc.* **1969**, *91*, 5350–5357.
- [119] Koster, J. L.; Ruttink, P. J. A. Non-empirical approximate calculations for the ground states of H_2 and H_3 including complete configuration interactions, *Chem. Phys. Lett.* **1972**, *17*, 419–421.
- [120] Birner, P.; Köhler, H. J.; Weiss, C. C–H Acidity Comparative CNDO/2 and NDDO Calculations on the Reactivity of Azabenzenes, *Chem. Phys. Lett.* **1974**, *27*, 347–350.
- [121] Chandler, G. S.; Grader, F. E. A Re-Examination of the Justification of Neglect of Differential Overlap Approximations in Terms of a Power Series Expansion in S , *Theor. Chim. Acta* **1980**, *54*, 131–144.
- [122] Duke, B. J.; Collins, M. P. S. The Ab Initio Neglect of Differential Diatomic Overlap Method, *Theor. Chim. Acta* **1981**, *58*, 233–244.
- [123] Tu, Y.; Jacobsson, S. P.; Laaksonen, A. Re-examination of the NDDO approximation and introduction of a new model beyond it, *Mol. Phys.* **2003**, *101*, 3009–3015.
- [124] Cao, X.; Dolg, M. Pseudopotentials and Modelpotentials, *WIREs Comput. Mol. Sci.* **2011**, *1*, 200–210.
- [125] Dolg, M.; Cao, X. Relativistic Pseudopotentials: Their Development and Scope of Applications, *Chem. Rev.* **2012**, *112*, 403–480.
- [126] Zerner, M. C. Removal of Core Orbitals in ‘Valence Orbital Only’ Calculations, *Mol. Phys.* **1972**, *23*, 963–978.

- [127] Ridley, J.; Zerner, M. An Intermediate Neglect of Differential Overlap Technique for Spectroscopy: Pyrrole and the Azines, *Theor. Chim. Acta* **1973**, *32*, 111–134.
- [128] Freed, K. F. Is There a Bridge between Ab Initio and Semiempirical Theories of Valence?, *Acc. Chem. Res.* **1983**, *16*, 137–144.
- [129] Freed, K. F. Building A Bridge Between Ab Initio and Semiempirical Theories of Molecular Electronic Structure. In *Structure and Dynamics of Atoms and Molecules: Conceptual Trends*; Calais, J. L.; Kryachko, E. S., Eds.; Springer: Dordrecht, 1995.
- [130] Kołos, W. Possible Improvements of the Interaction Energy Calculated Using Minimal Basis Sets, *Theor. Chim. Acta* **1979**, *51*, 219–240.
- [131] Francl, M. M.; Pietro, W. J.; Hehre, W. J.; Binkley, J. S.; Gordon, M. S.; DeFrees, D. J.; Pople, J. A. Self-consistent Molecular Orbital Methods. XXIII. A Polarization-type Basis Set for Second-row Elements, *J. Chem. Phys.* **1982**, *77*, 3654–3665.
- [132] Davidson, E. R.; Feller, D. Basis Set Selection for Molecular Calculations, *Chem. Rev.* **1986**, *86*, 681–696.
- [133] Giese, T. J.; York, D. M. Improvement of Semiempirical Response Properties with Charge-Dependent Response Density, *J. Chem. Phys.* **2005**, *123*, 164108.
- [134] Li, A.; Muddana, H. S.; Gilson, M. K. Quantum Mechanical Calculation of Noncovalent Interactions: A Large-Scale Evaluation of PMx, DFT, and SAPT Approaches, *J. Chem. Theory Comput.* **2014**, *10*, 1563–1575.
- [135] Pople, J. A. A Priori Geometry Predictions. In *Modern Theoretical Chemistry*, Vol. 4; Schaefer III, H. F., Ed.; Springer: New York, 1977.
- [136] Kulik, H. J.; Luehr, N.; Ufimtsev, I. S.; Martinez, T. J. Ab Initio Quantum Chemistry for Protein Structures, *J. Phys. Chem. B* **2012**, *116*, 12501–12509.
- [137] Sure, R.; Grimme, S. Corrected Small Basis Set Hartree-Fock Method for Large Systems, *J. Comput. Chem.* **2013**, *34*, 1672–1685.
- [138] Dewar, M. J. S.; Thiel, W. Ground States of Molecules. 39. MNDO Results for Molecules Containing Hydrogen, Carbon, Nitrogen, and Oxygen, *J. Am. Chem. Soc.* **1977**, *99*, 4907–4917.

- [139] Stewart, J. J. P. Optimization of parameters for semiempirical methods IV: extension of MNDO, AM1, and PM3 to more main group elements, *J. Mol. Model.* **2004**, *10*, 155–164 and the references cited herein.
- [140] Nanda, D. N.; Narasimhan, P. T. On Invariance Requirements in Approximate SCF MO Theory, *Int. J. Quantum Chem.* **1977**, *12*, 215–223.
- [141] Klopman, G. A Semiempirical Treatment of Molecular Structures. II. Molecular Terms and Application to Diatomic Molecules, *J. Am. Chem. Soc.* **1964**, *86*, 4550–4557.
- [142] Dewar, M. J. S.; Klopman, G. Ground States of σ -Bonded Molecules. I. Semiempirical S.C.F. Molecular Orbital Treatment of Hydrocarbons, *J. Am. Chem. Soc.* **1967**, *89*, 3089–3098.
- [143] Voigt, B. On Bridging the Gap between the INDO and the NDDO Schemes, *Theor. Chim. Acta* **1973**, *31*, 289–295.
- [144] Dewar, M. J. S.; Lo, D. H. Ground States of σ -Bonded Molecules. XVII. Fluorine Compounds, *J. Am. Chem. Soc.* **1972**, *94*, 5296–5303.
- [145] Denton, J.; McCourt, M.; McIver, J. W. New Formulas for Integrals in Semiempirical Molecular Orbital Methods: Part 2. Coulomb Integrals and Their First and Second Cartesian Derivatives in the NDDO Theory, *J. Mol. Struct. Theochem* **1988**, *163*, 355–388.
- [146] Dewar, M. J. S.; Jie, C.; Yu, J. SAM1; The First of a New Series of General Purpose Quantum Mechanical Molecular Models, *Tetrahedron* **1993**, *49*, 5003–5038.
- [147] Holder, A. J.; Dennington, R. D.; Jie, C. Addendum to SAM1 Results Previously Published, *Tetrahedron* **1994**, *50*, 627–638.
- [148] Holder, A. J.; Evleth, E. M. SAM1: General Description and Performance Evaluation for Hydrogen Bonds. In *Modeling the Hydrogen Bond*, Vol. 569; Smith, D. A., Ed.; American Chemical Society: Washington, DC, 1994.
- [149] Stewart, J. J. P. Application of the PM6 Method to Modeling the Solid State, *J. Mol. Model.* **2008**, *14*, 499–535.
- [150] Margraf, J. T.; Hennemann, M.; Meyer, B.; Clark, T. EMPIRE: a highly parallel semiempirical molecular orbital program: 2: periodic boundary conditions, *J. Mol. Model.* **2015**, *21*, 144.

- [151] Weber, W. *Ein neues semiempirisches NDDO-Verfahren mit Orthogonalisierungskorrekturen : Entwicklung des Modells, Implementierung, Parametrisierung und Anwendungen*, Thesis, Universität Zürich, 1996.
- [152] Scholten, M. *Semiempirische Verfahren mit Orthogonalisierungskorrekturen: Die OM3 Methode*, Thesis, Heinrich-Heine-Universität Düsseldorf, 2003.
- [153] Brown, R. D.; Roby, K. R. Approximate Molecular Orbital Theory for Inorganic Molecules, *Theor. Chim. Acta* **1970**, *16*, 175–193.
- [154] Spanget-Larsen, J. On Bridging the Gap between Extended Hückel and NDO Type LCAO-MO Theories, *Theor. Chim. Acta* **1980**, *55*, 165–172.
- [155] De Bruijn, S. Analysis of the Inadequacies of Some Semi-Empirical MO Methods as Theories of Structure and Reactivity, *Int. J. Quantum Chem.* **1984**, *25*, 367–390.
- [156] Pople, J. A.; Segal, G. A. Approximate Self-Consistent Molecular Orbital Theory. III. CNDO Results for AB₂ and AB₃ Systems, *J. Chem. Phys.* **1966**, *44*, 3289–3296.
- [157] Goepfert-Mayer, M.; Sklar, A. L. Calculations of the Lower Excited Levels of Benzene, *J. Chem. Phys.* **1938**, *6*, 645–652.
- [158] Coffey, P. Potential Energy Integrals in Semiempirical MO Methods, *Int. J. Quantum Chem.* **1974**, *8*, 263–266.
- [159] Kollmar, C.; Böhm, M. C. An Analysis of the Zero Differential Overlap Approximation. Towards an Improved Semiempirical MO Method beyond It, *Theor. Chim. Acta* **1995**, *92*, 13–47.
- [160] Mulliken, R. S. The theory of molecular orbitals, *J. Chim. Phys.* **1949**, *46*, 497.
- [161] Jug, K. Operator Equations in Approximate Molecular Orbital Theories, *Theor. Chim. Acta* **1971**, *23*, 183–194.
- [162] Coffey, P.; Jug, K. Semiempirical Molecular Orbital Calculations and Molecular Energies. A New Formula for the β Parameter, *J. Am. Chem. Soc.* **1973**, *95*, 7575–7580.
- [163] De Bruijn, S. Resonance Integrals in Semi-Empirical MO Theories, *Chem. Phys. Lett.* **1978**, *54*, 399–406.

- [164] Horn, A. H. C.; Lin, Jr-H.; Clark, T. Multipole electrostatic model for MNDO-like techniques with minimal valence *spd*-basis sets, *Theor. Chem. Acc.* **2005**, *114*, 159–168.
- [165] Horn, A. H. C.; Lin, Jr-H.; Clark, T. Erratum: Multipole electrostatic model for MNDO-like techniques with minimal valence *spd*-basis sets, *Theor. Chem. Acc.* **2007**, *117*, 461–465.
- [166] Burstein, K. Y.; Isaev, A. N. MNDO Calculations on Hydrogen Bonds. Modified Function for Core-Core Repulsion, *Theor. Chim. Acta* **1984**, *64*, 397–401.
- [167] Voityuk, A. A.; Rösch, N. AM1/d Parameters for Molybdenum, *J. Phys. Chem. A* **2000**, *104*, 4089–4094.
- [168] Winget, P.; Horn, A. H. C.; Selçuki, C.; Martin, B.; Clark, T. AM1* Parameters for Phosphorus, Sulfur and Chlorine, *J. Mol. Model.* **2003**, *9*, 408–414.
- [169] Winget, P.; Clark, T. AM1* Parameters for Aluminum, Silicon, Titanium and Zirconium, *J. Mol. Model.* **2005**, *11*, 439–456.
- [170] Kayi, H.; Clark, T. AM1* Parameters for Copper and Zinc, *J. Mol. Model.* **2007**, *13*, 965–979.
- [171] Kayi, H.; Clark, T. AM1* Parameters for Vanadium and Chromium, *J. Mol. Model.* **2009**, *15*, 1253–1269.
- [172] Kayi, H.; Clark, T. AM1* Parameters for Bromine and Iodine, *J. Mol. Model.* **2009**, *15*, 295–308.
- [173] Kayi, H.; Clark, T. AM1* Parameters for Manganese and Iron, *J. Mol. Model.* **2010**, *16*, 1109–1126.
- [174] Kayi, H.; Clark, T. AM1* Parameters for Cobalt and Nickel, *J. Mol. Model.* **2010**, *16*, 29–47.
- [175] Kayi, H. AM1* Parameters for Gold, *J. Mol. Model.* **2010**, *16*, 1029–1038.
- [176] Kayi, H.; Clark, T. AM1* Parameters for Palladium and Silver, *J. Mol. Model.* **2011**, *17*, 2585–2600.
- [177] Hennemann, M.; Clark, T. EMPIRE: A highly parallel semiempirical molecular orbital program: 1: Self-Consistent Field Calculations *J. Mol. Model.* **2014**, *20*, 2331–2342.

- [178] Stewart, J. P. P. MOPAC, version 17.231, Stewart Computational Chemistry, Colorado Springs, CO, USA, <http://OpenMOPAC.net> (Accessed: 20. April 2018).
- [179] Grimme, S.; Hansen, A.; Brandenburg, J. G.; Bannwarth, C. Dispersion-Corrected Mean-Field Electronic Structure Methods, *Chem. Rev.* **2016**, *116*, 5105–5154.
- [180] Brandenburg, J. G.; Hochheim, M.; Bredow, T.; Grimme, S. Low-Cost Quantum Chemical Methods for Noncovalent Interactions, *J. Phys. Chem. Lett.* **2014**, *5*, 4275–4284.
- [181] Sure, R.; Grimme, S. Comprehensive Benchmark of Association (Free) Energies of Realistic Host–Guest Complexes, *J. Chem. Theory Comput.* **2015**, *11*, 3785–3801.
- [182] Kolb, M. *Ein neues semiempirisches Verfahren auf Grundlage der NDDO-Näherung: Entwicklung der Methode, Parametrisierung und Anwendungen*, Thesis, Universität Wuppertal, 1991.
- [183] Oleari, L.; Sipio, L. D.; Michelis, G. D. The Evaluation of the One-Centre Integrals in the Semi-Empirical Molecular Orbital Theory, *Mol. Phys.* **1966**, *10*, 97–109.
- [184] Gleghorn, J. T.; McConkey, F. W. Extended Basis NDDO Calculations on Diatomic Molecules, *Theor. Chim. Acta* **1982**, *61*, 283–293.
- [185] Zhidomirov, G. M.; Zhanpeisov, N. U.; Zilberberg, I. L.; Yudanov, I. V. On Some Ways of Modifying Semiempirical Quantum Chemical Methods, *Int. J. Quantum Chem.* **1996**, *58*, 175–184.
- [186] Spanget-Larsen, J. The Alternant Hydrocarbon Pairing Theorem and All-Valence Electrons Theory. An Approximate LCAO Theory for the Electronic Absorption and MCD Spectra of Conjugated Organic Compounds, Part 2, *Theor. Chem. Acc.* **1997**, *98*, 137–153.
- [187] Kollmar, C. A New Concept for an Approximate MO Formalism, *Chem. Phys. Lett.* **1997**, *269*, 215–221.
- [188] Nanda, D. N.; Jug, K. SINDO1. A Semiempirical SCF MO Method for Molecular Binding Energy and Geometry I. Approximations and Parametrization, *Theor. Chim. Acta* **1980**, *57*, 95–106.

- [189] Filatov, M. J.; Gritsenko, O. V.; Zhidomirov, G. M. CNDO-S2—a Semiempirical SCF MO Method for Transition Metal Organometallics, *Theor. Chim. Acta* **1987**, *72*, 211–222.
- [190] Jug, K.; Iffert, R.; Schulz, J. Development and Parametrization of SINDO1 for Second-Row Elements, *Int. J. Quantum Chem.* **1987**, *32*, 265–277.
- [191] Gray, N. A. B.; Stone, A. J. Justifiability of the ZDO approximation in terms of a power series expansion, *Theor. Chim. Acta* **1970**, *18*, 389–390.
- [192] Wadt, W. R.; Hay, P. J. Ab Initio Effective Core Potentials for Molecular Calculations. Potentials for Main Group Elements Na to Bi, *J. Chem. Phys.* **1985**, *82*, 284–298.
- [193] Chandrasekhar, J.; Mehrotra, P. K.; Subramanian, S.; Manoharan, P. T. NDDO MO Calculations, *Theor. Chim. Acta* **1976**, *41*, 243–256.
- [194] Chandrasekhar, J.; Mehrotra, P. K.; Subramanian, S.; Manoharan, P. T. NDDO MO Calculations, *Theor. Chim. Acta* **1979**, *52*, 303–310.
- [195] Laikov, D. N. Neglect of Four- and Approximation of One-, Two-, and Three-Center Two-Electron Integrals in a Symmetrically Orthogonalized Basis, *J. Comput. Chem.* **2007**, *28*, 698–702.
- [196] Chang, D. T.; Schenter, G. K.; Garrett, B. C. Self-Consistent Polarization Neglect of Diatomic Differential Overlap: Application to Water Clusters, *J. Chem. Phys.* **2008**, *128*, 164111.
- [197] Laikov, D. N. Intrinsic Minimal Atomic Basis Representation of Molecular Electronic Wavefunctions, *Int. J. Quantum Chem.* **2011**, *111*, 2851–2867.
- [198] Laikov, D. N. A New Parametrizable Model of Molecular Electronic Structure, *J. Chem. Phys.* **2011**, *135*, 134120.
- [199] Jug, K. Mechanism of Cyclopropane-Propene Isomerization, *Theor. Chim. Acta* **1976**, *42*, 303–310.
- [200] Jug, K.; Geudtner, G. Treatment of Hydrogen Bonding in SINDO1, *J. Comput. Chem.* **1993**, *14*, 639–646.

- [201] Zuber, G.; Hug, W. Rarefied Basis Sets for the Calculation of Optical Tensors. 1. The Importance of Gradients on Hydrogen Atoms for the Raman Scattering Tensor, *J. Phys. Chem. A* **2004**, *108*, 2108–2118.
- [202] Hinze, J.; Jaffé, H. H. Electronegativity. I. Orbital Electronegativity of Neutral Atoms, *J. Am. Chem. Soc.* **1962**, *84*, 540–546.
- [203] Cohen, A. J.; Mori-Sánchez, P.; Yang, W. Challenges for Density Functional Theory, *Chem. Rev.* **2012**, *112*, 298–320.
- [204] Perdew, J. P.; Parr, R. G.; Levy, M.; Balduz, Jr., J. L. Density-Functional Theory for Fractional Particle Number: Derivative Discontinuities of the Energy, *Phys. Rev. Lett.* **1982**, *49*, 1691–1694.
- [205] Cohen, A. J.; Mori-Sánchez, P.; Yang, W. Insights into Current Limitations of Density Functional Theory, *Science* **2008**, *321*, 792–794.
- [206] Mori-Sánchez, P.; Cohen, A. J. The derivative discontinuity of the exchange-correlation functional, *Phys. Chem. Chem. Phys.* **2014**, *16*, 14378–14387.
- [207] Sichel, J. M.; Whitehead, M. A. Atomic Parameters for Semi-Empirical SCF-LCAO-MO Calculations, *Theor. Chim. Acta* **1967**, *7*, 32–40.
- [208] Di Sipio, L.; Tondello, E.; De Michelis, G.; Oleari, L. Semi-Empirical Molecular Orbital Theory. The One-Centre Quantities for the Elements of the First and Second Transition Series, *Chem. Phys. Lett.* **1971**, *11*, 287–289.
- [209] Margraf, J. T.; Claudino, D.; Bartlett, R. J. Determination of Consistent Semiempirical One-Centre Integrals Based on Coupled-Cluster Theory, *Mol. Phys.* **2017**, *115*, 538–544.
- [210] Bingham, R. C.; Dewar, M. J. S.; Lo, D. H. Ground States of Molecules. XXV. MINDO/3. Improved Version of the MINDO Semiempirical SCF-MO Method, *J. Am. Chem. Soc.* **1975**, *97*, 1285–1293.
- [211] Hicks, M. G.; Thiel, W. Reference energies in semiempirical parametrizations, *J. Comput. Chem.* **1986**, *7*, 213–218.
- [212] Rossi, I.; Truhlar, D. G. Parameterization of NDDO Wavefunctions Using Genetic Algorithms. An Evolutionary Approach to Parameterizing Potential Energy Surfaces and Direct Dynamics Calculations for Organic Reactions, *Chem. Phys. Lett.* **1995**, *233*, 231–236.

- [213] Brothers, E. N.; Merz, K. M. Sodium Parameters for AM1 and PM3 Optimized Using a Modified Genetic Algorithm, *J. Phys. Chem. B* **2002**, *106*, 2779–2785.
- [214] Hutter, M. C.; Reimers, J. R.; Hush, N. S. Modeling the Bacterial Photosynthetic Reaction Center. 1. Magnesium Parameters for the Semiempirical AM1 Method Developed Using a Genetic Algorithm, *J. Phys. Chem. B* **1998**, *102*, 8080–8090.
- [215] Cox, J. D.; Wagman, D. D.; Medvedev, V. A. *CODATA Key Values for Thermodynamics*; Hemisphere Publishing Corporation: New York, 1989.
- [216] McQuarrie, D. A. *Statistical Mechanics*; University Science Books: Sausalito, 2000.
- [217] Repasky, M. P.; Chandrasekhar, J.; Jorgensen, W. L. Improved Semiempirical Heats of Formation through the Use of Bond and Group Equivalents, *J. Comput. Chem.* **2002**, *23*, 498–510.
- [218] Kromann, J. C.; Welford, A.; Christensen, A. S.; Jensen, J. H. Random Versus Systematic Errors in Reaction Enthalpies Computed Using Semi-Empirical and Minimal Basis Set Methods, *ACS Omega* **2018**, *3*, 4372–4377.
- [219] Winget, P.; Selçuki, C.; Horn, A. H. C.; Martin, B.; Clark, T. Towards a “next Generation” Neglect of Diatomic Differential Overlap Based Semiempirical Molecular Orbital Technique, *Theor. Chem. Acc.* **2003**, *110*, 254–266.
- [220] Proppe, J.; Reiher, M. Reliable Estimation of Prediction Uncertainty for Physicochemical Property Models, *J. Chem. Theory Comput.* **2017**, *13*, 3297–3317.
- [221] Weymuth, T.; Proppe, J.; Reiher, M. Statistical Analysis of Semi-classical Dispersion Corrections, *J. Chem. Theory Comput.* **2018**, *14*, 2480–2494.
- [222] Efron, B. Bootstrap Methods: Another Look at the Jackknife, *Ann. Stat.* **1979**, *7*, 1–26.
- [223] Hastie, T.; Tibshirani, R. J.; Friedman, J. *The Elements of Statistical Learning: Data Mining, Inference, and Prediction*; Springer: New York, 2016.

- [224] Oreluk, J.; Liu, Z.; Hegde, A.; Li, W.; Packard, A.; Frenklach, M.; Zubarev, D. Diagnostics of Data-Driven Models: Uncertainty Quantification of PM7 Semi-Empirical Quantum Chemical Method, **2018**, submitted, [arXiv: 1806.04813].
- [225] Jiang, W.; DeYonker, N. J.; Wilson, A. K. Multireference Character for 3d Transition-Metal-Containing Molecules, *J. Chem. Theory Comput.* **2012**, *8*, 460–468.
- [226] http://openmopac.net/PM7_accuracy/molecules.html (Accessed: 20. April 2018).
- [227] Nieke, C.; Reinhold, J. NDDO Study of the Jahn—Teller Distortions of Octahedral Transition Metal Compounds, *J. Mol. Struct. Theochem* **1985**, *124*, 87–92.
- [228] Nieke, C.; Reinhold, J. NDDO Study of the Coordination Structure of $M_2+(S_2CNH_2)_2$ Complexes ($M = Ni, Cu$), *J. Mol. Struct. Theochem* **1986**, *139*, 241–245.
- [229] Filatov, M. J.; Zilberberg, I. L.; Zhidomirov, G. M. NDDO/MC: A New Semiempirical SCFMO Method for Transition Metal Complexes, *Int. J. Quantum Chem.* **1992**, *44*, 565–585.
- [230] Bosque, R.; Maseras, F. Performance of the Semiempirical PM3 (Tm) Method in the Geometry Optimization of Transition Metal Complexes, *J. Comput. Chem.* **2000**, *21*, 562–571.
- [231] Minenkov, Y.; Sharapa, D. I.; Cavallo, L. Application of Semiempirical Methods to Transition Metal Complexes: Fast Results but Hard-to-Predict Accuracy, *J. Chem. Theory Comput.* doi:10.1021/acs.jctc.8b00018.
- [232] Husch, T.; Freitag, L.; Reiher, M. Calculation of Ligand Dissociation Energies in Large Transition-Metal Complexes, *J. Chem. Theory Comput.* **2018**, *14*, 2456–2468.
- [233] Weymuth, T.; Couzijn, E. P. A.; Chen, P.; Reiher, M. New Benchmark Set of Transition-Metal Coordination Reactions for the Assessment of Density Functionals, *J. Chem. Theory Comput.* **2014**, *10*, 3092–3103.
- [234] Korth, M.; Thiel, W. Benchmarking Semiempirical Methods for Thermochemistry, Kinetics, and Noncovalent Interactions: OMx Methods Are Almost As Accurate and Robust As DFT-GGA Methods for Organic Molecules, *J. Chem. Theory Comput.* **2011**, *7*, 2929–2936.

- [235] Dral, P. O.; Wu, X.; Spörkel, L.; Kosłowski, A.; Thiel, W. Semiempirical Quantum-Chemical Orthogonalization-Corrected Methods: Benchmarks for Ground-State Properties, *J. Chem. Theory Comput.* **2016**, *12*, 1097–1120.
- [236] Lopez, X.; York, D. M. Parameterization of Semiempirical Methods to Treat Nucleophilic Attacks to Biological Phosphates: AM1/d Parameters for Phosphorus, *Theor. Chem. Acc.* **2003**, *109*, 149–159.
- [237] Giese, T. J.; Sherer, E. C.; Cramer, C. J.; York, D. M. A Semiempirical Quantum Model for Hydrogen-Bonded Nucleic Acid Base Pairs, *J. Chem. Theory Comput.* **2005**, *1*, 1275–1285.
- [238] Nam, K.; Cui, Q.; Gao, J.; York, D. M. Specific Reaction Parameterization of the AM1/d Hamiltonian for Phosphoryl Transfer Reactions: H, O, and P Atoms, *J. Chem. Theory Comput.* **2007**, *3*, 486–504.
- [239] Tejero, I.; González-Lafont, À.; Lluch, J. M. A PM3/d Specific Reaction Parameterization for Iron Atom in the Hydrogen Abstraction Catalyzed by Soybean Lipoxygenase-1, *J. Comput. Chem.* **2007**, *28*, 997–1005.
- [240] Wu, X.; Thiel, W.; Pezeshki, S.; Lin, H. Specific Reaction Path Hamiltonian for Proton Transfer in Water: Reparameterized Semiempirical Models, *J. Chem. Theory Comput.* **2013**, *9*, 2672–2686.
- [241] Liang, S.; Roitberg, A. E. AM1 Specific Reaction Parameters for Reactions of Hydroxide Ion with Halomethanes in Complex Environments: Development and Testing, *J. Chem. Theory Comput.* **2013**, *9*, 4470–4480.
- [242] Zhou, Y.; Pu, J. Reaction Path Force Matching: A New Strategy of Fitting Specific Reaction Parameters for Semiempirical Methods in Combined QM/MM Simulations, *J. Chem. Theory Comput.* **2014**, *10*, 3038–3054.
- [243] Saito, T.; Kitagawa, Y.; Takano, Y. Reparameterization of PM6 Applied to Organic Diradical Molecules, *J. Phys. Chem. A* **2016**, *120*, 8750–8760.
- [244] Fredin, L. A.; Allison, T. C. Predicting Structures of Ru-Centered Dyes: A Computational Screening Tool, *J. Phys. Chem. A* **2016**, *120*, 2135–2143.

- [245] Bartók, A. P.; Kondor, R.; Csányi, G. On representing chemical environments, *Phys. Rev. B* **2013**, *87*, 184115.
- [246] Kee, R. J.; Miller, J. A.; Jefferson, T. H. CHEMKIN: a general-purpose, problem-independent, transportable, FORTRAN chemical kinetics code package, Technical Report SAND-80-8003, Sandia National Labs., Livermore, CA (USA), 1980.
- [247] Glowacki, D. R.; Liang, C.-H.; Morley, C.; Pilling, M. J.; Robertson, S. H. MESMER: An Open-Source Master Equation Solver for Multi-Energy Well Reactions, *J. Phys. Chem. A* **2012**, *116*, 9545–9560.
- [248] Proppe, J.; Husch, T.; Simm, G. N.; Reiher, M. Uncertainty quantification for quantum chemical models of complex reaction networks, *Faraday Discuss.* **2017**, *195*, 497–520.
- [249] Proppe, J.; Reiher, M. Mechanism Deduction from Noisy Chemical Reaction Networks, *J. Chem. Theory Comput.* **2018**, submitted, [arXiv: 1803.09346].
- [250] Maeda, S.; Ohno, K.; Morokuma, K. Systematic Exploration of the Mechanism of Chemical Reactions: The Global Reaction Route Mapping (GRRM) Strategy Using the ADDF and AFIR Methods, *Phys. Chem. Chem. Phys.* **2013**, *15*, 3683–3701.
- [251] Magoon, G. R.; Green, W. H. Design and Implementation of a Next-Generation Software Interface for on-the-Fly Quantum and Force Field Calculations in Automated Reaction Mechanism Generation, *Computers & Chemical Engineering* **2013**, *52*, 35–45.
- [252] Rappoport, D.; Galvin, C. J.; Zubarev, D. Y.; Aspuru-Guzik, A. Complex Chemical Reaction Networks from Heuristics-Aided Quantum Chemistry, *J. Chem. Theory Comput.* **2014**, *10*, 897–907.
- [253] Zimmerman, P. M. Navigating Molecular Space for Reaction Mechanisms: An Efficient, Automated Procedure, *Mol. Simul.* **2015**, *41*, 43–54.
- [254] Habershon, S. Automated Prediction of Catalytic Mechanism and Rate Law Using Graph-Based Reaction Path Sampling, *J. Chem. Theory Comput.* **2016**, *12*, 1786–1798.
- [255] Bergeler, M.; Simm, G. N.; Proppe, J.; Reiher, M. Heuristics-Guided Exploration of Reaction Mechanisms, *J. Chem. Theory Comput.* **2015**, *11*, 5712–5722.

- [256] Simm, G. N.; Reiher, M. Context-Driven Exploration of Complex Chemical Reaction Networks, *J. Chem. Theory Comput.* **2017**, *13*, 6108–6119.
- [257] Marx, D.; Hutter, J. *Ab Initio Molecular Dynamics: Basic Theory and Advanced Methods*; Cambridge University Press: Cambridge, 2009.
- [258] Wang, L.-P.; Titov, A.; McGibbon, R.; Liu, F.; Pande, V. S.; Martínez, T. J. Discovering Chemistry with an *Ab Initio* Nanoreactor, *Nat. Chem.* **2014**, *6*, 1044–1048.
- [259] Martínez, T. J. Ab Initio Reactive Computer Aided Molecular Design, *Acc. Chem. Res.* **2017**, *50*, 652–656.
- [260] Schweig, A.; Thiel, W. MNDOC Study of Excited States, *J. Am. Chem. Soc.* **1980**, *103*, 1425–1431.
- [261] Thiel, W. The MNDOC Method, a Correlated Version of the MNDO Model, *J. Am. Chem. Soc.* **1981**, *103*, 1413–1420.
- [262] Clark, T.; Chandrasekhar, J. NDDO-Based CI Methods for the Prediction of Electronic Spectra and Sum-Over-States Molecular Hyperpolarization, *Isr. J. Chem.* **1993**, *33*, 435–448.
- [263] Liotard, D. A.; Holder, A. An Implementation of Configuration Interaction in a General Purpose Semiempirical Context, *J. Chem. Inf. Comput. Sci.* **1999**, *39*, 587–593.
- [264] Toniolo, A.; Ben-Nun, M.; Martínez, T. J. Optimization of Conical Intersections with Floating Occupation Semiempirical Configuration Interaction Wave Functions, *J. Phys. Chem. A* **2002**, *106*, 4679–4689.
- [265] Toniolo, A.; Granucci, G.; Martínez, T. J. Conical Intersections in Solution: A QM/MM Study Using Floating Occupation Semiempirical Configuration Interaction Wave Functions, *J. Phys. Chem. A* **2003**, *107*, 3822–3830.
- [266] Koslowski, A.; Beck, M. E.; Thiel, W. Implementation of a General Multireference Configuration Interaction Procedure with Analytic Gradients in a Semiempirical Context Using the Graphical Unitary Group Approach, *J. Comput. Chem.* **2003**, *24*, 714–726.
- [267] Toniolo, A.; Thompson, A. L.; Martínez, T. J. Excited state direct dynamics of benzene with reparameterized multi-reference semiempirical configuration interaction methods, *Chem. Phys.* **2004**, *304*, 133–145.

- [268] Lei, Y.; Suo, B.; Dou, Y.; Wang, Y.; Wen, Z. New Implementations of MRCI in Semiempirical Frameworks, *J. Comput. Chem.* **2010**, *31*, 1752-1758.
- [269] Dral, P. O.; Clark, T. Semiempirical UNO-CAS and UNO-CI: Method and Applications in Nanoelectronics, *J. Phys. Chem. A* **2011**, *115*, 11303-11312.
- [270] Liu, J.; Thiel, W. An efficient implementation of semiempirical quantum-chemical orthogonalization-corrected methods for excited-state dynamics, *J. Chem. Phys.* **2018**, *148*, 154103.
- [271] Thiel, W. MNDOC study of reactive intermediates and transition states, *J. Am. Chem. Soc.* **1981**, *103*, 1420-1425.
- [272] Silva-Junior, M. R.; Thiel, W. Benchmark of Electronically Excited States for Semiempirical Methods: MNDO, AM1, PM3, OM1, OM2, OM3, INDO/S, and INDO/S2, *J. Chem. Theory Comput.* **2010**, *6*, 1546-1564.
- [273] Tuna, D.; Lu, Y.; Koslowski, A.; Thiel, W. Semiempirical Quantum-Chemical Orthogonalization-Corrected Methods: Benchmarks of Electronically Excited States, *J. Chem. Theory Comput.* **2016**, *12*, 4400-4422.
- [274] Grimme, S.; Waletzke, M. A combination of Kohn-Sham density functional theory and multi-reference configuration interaction methods, *J. Chem. Phys.* **1999**, *111*, 5645-5655.
- [275] Silva-Junior, M. R.; Schreiber, M.; Sauer, S. P. A.; Thiel, W. Benchmarks for electronically excited states: Time-dependent density functional theory and density functional theory based multireference configuration interaction, *J. Chem. Phys.* **2008**, *129*, 104103.
- [276] Simm, G. N.; Proppe, J.; Reiher, M. Error Assessment of Computational Models in Chemistry, *Chimia Int. J. Chem.* **2017**, *71*, 202-208.
- [277] Ramakrishnan, R.; Dral, P. O.; Rupp, M.; von Lilienfeld, O. A. Big Data Meets Quantum Chemistry Approximations: The Δ -Machine Learning Approach, *J. Chem. Theory Comput.* **2015**, *11*, 2087-2096.
- [278] Simm, G.; Reiher, M. Error-Controlled Exploration of Chemical Reaction Networks with Gaussian Processes, *J. Chem. Theory Comput.* **2018**, submitted, [arXiv: 1805.09886].

- [279] Software for Chemical Interaction and Networks (SCINE), www.scine.ethz.ch (Accessed 6. June 2018).
- [280] Sun, Q.; Berkelbach, T. C.; Blunt, N. S.; Booth, G. H.; Guo, S.; Li, Z.; Liu, J.; McClain, J. D.; Sayfutyarova, E. R.; Sharma, S.; Wouters, S.; Chan, G. K.-L. PySCF: the Python-based simulations of chemistry framework, *WIREs Comput. Mol. Sci* **2017**, *8*, e1340.
- [281] Sun, Q. Libcint: An efficient general integral library for Gaussian basis functions, *J. Comput. Chem.* **2015**, *36*, 1664–1671.
- [282] Thiel, W. MNDO2005, Max-Planck-Institut für Kohlenforschung: Mülheim an der Ruhr, Germany, 2005.
- [283] Dewar, M. J. S.; Zoebisch, E. G. Extension of AM1 to the Halogens, *Journal of Molecular Structure: THEOCHEM* **1988**, *180*, 1–21.
- [284] Dewar, M. J. S.; Jie, C.; Zoebisch, E. G. AM1 Calculations for Compounds Containing Boron, *Organometallics* **1988**, *7*, 513–521.
- [285] Kayi, H.; Clark, T. AM1* Parameters for Copper and Zinc, *J Mol Model* **2007**, *13*, 965–979.
- [286] Stewart, J. J. P. MOPAC: A semiempirical molecular orbital program, *J. Comput. Aided Mol. Des.* **1990**, *4*, 1–105.
- [287] Stewart, J. J. P. Optimization of parameters for semiempirical methods. III Extension of PM3 to Be, Mg, Zn, Ga, Ge, As, Se, Cd, In, Sn, Sb, Te, Hg, Tl, Pb, and Bi, *J. Comput. Chem.* **1991**, *12*, 320–341.
- [288] <http://openmopac.net/manual/hcore.html> (Accessed: 20. April 2018).
- [289] Steinmann, C.; Blædel, K. L.; Christensen, A. S.; Jensen, J. H. Interface of the Polarizable Continuum Model of Solvation with Semi-Empirical Methods in the GAMESS Program, *PLoS ONE* **2013**, *8*, e67725.
- [290] Dewar, M. J. S.; Yamaguchi, Y.; Suck, S. H. MNDO Calculations of Molecular Electric Polarizabilities, Hyperpolarizabilities, and Nonlinear Optical Coefficients, *Chem. Phys. Lett.* **1978**, *59*, 541–544.
- [291] Manion, J. A. Evaluated Enthalpies of Formation of the Stable Closed Shell C1 and C2 Chlorinated Hydrocarbons, *J. Phys. Chem. Ref. Data* **2002**, *31*, 123–172.

- [292] Knowlton, J. W.; Rossini, F. D. Heats of Combustion and Formation of Cyclopropane, *J. Res. Natl. Bur. Stand.* **1949**, *43*, 113–115.
- [293] Kaarsemaker, S.; Coops, J. Thermal Quantities of Some Cycloparaffins. Part III. Results of Measurements, *Recl. Trav. Chim. Pays-Bas* **1952**, *71*, 261–276.
- [294] Roux, M. V.; Temprado, M.; Chickos, J. S.; Nagano, Y. Critically Evaluated Thermochemical Properties of Polycyclic Aromatic Hydrocarbons, *J. Phys. Chem. Ref. Data* **2008**, *37*, 1855–1996.
- [295] Good, W. D. The Enthalpies of Combustion and Formation of the Isomeric Pentanes, *J. Chem. Thermodyn.* **1970**, *2*, 237–244.
- [296] Pittam, D. A.; Pilcher, G. Measurements of Heats of Combustion by Flame Calorimetry. Part 8.—Methane, Ethane, Propane, n-Butane and 2-Methylpropane, *J. Chem. Soc. Faraday Trans.* **1972**, *68*, 2224–2229.
- [297] Clark, T.; Knox, T. M.; McKervey, M. A.; Mackle, H.; Rooney, J. J. Thermochemistry of Bridged-Ring Substances. Enthalpies of Formation of Some Diamondoid Hydrocarbons and of Perhydroquinacene. Comparisons with Data from Empirical Force Field Calculations, *J. Am. Chem. Soc.* **1979**, *101*, 2404–2410.
- [298] Rogers, D. W.; Matsunaga, N.; Zavitsas, A. A.; McLafferty, F. J.; Liebman, J. F. The Conjugation Stabilization of 1,3-Butadiyne Is Zero, *Org. Lett.* **2003**, *5*, 2373–2375.